Thermal analysis of liquid immersed electronics for data centres

By

Abdulmajeed Hamad Almaneea

Submitted in accordance with the requirements for the degree of

Doctor of Philosophy

The University of Leeds

School of Mechanical Engineering

October, 2014

The candidate confirms that the work submitted is his own, except where work has formed jointly-authored publication has been included. The contribution of the candidate and other authors to this work has been explicitly indicated overleaf. The candidate confirms that appropriate credit has been given within the thesis where reference has been made to the work of others.

This copy has been supplied on the understanding that it is copyrighted material and that no quotation from the thesis may be published without proper acknowledgement.

© 2014 The University of Leeds and Abdulmajeed H Almaneea

Work Formed from Jointly Authored Publication

The candidate has publications from work contained in this thesis. These were submitted with support of the supervisors. The contribution of the candidate to these works is explicitly mentioned below.

1. Best paper award of conference paper for sections 5.1, 5.2, 5.3 and 5.4 of this thesis. It is jointly- authored: A. Almaneea, J. Summers, H. Thompson and N. Kapur, “Optimal Heat Sink Fin and Cold Lid Heights for Liquid Immersed Servers”, Proceeding of the 2013 COMSOL Conference in Rottrdam [1].
2. Chapter 7 of this thesis is Journal paper jointly authored: Almaneea, A, H. Thompson A, J. Summers A and N. Kapur., Cooling system analysis for a data centre using liquid immersed servers. International Journal of Thermal Technologies, 2014. Vol.(4), No. 3: p. 200-207 [2].
3. Section 6.3.4 of chapter 6 is Journal paper jointly authored: Almaneea, A, H. Thompson A, J. Summers A and N. Kapur., The Effect of CPU Location in Total Immersion of Microelectronics. Engineering and Technology International Journal of Electrical, Computer, Electronics and Communication Engineering 2015. Vol. (9), No. 4: p. 370-273 [3].

The candidate has conducted the majority of the work that appears in the published papers, such as developing the model, presenting and analysing the results. The co-authors provided valuable review and guidance to the candidate.

Acknowledgements

I owe sincere and earnest thanks to my supervisors Dr Summers, Prof. Harvey and Prof Kapur for their advice, supportive guidance, encouragement, and assistance throughout the entire research.

Moreover, I take privilege in acknowledging my family, especially my parents and my wife ‘Alla’, each of whom have helped me at good and hard time, either directly or indirectly. This work would not have been achieved without their support.

Finally, I am grateful to University of Leeds for granting me access to their facilities, such as library and ARC1.

Abstract

Data centres have racks that include servers which support digital services. The growing demand on digital services such as streaming content, web services, telecommunications, financial and social media has led to an unprecedented growth in data centres and therefore their electrical power consumption. A significant portion of data centre energy is consumed by the cooling systems within data centres. Energy consumption of data centres can be reduced by improving their cooling systems. Some data centres are cooled by air cooling while others are cooled by liquid. The liquid cooling approach has greater opportunities for efficient cooling, particularly in high density data centres. The liquid cooling methods can be classified as rack heat exchanger, in server and on chip heat exchangers and total liquid immersion. The liquid immersed concept submerges the server in a dielectric liquid. This liquid is in direct contact with all of the microelectronics and it has properties that do not cause any electrical discharge. The heat from server components, such as the CPU, is transferred via natural convection in the dielectric liquid to water channels, which transport the heat.

The main interest of this thesis is to study liquid immersed microelectronics for data centres. The thesis starts with validation of numerical and experimental work to develop the correct physics for immersed server simulation model. Investigations for optimal heat transfer within the servers include varying the fin height and cold plate height and the adoption of

baffles on the server water jackets (similar to a cold plate). How such servers can be integrated into a data centre is also investigated.

The overview results show that the heat transfer performance when immersing servers is improved when heights of the heat sink fins and distances of the cold plate are optimised. Baffles with a rectangular cross sectional area attached to the water jacket demonstrated the best results where the heat transfer can be improved by up to 71% compared to water jackets with no baffles. Extending these results into a data centre scenario showed that increasing the rack occupancy had a positive effect on the Power Usage Effectiveness (PUE), which indicates an improvement in the cooling system.

Table of Contents

List of Tables....................xi

List of Figures....................xii

List of Abbreviations....................xvii

Chapter 1: Introdction....................1

1.1 General overview....................1

1.2 Aim and objective of this work....................5

1.3 Thesis Organization....................6

Chapter 2: LITERATURE REVIEW....................8

2.1 Introduction....................8

2.2 Data Centre....................9

2.3 Energy Use in Data Centre....................10

2.4 Cooling Uses Energy....................12

2.5 The power usage effectiveness (PUE)....................14

2.6 Methods of Cooling....................15

2.7 Air Cooling....................15

2.7.1 Hot Aisle and Cold Aisle Layout....................18

2.7.2 Aisle Containment....................19

2.7.3 Blanking Panels....................22

2.7.4 Plenum....................24

2.7.5 Vents Location....................24

2.7.6 Environmental requirement of air cooling method ... 26
2.8 Liquid Cooling ... 27
2.8.1 Rack Back Door Heat Exchanger ... 29
2.8.2 Indirect contact with cold plate approaches ... 32
2.8.3 Direct contact with immersion ... 37
2.9 Summary ... 41
Chapter 3: Mathematical Modelling and simulation of liquid cooling of microelectronics ... 43
3.1 Introduction ... 43
3.2 Introduction of Computational Fluid Dynamics (CFD) ... 44
3.2.1 Finite element method ... 47
3.3 Data Centre Modelling Using CFD ... 47
3.4 Boundary conditions ... 48
3.4.1 Inlet and outlet ... 48
3.4.2 Walls ... 49
3.4.3 Symmetry ... 51
3.4.4 Conjugate heat transfer ... 51
3.5 Laminar flow modelling ... 53
3.6 Turbulence modelling ... 56
3.6.1 Turbulent flow – RANS ... 57
3.6.2 K-ε turbulence model ... 58
3.6.3 k-ω turbulence model ... 59

3.6.4 Low Reynolds Number k-ε turbulence model 61

3.7 Summary.. 62

Chapter 4: Validation of model and simulation 63

4.1 Introduction 63

4.2 Natural convection flows in enclosure... 64

4.2.1 Mathematical formulation 65

4.2.2 Building model use COMSOL.. 71

4.2.3 Results 72

4.3 Comparison of natural convection in square cavity using different CFD packages... 77

4.3.1 Mesh sensitivity study.. 79

4.3.2 CFD packages comparison results.. 80

4.4 Validation of numerical solution of heat source on enclosure 83

4.5 Turbulent finned enclosure 93

4.6 Cold plate validation.. 97

4.6.2 Cold plate validation results... 103

4.7 Summary.. 105

Chapter 5: Optimal Heat Sink Fin and Cold plate Heights for Liquid Immersed Servers of model and simulation 107

5.1 Introduction 107

5.2 Modelling methodology 108

5.2.1 Model geometry... 108

5.2.2 Mathematical Model 109

5.2.3 Boundary conditions 112

5.2.4 Heat flux calculation 113

5.2.5 The number of fins 117

5.2.6 Fluid and material properties 118

5.2.7 Mesh sensitivity study 119

5.3 Optimisation method 120

5.4 Optimisation analyses 122

5.4.1 Unconstrained optimisation problem 122

5.4.2 Investigation of lowest T_{case} models 124

5.4.3 Constraint optimisation problem 127

5.5 Summary 129

Chapter 6: Investigation of different baffle cross sections for improving the cooling in liquid immersed servers 131

6.1 Introduction 131

6.2 Modelling of immersed server 132

6.2.1 Immersed server modelling 132

6.2.2 Mathematical formulation 137

6.2.3 Boundary conditions 139

6.2.4 Numerical solution 141

6.3 Result and discussion 142

6.3.1 Parametric study of immersed server 143

6.3.2 Investigation of best heat transfer parameter 145

6.3.3 Study of effect the heat flux on best baffle cross section....... 149

6.3.4 Effect of CPU location on heat transfer 151

6.4 Summary... 155

Chapter 7: Cooling system analysis for a data centre using liquid immersed servers 156

7.1 Introduction 156

7.2 Cooling data centre system.. 157

7.3 Methodology of flow rate and temperature calculations 159

7.4 Results of rack inlet temperature and the simulation model......... 164

7.5 PUE of the cooling system 168

7.6 PUE for different number of servers... 172

7.7 Summary... 173

Chapter 8: Conclusion.. 175

8.1 General discussion 175

8.2 Future Work 181

REFERENCES 183

LIST OF TABLES

Table 2.1: Immersed cooling verses the air cooling 38

Table 4.1: Comparison of temperature contours inside the cavity between present study (right) and De Vahl Davis 73

Table 4.2: Numerical comparison between present validation and De Vahl Davis [92] 76

Table 4.3: Square cavity length of different liquids 77

Table 4.4: Thermal properties of water and HFE 7300 78

Table 4.5: u_{max} in middle of square cavity in y direction of different number of elements 79

Table 4.6: Wall lift off inside the water pipe in the cold plate for different velocities 102

Table 5.1: Working fluid thermal properties 119

Table 5.2: Compare between the predicted T_{case} and simulated optimum design variables. 123

Table 5.3: Lowest T_{case} cases 125

Table 6.1: Geometrical parameter values 135

Table 6.2: Baffles cross section surface area that contact with fluid 146

Table 6.3: CPU location 151

LIST OF FIGURES

Figure 1.1: Data centre using air cooling method [3]..................................... 2

Figure 1.2: Immersed server diagram 3

Figure 1.3: Server baffles diagram.. 6

Figure 2.1: Data centre arrangement [21] 9

Figure 2.2: projected trends of IT heat load [26] 11

Figure 2.3: Energy use of worldwide data centres in 2000 and 2005 [32]... 13

Figure 2.4: Electricity consumption of the data centre [33].......................... 13

Figure 2.5: Standard air cooling [40] 17

Figure 2.6: The airflow recalculation in data centre [41].............................. 18

Figure 2.7: Hot aisles cold aisle layout [42]... 19

Figure 2.8: Standard Aisle Configuration [45] 20

Figure 2.9: Cold Aisle Containment [45]... 21

Figure 2.10: Hot Aisle Containment [46] 22

Figure 2.11: Air flow with and without blanking panels [47]......................... 23

Figure 2.12: Floor vents location [48]... 25

Figure 2.13: Environmental condition by ASRAE for the data centre.......... 26

Figure 2.14: Heat flux and processors technologies [55] 28

Figure 2.15: Rack back door heat exchanger 30

Figure 2.16: Free cooling a: Total Free cooling in winter, b: Partial Free cooling in spring, c: No Free cooling in summer [60].................................. 32

Figure 2.17: Growth of chip heat flux densities [62] 33

Figure 2.18: Cold plate... 34

Figure 2.19: Liquid system diagram 35

Figure 2.20: Types of fan 35

Figure 2.21: Fin array of IBM original cooling system 36

Figure 2.22: The liquid cooling system configuration 36

Figure 2.23: Data centre immersion concept [67] 39

Figure 2.24: Cross section Iceotope cooling module [69]............................ 41

Figure 3.1: CFD combinations [71].. 44

Figure 3.2: the velocity developed layer in pipe [77] 49

Figure 3.3:The distance between computational domain and the wall δw. [79] 50

Figure 3.4: Diagram showing the conjugate heat transfer for solid and fluid domains. 52

Figure 3.5: Laminar flow between two plates one moving while the other is stationary [82]. 53

Figure 3.6: Rectangular enclosure geometry [12] 55

Figure 3.7: Fluid behaviour of Natural convection fluid flow in rectangular enclosure [12] 55

Figure 3.8: The fluid behaviour of Turbulent and laminar flow [81] 56

Figure 4.1: Geometry of square cavity 65

Figure 4.2: COMSOL interface for the Natural convection model 72

Figure 4.4: Horizontal velocity (u’) at x= 0.5 for different Ra, the diagram in the corner is showing the cut line in the square cavity at x=0.5 and the horizontal velocity in X direction (u’).. 74

Figure 4.5: Vertical velocity (v’) at y= 0.5 for different Ra, the diagram in the corner is showing the cut line in the square cavity at y= 0.5 and the vertical velocity in Y direction (v’) 75

Figure 4.6: u_{max} in x-direction for HFE 7300 at L=1x10^{-3} m 81

Figure 4.7: u_{max} in x-direction for HFE 7300 at $L=2x10^{-3}$ m 81

Figure 4.8: u_{max} in x-direction for water at $L=1x10^{-3}$ m 82

Figure 4.9: u_{max} in x-direction for water at $L=2x10^{-3}$ m 82

Figure 4.10: Schematic diagram of non-dimensional simulation model of three chips in an enclosure 84

Figure 4.11: Temperature profile along substrate surface to compare simulation model and Liu and Phan-Thien results. 93

Figure 4.12: Schematic diagram of experiment setup of finned enclosure[16]. 94

Figure 4.13: Finned enclosure of model simulation in this work where N = 3, L/H =0.5 and S/H=2 95

Figure 4.14: Comparison of present study model with experiment for Nusselt number. 97

Figure 4.15: Simulation model components of validation AVVID cold plate 99

Figure 4.16: AVVID model geometry showing the different cross section of real cold plate.. 100

Figure 4.17: Zoom-in to different cross section areas that the water passes through in clod plate pipe 100

Figure 4.18: The validation of simulation model and AAVID results by varying the flow rate and measuring the pressure drop. 103

Figure 4.19: The validation of simulation model and AAVID results by varying the flow rate and measure the Thermal resistance drop............... 105

Figure 5.1: Geometry of a) Computational domain b) Server.................... 109

Figure 5.2: Schematic diagram of cut plane in the centre of the model to show the boundary conditions of the model and the conjugate heat......... 113

Figure 5.3: CPU and server dimensions 114

Figure 5.4: Temperature in centre of CPU along Z direction. 116

Figure 5.5: Top view of different number of fins a) one fin b) two fins c) three fins. 117

Figure 5.6: Show the temperature along Z axis in order to compare between the numbers of fins.. 118

Figure 5.7. Wall lift off of the simulation model.. 120

Figure 5.8: Design of experiment 122

Figure 5.9. Response surface of T_{case} 124

Figure 5.10. Temperature line along the top centre of the CPU in Z direction 126

Figure 5.11: Velocity field Z component, m/s 128

Figure 6.1: Server assembly geometry (turned to horizontal orientation for clarity) with a zoom-in to the interesting parts of the heat sink and the cold plat and baffles showing the fine details of the geometry design. 133

Figure 6.2: Server diagram (turned into horizontal orientation for clarity) a) Full server. b) Computational domain of the server.................................. 134

Figure 6.3: baffles different cross sections 136

Figure 6.4: Schematic diagram of cut plane in the centre of the model to show the boundary conditions of the model and the conjugate heat......... 140

Figure 6.5: comparison of variation T_{out} with flow rate of the analytical and computational model. 142

Figure 6.6: Variation of the Nu with heat flux load, where Q_{in} =3x10^{-7} m^3/s and T_{in}=303 K.. 145

Figure 6.7: Flow rate between the baffles for a different baffles cross section area along the server. 147

Figure 6.8: Temperature contour of Cut-plane in centre of the server for different baffles cross sections 148

Figure 6.9: Flow rate long the server between the rectangular baffle for a different heat flux load. 150

Figure 6.10: Temperature in centre line between rectangular baffles along the server for different heat flux load 150

Figure 6.11: CPU locations, where S is varying as shown in Table 6.3 151

Figure 6.12: the location of CPU for server using air for cooling [106]. 152

Figure 6.13: variation of heat flux load for different CPU location. 153

Figure 6.14: Effect of the CPU location on the velocity for different cases at q_L= 100%, Q_{in}= 3x10^{-7} m^3/s and T_{in}= 303 k 154

Figure 7.1: Schematic diagram of the data centre cooling system 158

Figure 7.2: Average temperature of Leeds, England [107]........................ 159

Figure 7.3: The variation of ΔT_{apr} with flow rate Q_{inr}, dry cooler fan spins at 169 rpm 160

Figure 7.4: The variation of ΔT_{aps} with Q_{ins} and Q_{inr}.................................. 162

Figure 7.5: Flow chart of calculations to find T_1 using MATLAB v7.11. 163

Figure 7.6 : Water inlet temperature of rack (T_1) varying Q_{inr} for different Q_{ins} 165

Figure 7.7: the geometry of the symmetry simulation model used in COMSOL a) Isometric view b) Side view c) Front View 167

Figure 7.8: variation of PUE by changing the number of the servers per rack 173

LIST OF ABBREVIATIONS

Nomenclature

Pr	Prantl number
Ra	Rayleigh number
Re	Reynolds number
Nu	Nusselt number
D	Diameter
T	Temperature
N	normal vector
U	velocity
u_τ	friction velocity
T_f	Fluid temperature
T_s	Solid temperature
C_p	specific heat
l_w	the distance to near wall
K	turbulent kinetic energy
T_h	Hot wall temperature
T_c	Cold wall temperature
F_y	Body force
u_{max}	the maximum velocity in X direction
v_{max}	the maximum velocity in Y direction
k_{chip}	chip thermal conductivity

k_s	substrate thermal conductivity
T_{case}	the top centre temperature of the CPU
Pr_T	turbulent Prantl Number
λ_s	thermal conductivity for the heat sink
H_{fin}	heat sink fin height
H_{plate}	cold plate height
Q_{inr}	flow rate from dry cooler to buffer heat exchange
Q_{ins}	flow rate from the buffer heat exchanger to the rack
T_3	the cold water temperature entering the buffer heat exchanger
T_1	the water inlet temperature of server
T_5	ambient temperature
Q_f	air flow rate
f	The fanning factor friction
L_e	Entrance length
D_r	root diameter
P_T	tube pitch
D_f	the diameter of the fans
P_f	power required for fan
P_c	power required for cooling
v'	non-dimensional velocity in Y direction
p'	non-dimensional pressure
T'	non-dimensional represent temperature

T'_o	non-dimensional reference temperature

Greek Symbols

λ	thermal conductivity
P	fluid density
δ_w	distance between the wall and the computational domain mesh
M	fluid dynamic viscosity
Κ	Karaman number
λ_s	Solid thermal conductivity
λ_f	Fluid thermal conductivity
B	coefficient of thermal expansion
Α	Thermal diffusivity
Ν	Kinematic viscosity
μ_t	turbulent viscosity
σ_ε	Prandtl number of ε
σ_k	Prandtl number of k
Ε	turbulent dissipation rate
Ω	turbulent specific dissipation rate

Acronyms

PUE	Power usage effectiveness
PDU	power distribution unit
CRAC	Computer room air conditioners
CFD	Computational Fluid Dynamics
GPM	Gallon per minute
DoE	design of experiment
R square	Coefficient of determination
UPS	Uninterruptible Power supply
IT	Information Technology
CPU	Central Processing Unit
HDD	Hard Disk Drive
DIMM	dual in-line memory module

CHAPTER 1:

INTRODCTION

1.1 General overview

The data centre (see Figure 1.1) is a big warehouse that contains electronic equipment to deal with processing and storing data. The high demand on digital and telecommunication services, which has increased the usage of data centres and the required powerful servers. Since more power means more heat; removing heat has become a challenge that needs to be overcome. Cooling the data centre can consume a major share (over 30%) of the overall energy consumption of the data centre [4, 5].

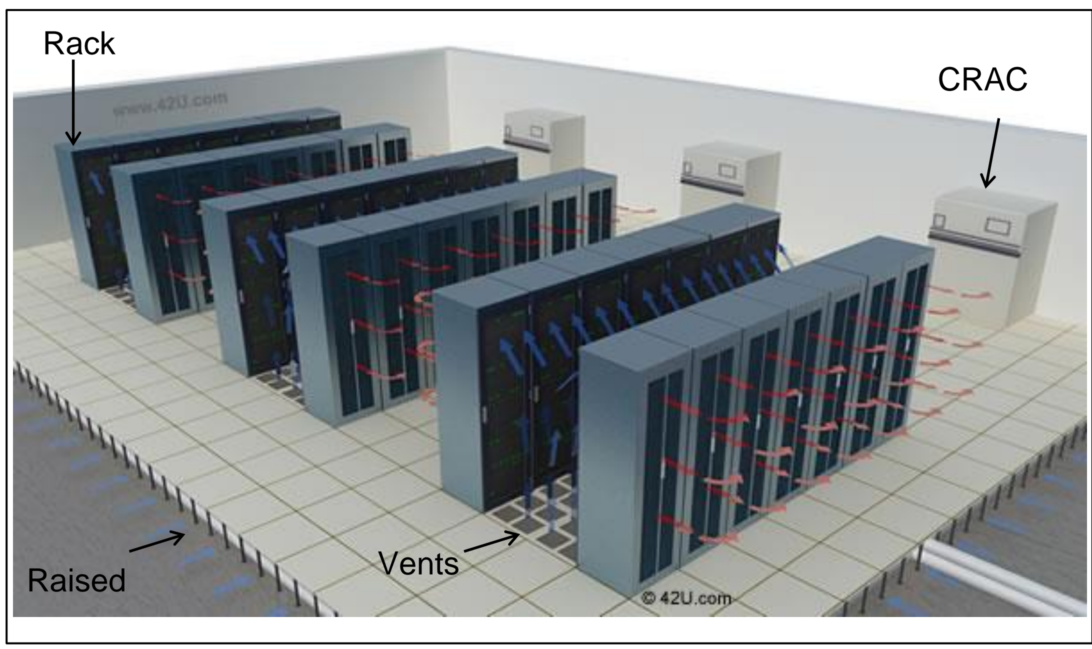

Figure 1.1: Data centre using air cooling method [6]

Air and liquid are the two heat transfer media that are used for cooling data centres. The cold air in a data centre supplied by computer room air conditioning (CRAC) where the cold air pass through the raised floor then via pressure differences through the electronic equipment to remove the heat, finally returning to the CRAC to be cooled as shown in Figure 1.1. Generally the large air volume that needs to manage and circulate is really expensive and the heat capacity and density of air is small compare to the liquid [7]. This fact has motivated the use of liquid cooling in some data centres. Using liquid in data centres is a promising approach that has advantages of handling high heat density. However, with liquid cooling there is an increase in infrastructure, i.e. pipe work and leak detection, and it may also offer difficulties in concurrent maintenance as well as other risks. Some liquid cooling methods bring the liquid close to the rack [8] other methods are based on bringing the liquid into the rack itself, but not in a direct contact

with the semiconductors [9]. Another technique is based on immersing the server into dielectric liquid [10]. These techniques will be described in more detail in chapter 2. The dielectric liquid is in direct contact with the microelectronics to improve the heat transfer performance and it prevents the electric discharge. The dielectric liquid has a so called dielectric strength that is sufficiently large to act as an electrical insulator [11].

This study focuses on the immersed server concept, in which the server is in a direct contact with the dielectric liquid as shown in Figure 1.2. The CPU generates the heat which is conducted towards the heat sink then naturally convected by the dielectric liquid. Then, the dielectric liquid cools down via cold plate where the cold water passes through a channel.

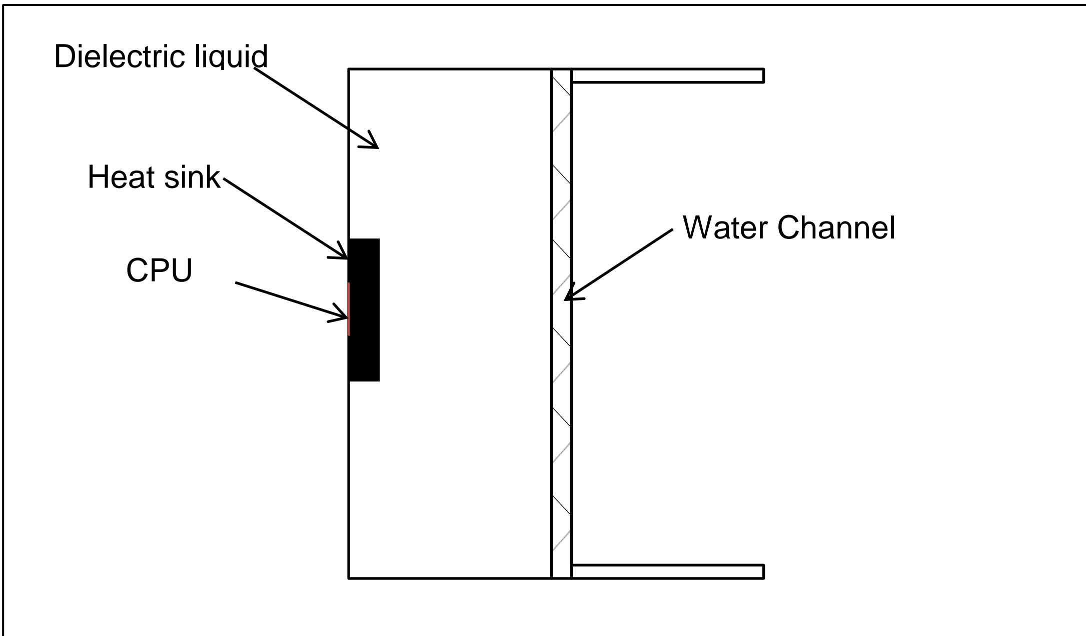

Figure 1.2: Immersed server diagram

The server is closed and there is no pump or blower inside the server so the heat transfer occurs by natural convection. In case of cubic and rectangular enclosures with one wall hot while the other is cold, there have been a number of investigations [12-14] . Fluid flow behaviour in rectangle enclosures has been studied for the range of rectangular aspect ratios, from 1 to 40 and the studies showed that for Rayleigh number (Ra) > 10^7 the fluid became turbulent [15]. For chip or heat source in rectangular enclosure Phan-Thien [16] studied three heat sources on rectangular enclosures and the results showed that the temperature can drop by up to 10% with the optimum heat source location. Chang [17] performed a 3D rectangular model and changed the chips location with varying Rayleigh number from 10^3 to 10^6, where the fluid is considered to be laminar. The results show that the highest average chips temperature is for placing the chips vertically.

However, there are a few studies that have been carried out for the enclosure with fins inside it to improve the rate of heat transfer. For the fins attached on walls, Frederick [18] numerically studied different Rayleigh numbers varying from 10^3 to 10^6 for 3D natural convection in a cube, where the fins were placed horizontally on the hot wall. Nada [19] has investigated rectangular enclosures experimentally in both horizontal and vertical orientations and also by changing the fin spacing and fin length on the hot surface. The results in their study show that the rate of heat transfer increased by increasing the fin height. Ycel [20] numerically investigated 2D natural convection in vertical rectangular enclosure with fins or baffles placed on the cold wall. They found that the increase the number of fins and length can increases the heat transfer.

In this work, the main model is the immersed server, where the server is filled with a dielectric liquid. The aim and objectives of the study in this thesis are presented in the next section. The outline of the thesis is also presented in this chapter.

1.2 Aim and objective of this work

This work is aiming to study immersed server of the data centre. The objectives of this work can be divided into four phases, as follows:

1. Phase one focused on developing the correct physics to build into a CFD model of an immersed server. This phase validate the CFD model with conjugate heat and buoyancy driven flow problems.
2. Phase two: After building the correct physics of conjugate heat and buoyancy driven flow, the simulations of an immersed server are produced. In addition, the optimisation approach is used to find the optimum cold plate (H_{plate}) and fin heights (H_{fin}) as shown in Figure 1.3 in order to reduce the CPU temperature.
3. Phase three: the suitable fin and cold plate heights for immersed server based on the previous phase are used to add baffles (see Figure 1.3) on the cold plate. The study in this phase is investigated with different cross sectional areas and shapes of baffles to improve the heat transfer performance.
4. Phase four: the fully optimised immersed server with baffles is placed in a data centre scenario to determine the effectiveness of the cooling via the power usage effectiveness (PUE) metric. Then, different

numbers of servers are used to obtain the effect of the number of severs on the PUE.

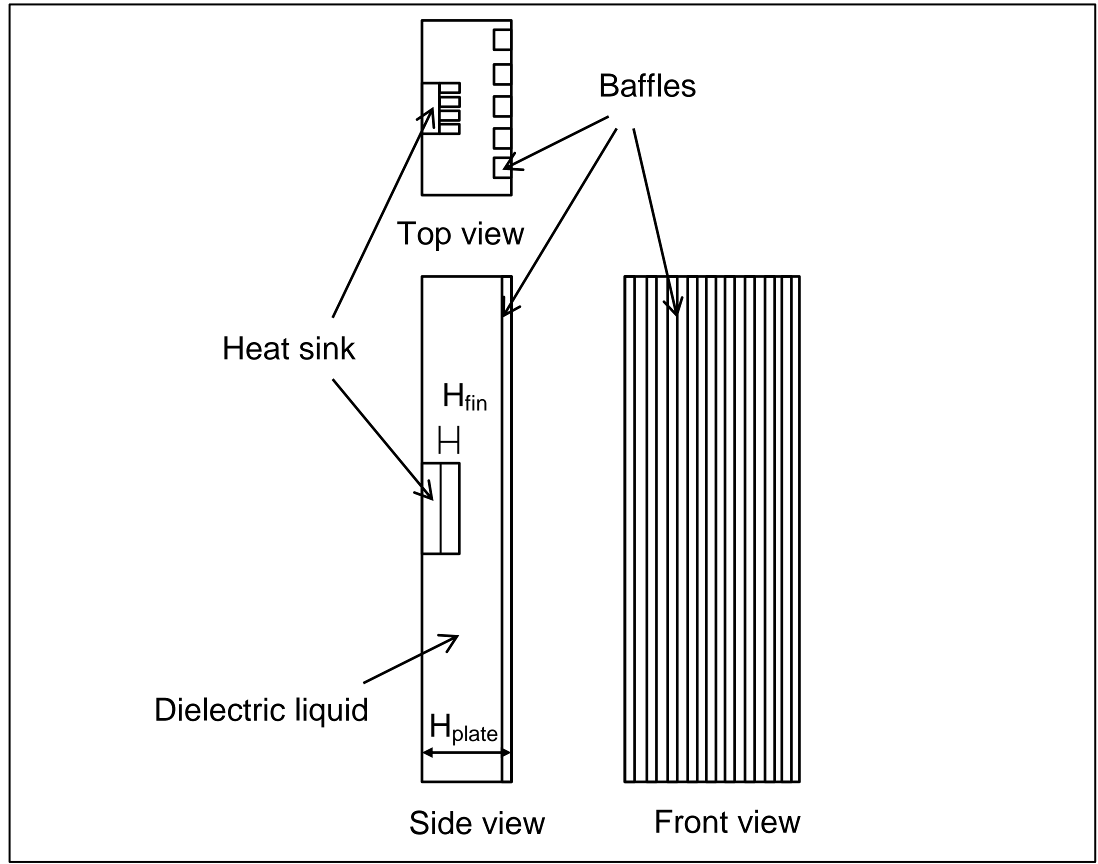

Figure 1.3: Server baffles diagram

1.3 Thesis Organization

To achieve the aims and objectives of this thesis, it is broken down into 8 chapters. The thesis is organised as follow:

A. Chapter 2: contains the literature review, where a general introduction to data centres is given. Then a detailed explanation of power consumption and cooling methods used in data centres is presented.

B. Chapter 3: this chapter describes mathematical modelling and simulation of liquid cooling of microelectronics. It provides an introduction to CFD and presents the model boundary conditions, fluid flow behaviours, and fluid governing equations.

C. Chapter 4: in this chapter different works have been validated in order to prove that the CFD using COMSOL is a capable tool to build the correct physical model for the conjugate heat transfer problem of liquid immersed servers in buoyancy driven flows.

D. Chapter 5: describes the immersed server model. The optimisation method and analysis that used to find the optimum fin and cold plate heights.

E. Chapter 6: investigates different cross section area of baffles that attached on the cold plate in order to improve the heat transfer performance.

F. Chapter 7: the immersed server model is placed in data centre in order to determine the Power Usage Effectiveness (PUE) of the cooling system.

G. Chapter 8: the conclusion is provided in this chapter based on previous chapters. In addition, some suggestion in this chapter is given for future work.

CHAPTER 2:

LITERATURE REVIEW

2.1 Introduction

This chapter reviews cooling techniques adopted in data centres. The increasing demand for digital services has led to high growth in data centres and their energy consumption. A significant portion of data centre energy is consumed by the cooling infrastructure. Data centres can be cooled by either air or liquids, or even a combination, to transport the heat away from the microelectronic components. Air and liquid cooling techniques are addressed in this chapter, and liquid cooling is classified into three main methods; back door heat exchanger, indirect liquid cooling (cold plate) and direct liquid cooling (immersed server) which will be explained thoroughly in this chapter.

2.2 Data Centre

Data centres are buildings that contain microelectronic equipment which deals with data storage, processing, management and the exchange of information and digital data [21].

The approximate area occupied by data centres in the UK is $7.6\text{x}10^6$ m^2 [22]. The area required for a typical single data centre ranges from 100 to 10000 m^2 and needs nearly 100 kW to 10 MW of power for running the servers, lights and cooling equipment, etc. [23]. The data centre consists of number of cabinets known as racks. The racks placed usually in rows as shown in Figure 2.1. The typical height of a rack is 2 m and it is occupied by servers, storage devices and network switches. The data are processed by servers, stored on the storage devices and transmitted locally and globally by the network switches.

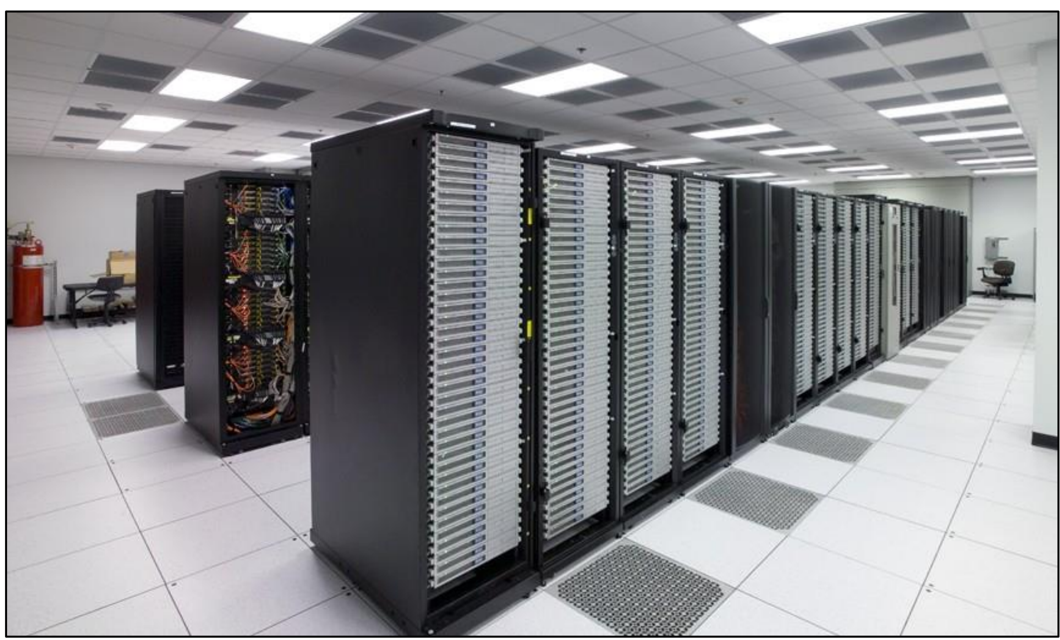

Figure 2.1: Data centre arrangement [24]

The data centre is used to deal with every conceivable digital service, for example bank transactions, telecommunications, simulation computing, big data, and web hosting. As an example data centre, Facebook uses more than 180,000 servers [25] to process and store uploaded photos, videos and messages. Data centres need to be working all of the time, 24 by 7. Maintaining the data centre's thermal environment is a challenging problem, as overheating can damage or turn off IT equipment resulting in loss of service for customers – an issue that can be catastrophic for certain businesses [26].

2.3 Energy Use in Data Centre

As more and more people adopt the information and communication technologies in their activities, the data centres are now growing and developing. Nearly 40% of world's population use the internet [27].

The growth and development of the data centres are not associated with the expansion of space, So that led to increase data centres power density. Figure 2.2 demonstrates the chart of the projected trends of six digital equipment classifications till the year 2014, which gives an idea about the power consumption by the data centres which according to Pacific Gas and Electrical company [28] the estimates are up to 50 times that of regular office space. In 1992, the computer server had the heat load density of about 3 kW/m^2, which was increased to 40 kW/m^2 by 2011. It was expected that this would further increase to 50kW/m^2 in 2014 [28].

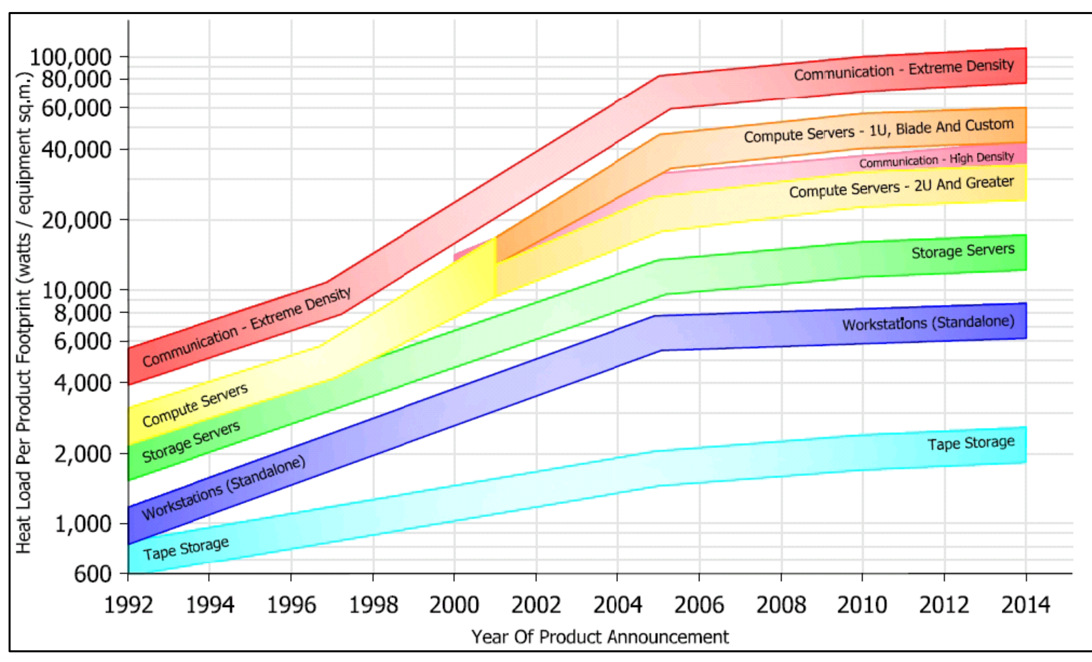

Figure 2.2: projected trends of IT heat load [29]

Smith [30] states that between 2005 and 2010, ten additional power plants (1 GW) will be constructed to cover the electrical energy consumption of data centres throughout the world. The paper also showed that, the electrical consumption in Western Europe in 2007 was 56 TWh/Year, while in 2020 electrical consumption is estimated to increase to 104 TWh/Year which is equivalent to the energy consumption of more than 30 million UK households [31]. It is also estimated that this increase will be due to a significant growth in power consumed by data centres requiring advancements in their cooling facilities.

The 2011 Data Centre Industry Census [32] showed that the growth of power consumption in data centre was raised by 6.7% in 12 months in the UK. By 2020, it is expected, that the IT carbon footprint globally will increase by 50%, while in the current situation IT accounts for 2% of the carbon emissions [33].

2.4 Cooling Uses Energy

The data centres are considered as huge devices that consume a lot of electrical power and in turn produce heat. The data centres have to be attached with a cooling unit to get rid of this heat, before damaging the components by overheating, which in turn requires more electrical power. The cooling units also have to be cooled, thus requiring more energy. Therefore, operation costs of data centres are greater than the construction costs which are considered proportional to the amount of power delivered and the amount of heat removed [34].

As demonstrated in Figure 2.3, the global electricity consumption of data centres further doubled from 2000 to 2005. From the IT load about 80% was due to the electricity consumed by the servers, while 10% was owing to the data centre’s network communications and 10% for the storage equipment. Power distribution and cooling of data centres consume nearly half of the total energy used by data centres, although in recent years the effectiveness of the cooling systems has improved.

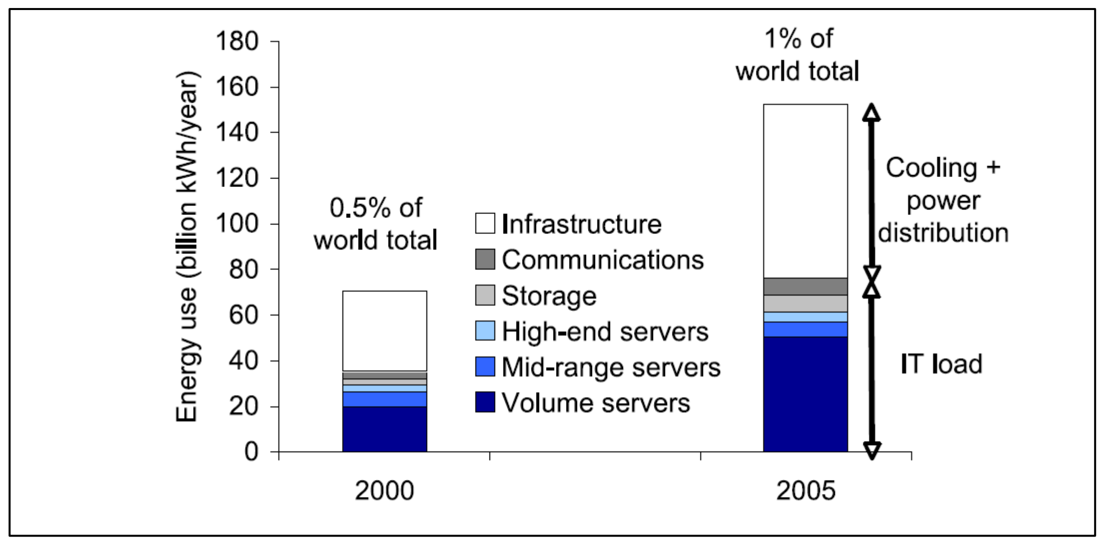

Figure 2.3: Energy use of worldwide data centres in 2000 and 2005 [35]

Figure 2.4 shows the statistic from a study conducted by Rasmussen [36] for the Lawrence Berkley National Laboratories and APC Corp. In this study the power consumption of the data centres was broken down according to the usage. This showed that more than one third of the total consumption was due to the cooling load. Thus the energy efficiency of the data centre can be improved by the reduction in the cooling loads.

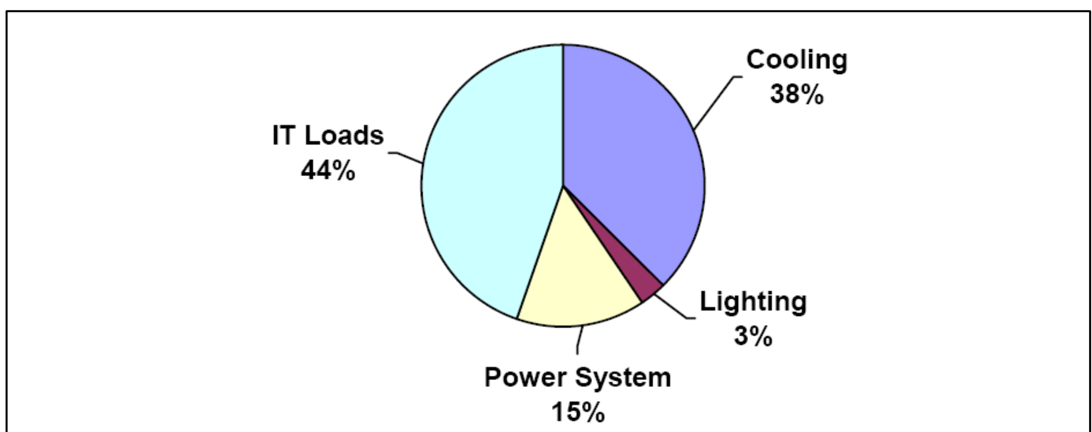

Figure 2.4: Electricity consumption of the data centre [36]

2.5 The power usage effectiveness (PUE)

The effectiveness of the IT supporting infrastructure of a data centre can be determined by the power usage effectiveness (PUE). The PUE is the ratio between the entire data centre power to the power consumed by the IT equipment. The lowest PUE that a data centre can achieve is 1 [37]. The closer the PUE to 1, the better the data centre energy infrastructure effectiveness. The equation that is used to calculate the PUE can be expressed as following [38, 39],

$$PUE = \frac{Total\ Power}{IT\ Power}$$

PUE measures for data centres can be measured in different ways to account for the changing seasons and therefore varying cooling requirements. Therefore sometimes PUE is reported as an annualized value, which is the total energy consumption of whole data centre in one year divided by total energy consumed by the IT in one year [40]. Usually the data centre is associated with other buildings so it sometimes not clears what needs to be taken in account to calculate the data centre total power and IT load. Avelar [41] provided a standard method to measure the power that is required to determine the data centre PUE. The main points that the standard highlighted to find the PUE are:

- The standard classifies the data subsystem under three categories, which are IT load, Physical infrastructure and not included.

- Use the approximation assumption in case of the subsystem is difficult to measure or the subsystem is connected with non-data centre load.
- Estimation of power consummation of devices complex to measure such as power distribution unit (PDU). The IT load may excess 10% due to the PDUs losses which affect the value of PUE. However, most of data centre workers ignore the PDUs excess due to measurements difficulties.

2.6 Methods of Cooling

In the past the energy costs were insignificant for the data centre organizations. This was due to the low rack densities with low energy costs and lower demand of past years. The organizations therefore, did not hesitate to oversize the hardware in order to avoid the risk of shortage of capacity storage and downtime.

But now this is not the case, as oversizing and over specification practices will cost an organization in excess and will both waste energy and increase the carbon footprint. The reduction of the energy consumption such as, the cooling energy was the best solution. At the heat source level there are two heat transfer media, air and liquid.

2.7 Air Cooling

In a typical data centre there are a number of racks, data storage and networking equipment that are vertically aligned. Computer room air conditioners (CRACs) at the perimeters of the data centre are used to cool the data centre equipment [21].

A self-contained air cooling system is created in the CRAC, in which the air is circulated within the data centre space as shown in the Figure 2.5. The heat is removed through a chilled water loop. The pump delivers the chilled water to the CRAC units from the chillers located outside the facility. The chilled water is delivered to the CRAC units. The air is passed over the heat exchanger coil (fin and a tube) by the blower in the CRAC unit. This air is then passed into the data centre. Some of the CRAC units have a fan that works at variable speeds to vary the temperature, but others have the fan working at a fixed speed and the air temperature is varied through the variation in the chilled water value. This supply temperature is varied according to the temperature of the returning air, which is detected by the sensors on the CRAC return. The CRAC systems may be designed as a ‘downflow’ or the ‘upflow’ system according to the cooling scheme of the space. The upflow system is designed for an office or a telecommunication equipment facility. It produces cool air through the ducts that are passed through the room to the supply diffusers placed on the ceilings. The air is circulated through the racks, which removes the heat from the electronic equipment inside the server. The heated air is returned back to the CRAC units through the front or the sides of the unit.

Data centres prefer to use downflows instead of the upflow system in the CRAC units which, sends the air through into the plenum. This system is known as the raised floor plenum data centre [42].

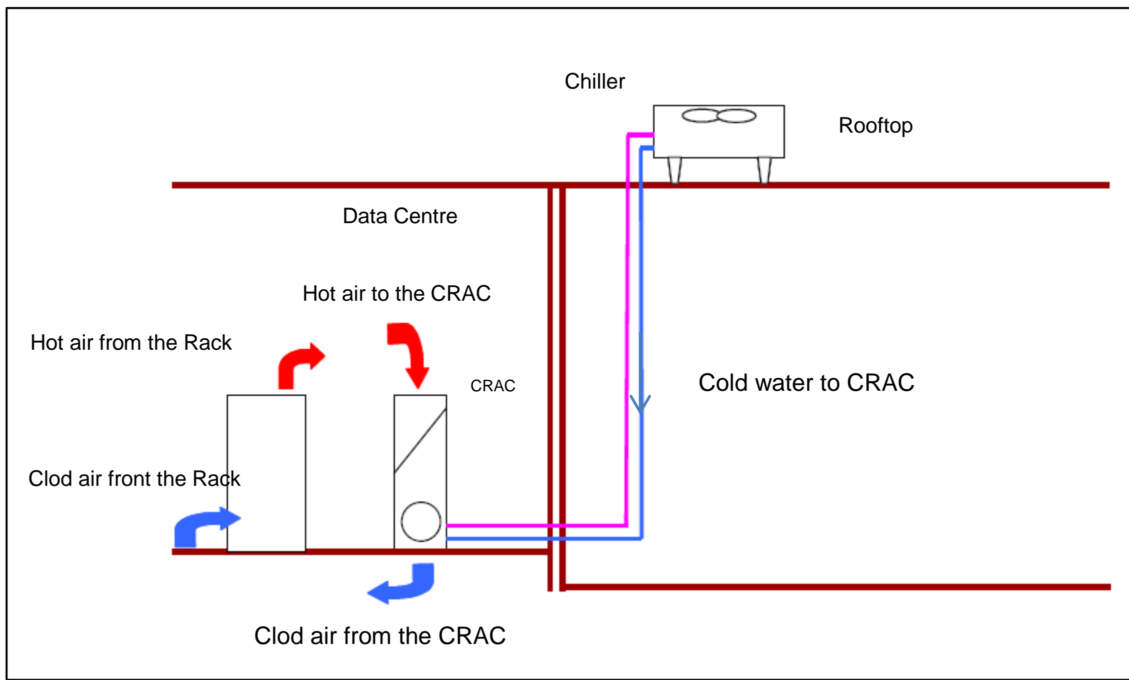

Figure 2.5: Standard air cooling [43]

The rack carries many electronic enclosures which act as heat sources so the air recirculation in and around the rack as shown in the Figure 2.6 is important in order to improve the cooling performance. There are two guiding principles that should be considered to improve the data centre airflow [36]:

1. There should be no obstructions that block the airflow.

2. There should be no mixing between supply cold air and return hot air.

In the subsequent sections, some common solutions will be discussed that are used on a routine basis to solve the above problems.

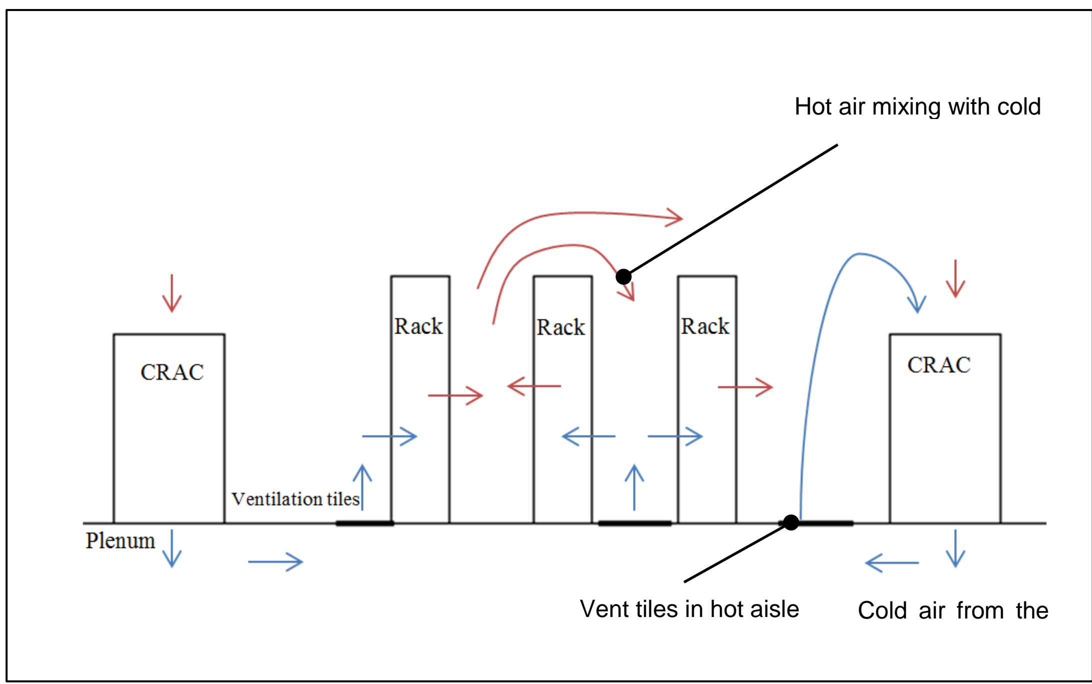

Figure 2.6: The airflow recalculation in data centre [44]

2.7.1 Hot Aisle and Cold Aisle Layout

As shown in the Figure 2.7, the cold aisle and the hot aisle concept is used to separate the cold air supply from the hot air return, which could result in the reduced the work required from the CRAC [28].

The cold air is blown into the plenum by the CRAC (Computer Room Air Conditioning) system. The cold air is passed through the tiles from the plenum. The tiles are placed in front of the racks, which is in the cold aisle. The cold air then passes through the racks and is heated by the server and after that and the air inside the hot aisle is returned to the CRAC. The air is cooled again by the CRAC by using the cold coils placed inside the CRAC. Thus the mixing of the cold and the hot air is reduced, increasing the efficiency [34].

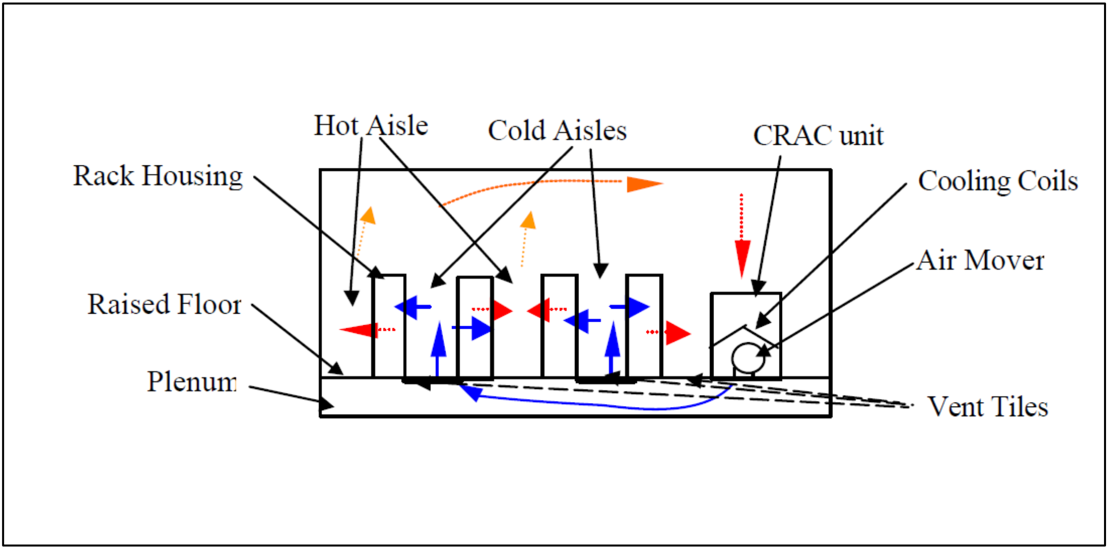

Figure 2.7: Hot aisles cold aisle layout [45].

Wang [46], has described and tested other layouts. These methods are applied to control the data centre layout with respect to the racks and CRACs without changing infrastructures. These methods have been used to improve the air delivery from CRACs to racks without mixing the hot and cold air stream hot and cold aisles layouts could be implemented to optimise the data centre cooling efficiency.

2.7.2 Aisle Containment

Aisle containment is an effective form of airflow management that leads to the optimum use of the cold air. There are two types of air containment used in data centres:

1. Hot aisle containment.
2. Cold aisle containment.

These two systems provide a cooling technique that can be adjusted to higher temperatures in order to save energy. These systems can also supply

heavy loads under safe operating temperatures. It reduces humidification and dehumidification costs. This allows appropriate size adjustments and helps in increasing efficiencies [47].

In cold aisle containment system, the entire room will be used as the hot air return plenum, while the cold air will be sent through the raised floor plenum to the cold aisles. The cold aisle is enclosed by the cold aisle containment which treats the entire data centre as a large hot air return plenum. When the cold aisles are contained, this result in the separation of the cold and the hot streams within the data centre and reduces the mixing between the cold and hot air. Figure 2.9 shows cold arrangement and the temperature improvement compare the slandered air configuration as shown in Figure 2.8.

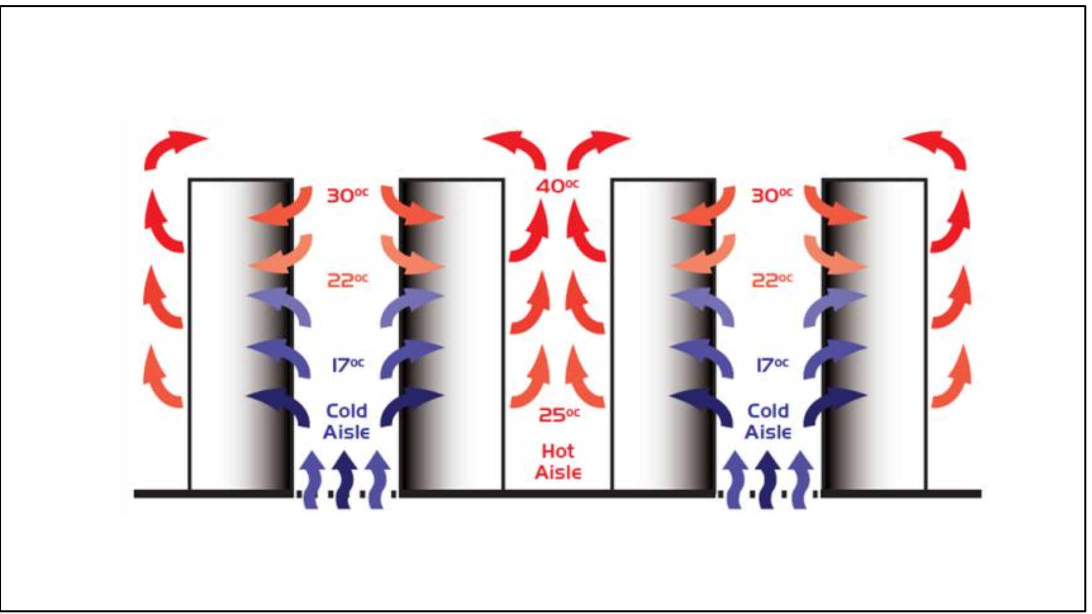

Figure 2.8: Standard Aisle Configuration [48]

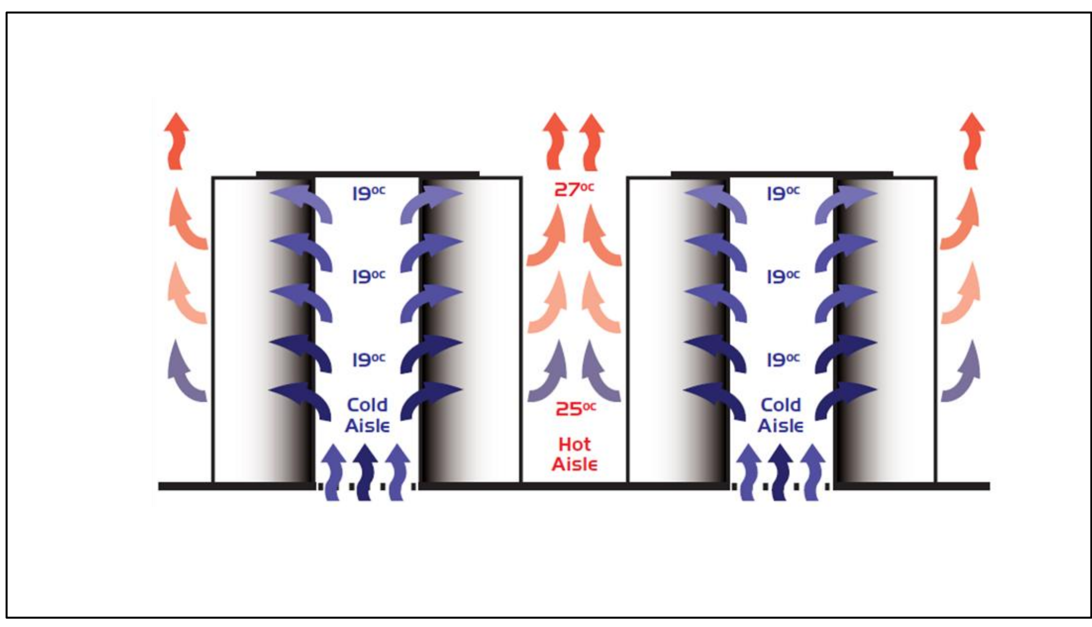

Figure 2.9: Cold Aisle Containment [48].

The hot aisle is enclosed by the hot air containment system, which collects the IT equipment's hot exhaust air and then cools it to make it available for the air to be taken in by the system as shown in Figure 2.10. The hot air containment system increases the efficiency by creating a self-contained system that is able to support high IT loads. The efficiency of the system is increased when the higher temperature air is returned to the computer room air conditioners (CRACs). The air is properly distributed throughout the system, when the air streams of supply and return are properly separated.

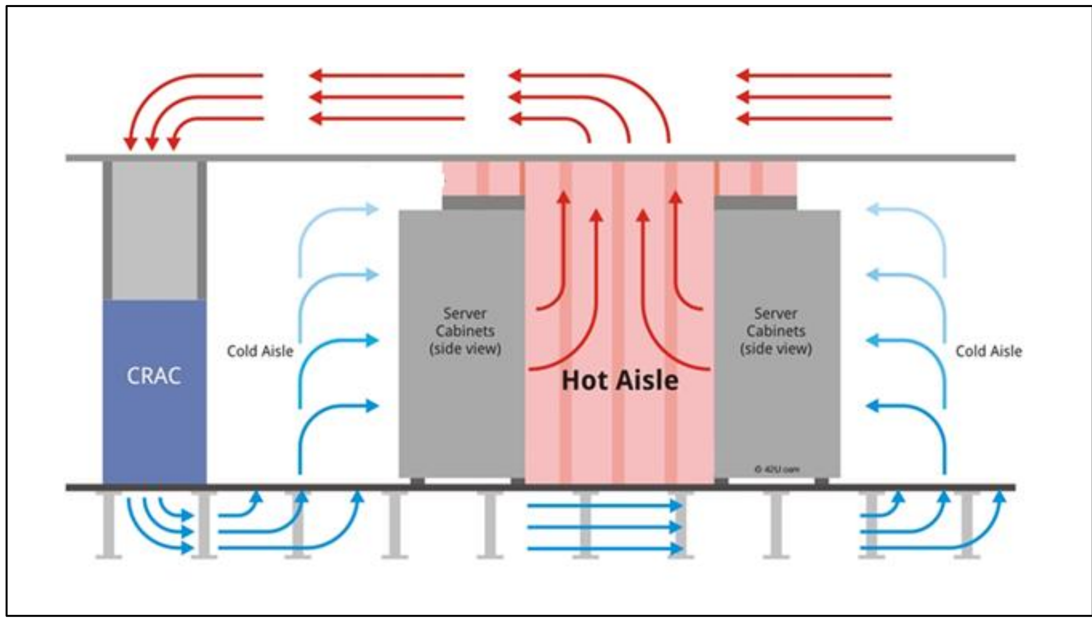

Figure 2.10: Hot Aisle Containment [49]

2.7.3 Blanking Panels

The rack provides a very critical function apart from just being a mechanical support, as it prevents the hot air exhaust to circulate in front of the rack. The hot air is pressurized to force it through servers, therefore if there is a path for it to combine with the suction at the equipment intake, it will flow back into the intake equipment causing a flow back. The length of the circulated air is greatly reduced by the rack, which acts as a natural barrier. This automatically minimizes the intake of hot air into the equipment. Figure 2.11 shows this process.

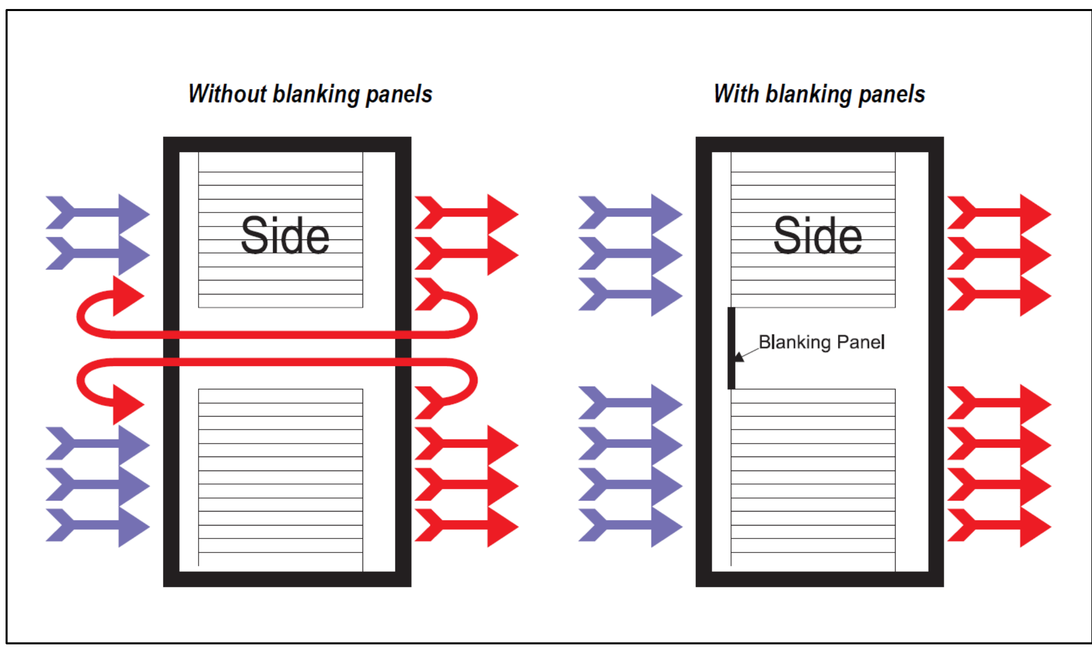

Figure 2.11: Air flow with and without blanking panels [50].

In spite of suggestions by major IT equipment manufacturers to include the blanking panels in the system, it is frequently observed that 90% of the data centres do not have the blanking panels in their systems. This leads to a rise in temperature by 8°C of the IT equipment [50].

The blanking panels can be easily installed in all the data centres at a very low cost and are beneficial as they are able to modify the rack air inflow.

2.7.4 Plenum

Data centres having raised floors have the subfloors acting as the plenum or the duct. This provides a path for the cool air to pass from the CRACs to the vented floors which are positioned at the front of the racks. The subfloors are useful as they can also act as means to carry the services such as, network cables, cooling pipes and power. In some subfloors there is fire detection or water systems [51].

The energy requirement for the system may increase owing to the hindrances in the paths of the airflows. These obstructions can be created in the plenum through the cabling and other structures in the path of the airflow. These obstructions create turbulence in the airflow thus increasing the flow resistance. These issues can be reduced with the incorporation of the overhead cabling trays for networking. Care should be taken to incorporate spaces between the floors through properly arranging cables when placing them in the floor [52].

2.7.5 Vents Location

If the floor vents are not properly positioned, then the cooled air can get mixed with the hot air. The benefits of the hot aisle and the cold aisle system can be destroyed by the poor location of the delivery or return vents. The best positions for the air delivery vents are near the equipment intakes, which therefore restricts the cool air in the cold aisle as much as possible. The vented tiles, in the subfloor or overhead air distribution, should be placed in the cold aisle only. Any vents near to not working rack should be closed because they can become of source returning air to the CRAC. This

returning air decreases the temperature and increase the dehumidification which reduce the CRAC performance[52].

As indicated in Figure 2.12, the floor vents that are positioned too near the CRAC units, will eventually begin to produce a negative pressure. That is the air will be drawn back from the room to underneath the floor. The vent tile location can be determined through the use of a simple air velocity measuring device that will assure an appropriate static pressure [51].

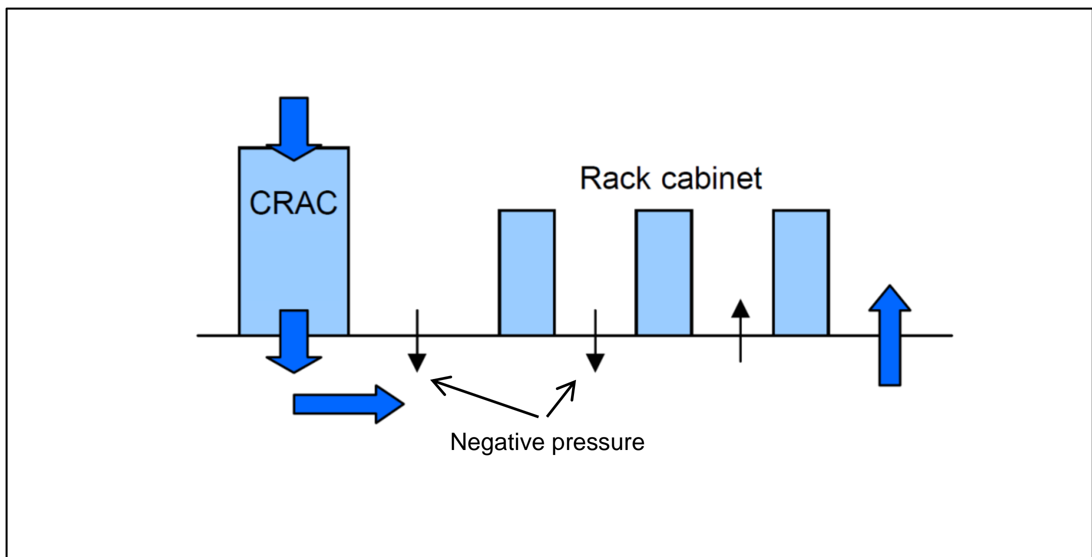

Figure 2.12: Floor vents location [51].

2.7.6 Environmental requirement of air cooling method

The temperature and humidity are required to be in proper level to keep the data centre in good working condition. The suitable inlet temperature according to ASHAEY TC 9.9 standards is between 15 and 25 °C and the humidity is accepted in the range between 40% and 60%. The IT equipment of data centre could be damages if it works in poor environmental conditions [53]. Psychometric chart in Figure 2.13 shows the recommended operating condition zone of data centre. The dry bulb temperature for recommended envelop is between 18 and 27 °C. The allowance operating condition envelops are A1, A2, A3 and A4. Each envelop has a limit of temperature and humidity. However, All the envelopes envelop can be used for a data centre [54].

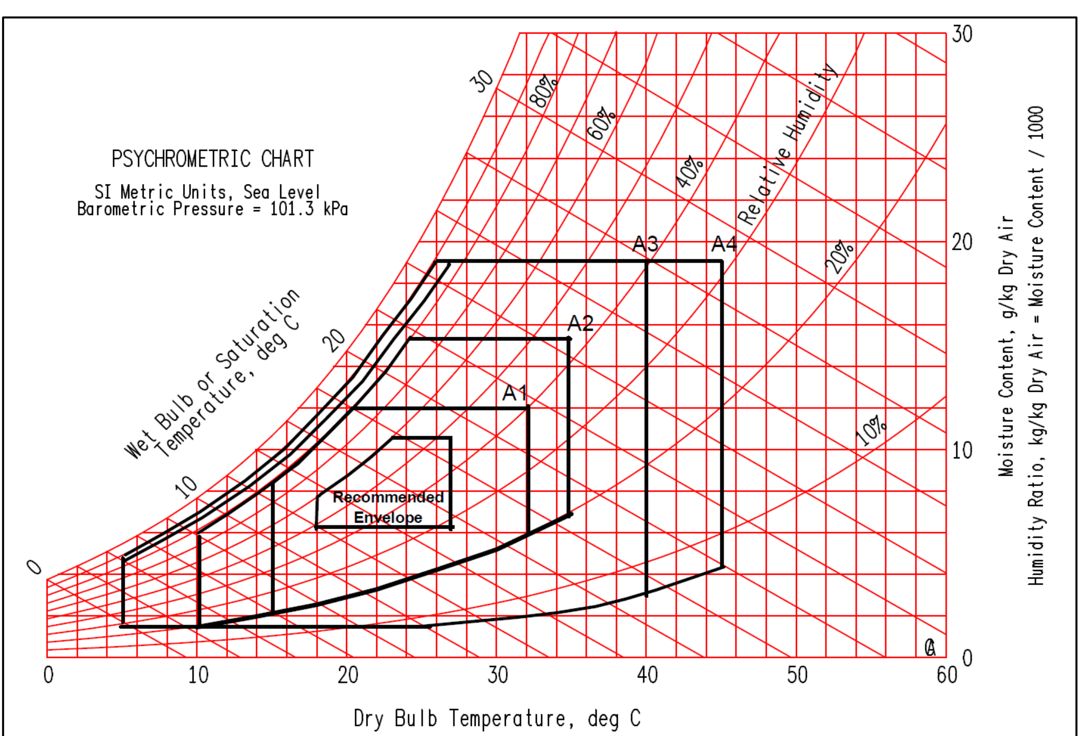

Figure 2.13: Environmental condition by ASRAE for the data centre.

One of the main environmental requirement for using the air as cooling medium is keeping the humidity of air at proper level. High humidity in air for cooling data centre could cause electrical discharge, however low humidity in the air could potentially provide a static electricity. Therefore, in case of low humidity, humidifier should use to increase the humidity in the air. In another case the dehumidification can by use to reduce the humidity in the air. Humidification and dehumidification cost money, so both humidification and dehumidification should be used only when it necessary [55].

2.8 Liquid Cooling

Using liquid for cooling processors is not new [56, 57]. Figure 2.14 shows that from 1960, computing systems using bipolar processor technology adopted water cooling as the heat flux per unit area increased. However, in 1995, with the introduction of CMOS (complementary metal-oxide semiconductor) processor technology, the heat fluxes from processors dropped dramatically and therefore air cooling became the dominant cooling approach. As seen in Figure 2.14, heat fluxes have again increased, which has brought back the requirement of liquid cooling.

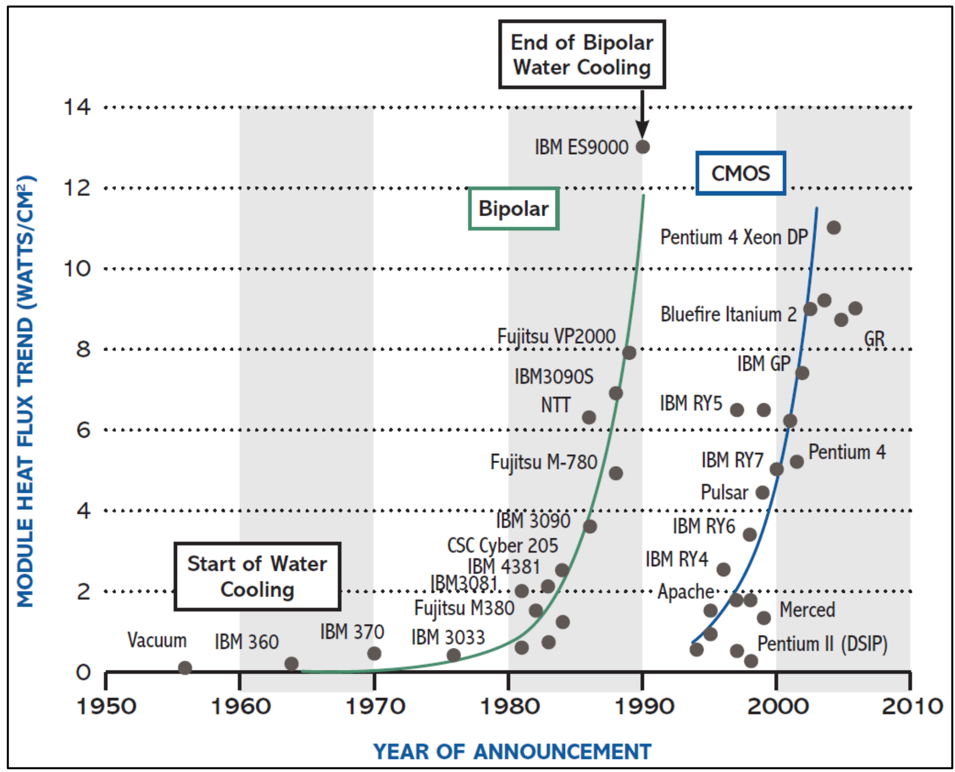

Figure 2.14: Heat flux and processors technologies [58]

Numerous methods are applied that use liquid cooling for the data centre equipment. This is because liquid cooling systems have the capacity of handling higher heat densities and still maintains its efficiency as compared to the air cooling system. For example, water cooling system can conduct about 3,500 more heat per unit volume compared to the system using air [28]. Thus the data centre benefits from this system by transferring the waste heat from the racks to the cooling loops placed as close to the heat source as possible. It has the ability to handle high temperatures.

In one condition, remove the heat by installing the cooling coils directly onto the racks. The coolant lines are run under the floor. These lines are connected to the rack coil via a flexible hose as shown in Figure 2.15.

Besides this method, there are many others available, which range from cooling the heat sink using water to submersion in a dielectric fluid.

2.8.1 Rack Back Door Heat Exchanger

In The Rack back door heat exchanger the distribution unit supply the cold water to the heat exchanger which attached to the back of the rack. The heat exchanger is able to remove about 40% to 90% of the heat from the air under typical conditions [59]. The air that exits from the rack is therefore much cooler. This reduces the adverse effects of the recirculation air. In addition, the heat exchanger placed at the rear door means that the cooler air that comes out of the racks will result in the reduction of the heat load in the CRAC units. Therefore the number of the CRAC units can be reduced, which will cut down on the energy required for the cooling of the servers. Sometimes only part of the heat is removed by the rack back door heat exchanger, thus decreasing the load on the room’s CRACs. Other systems are able to completely displace the heat and therefore are able to replace the CRAC systems completely [60].

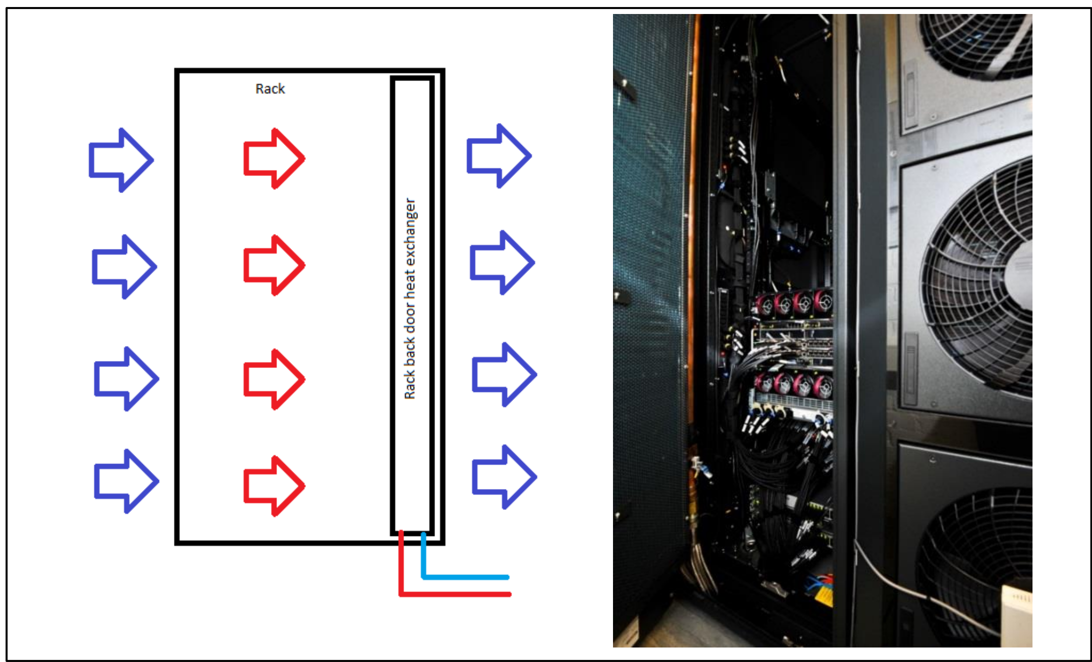

Figure 2.15: Rack back door heat exchanger

Three dimensional CFD analysis for the data centre was done by Almoli et al [59] to compare between active and passive back heat exchangers. It is shown that the active back door heat exchanger is better with respect to the exhaust air from the rack. This is due to bigger fans that are attached to the rear of the active back door heat exchanger, see the photograph in Figure 2.15. Both strategies (passive and active back door heat exchangers) are used to overcome the recirculation problem in the cold-hot aisle arrangement. Passive and active back door heat exchangers can remove 91% and 93% of the heat respectively.

According to a study by Udakeri [61], is used a CFD commercial code which is fluent to compare between the hybrid cooling solution of the overhead supply and the underflow supply system that focuses on the rack inlet temperatures. The system is the hybrid cooling system of the air cooling with the rack back door heat exchanger. The study shows that the hot air

circulating and a large amount of the heat can be reduced by the use of back door heat exchanger Also it will reduce the air temperature from the back of the rack in both the overhead and the underflow supply systems.

The disadvantage of the rack back door heat exchanger that is the system requires chilled water that needs to be brought back to the rack. This increases the cost owing to the chiller's power consumption and additional cost of plumbing. In addition there is a risk of a water leakage on the data centre floor [34]. However, the "free cooling" could be used on the chillers to save the power by using the fresh outside air as shown in Figure 2.16. The restriction with this method is that it can only be implemented to the cold weather countries with suitable humidity and throughout part of the year [62]. Figure 2.16 shows that total free cooling can be achieved when the temperature of the weather outside is less or same as the chiller temperature. In (b) the dry cooler can help to reduce the inlet temperature for the chiller which reduces the chiller power in some parts of the year. In summer or when the weather is hot the free cooling cannot be used as shown in (c).

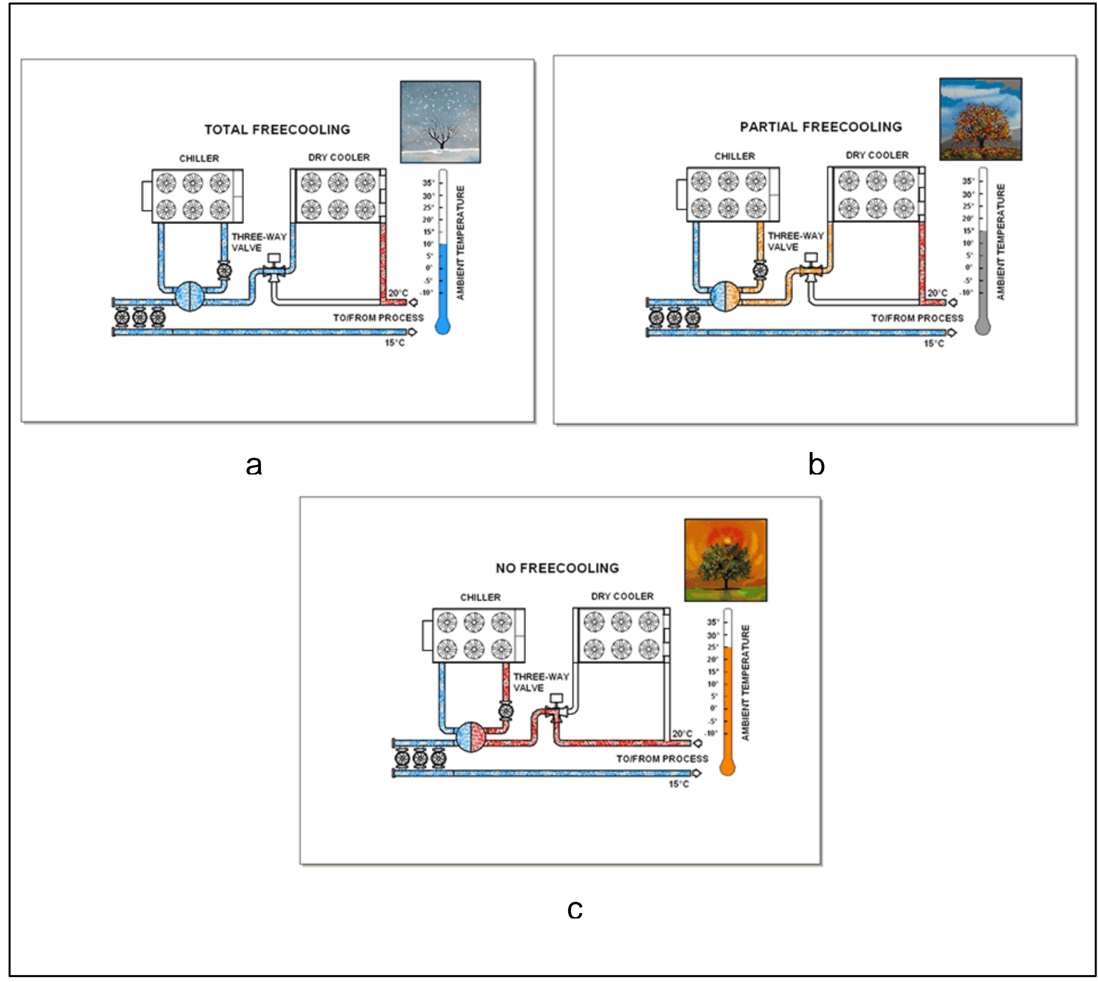

Figure 2.16: Free cooling a: Total Free cooling in winter, b: Partial Free cooling in spring, c: No Free cooling in summer [63]

2.8.2 Indirect contact with cold plate approaches

There is an increased amount of energy dissipated owing to developments of the semiconductor industry and the increased operation speed. Increasing in power dissipation and reduction of the semiconductor size lead to increase of power density as shown in Figure 2.17 .Due to the presence of heat transfer limits, the conventional air cooling techniques will be not sufficient to cool the expected heat flux [64]. Consequently, bringing the liquid close to the heat source would be a good cooling method to handle the high heat flux.

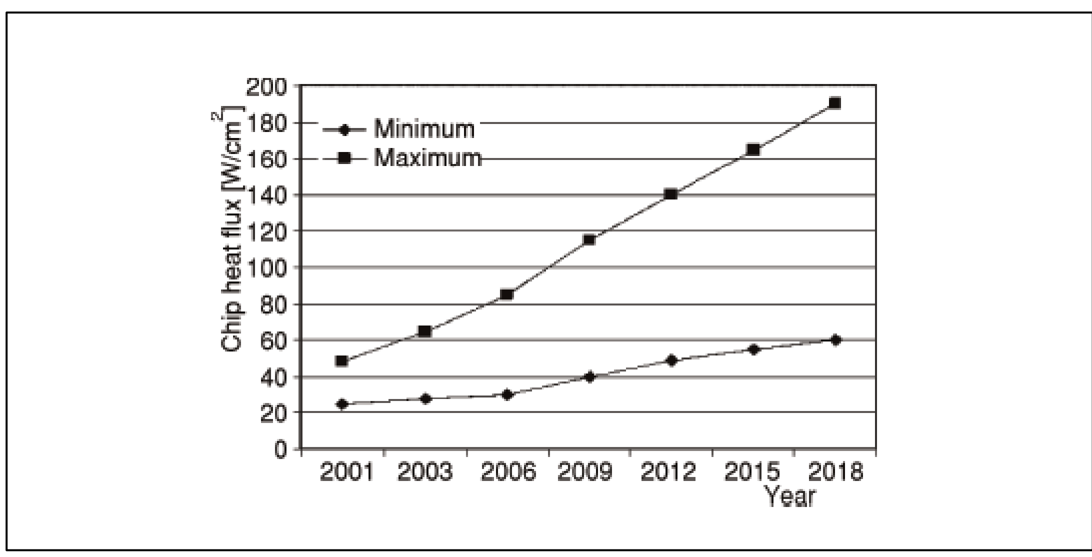

Figure 2.17: Growth of chip heat flux densities [65]

Indirect liquid cooling has been used in the past to dissipate the high heat from the chip. Generally, this can be approached by placing high thermal conductive metal (cold plate) such as Aluminum and copper on the chip as shown in Figure 2.18. The liquid pass thought the cold plate in order to cool the cold plate. The water is the common choice to use as liquid cooling in cold plate because it has good thermal conductivity. It is easily sourced and low cost compared to other liquid cooling [66].

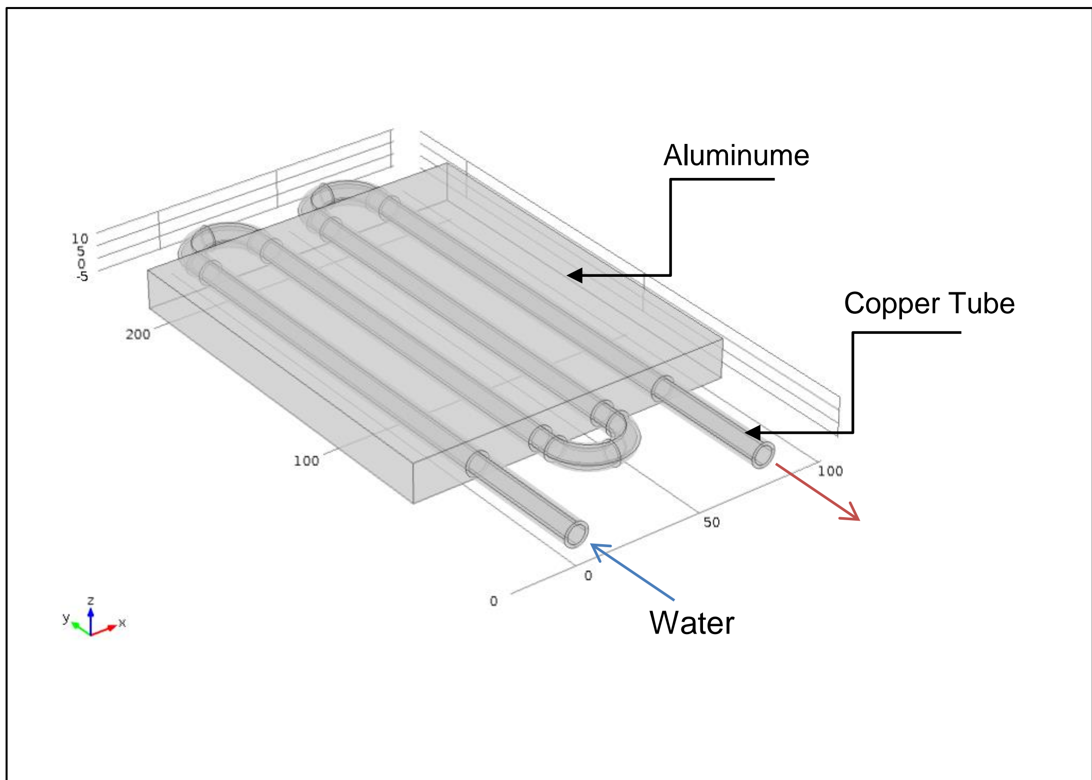

Figure 2.18: Cold plate

The performance of the liquid cooling system using cold plate was tested with the IBM power series server x3350 [67]. The liquid cooling system was assembled by incorporating the cold plate assembly, pump and flow direction, as shown in the Figure 2.19. From the inlet port the water was first sucked, which passed through the cold plate and then entered the impeller. Then the centrifugal force directs the water to the outlet port.

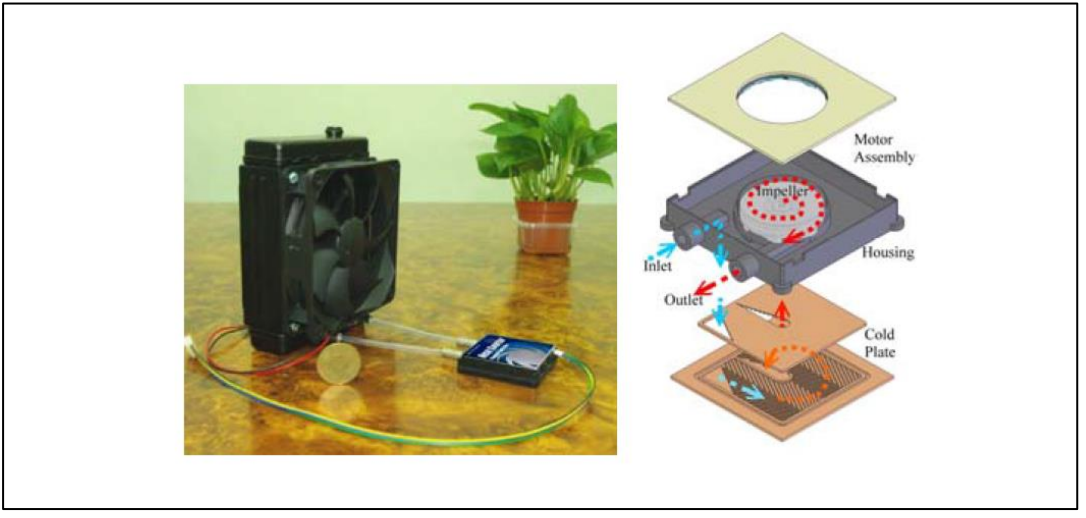

Figure 2.19: Liquid system diagram

There were 3 types of fin array and fan combination used for the heat sink of the liquid cooling system. The LC-1212, LC-0808 and the LC-0416 are shown in Figure 2.20, while the fin array of IBM original cooling system is shown in Figure 2.21.

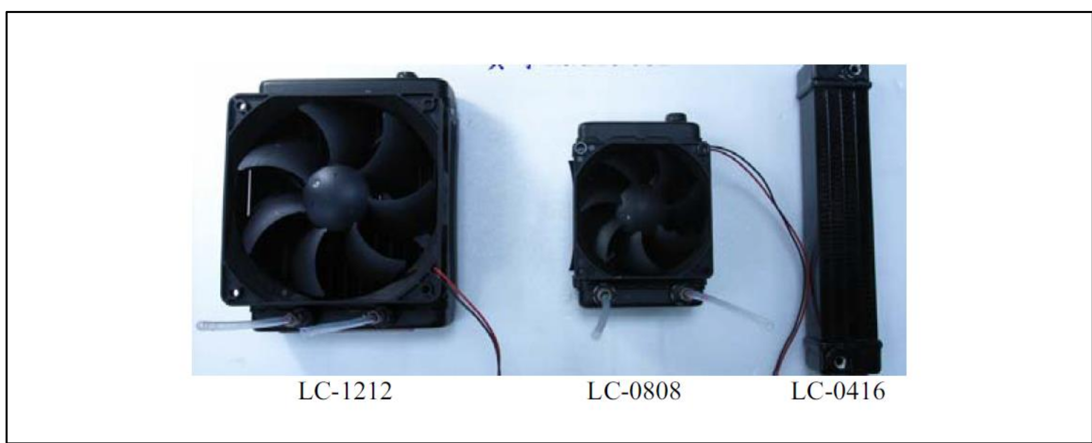

Figure 2.20: Types of fan

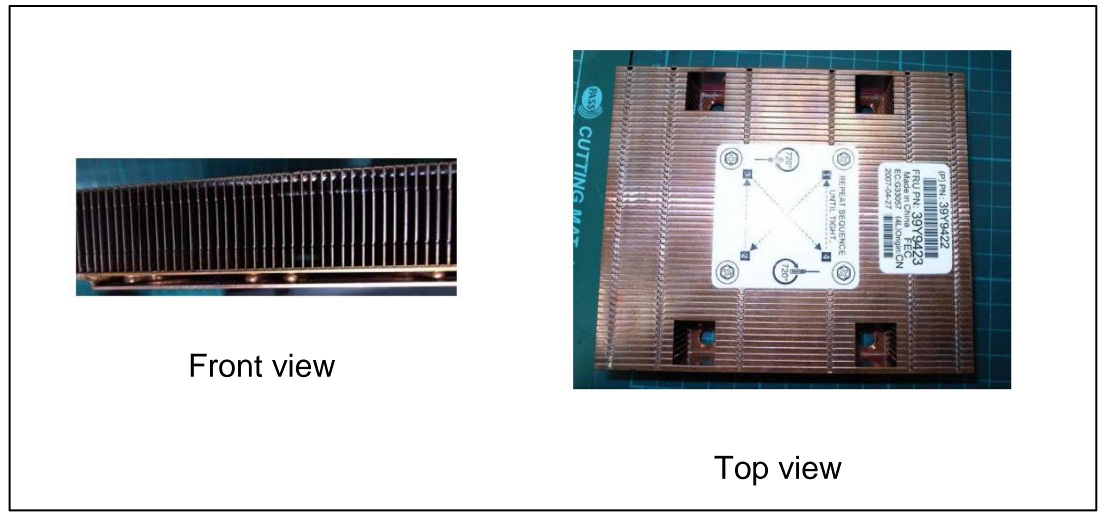

Figure 2.21: Fin array of IBM original cooling system

The Figure 2.22 shows the schematic diagram of the liquid cooling system arrangement, in which the cold plate was incorporated instead of the IBM fin array. While the cooling tests were being conducted, the power of three of four hot swaps was not connected during the liquid cooling tests. Among these, only one hot swap fans was to remain operational for cooling of other devices.

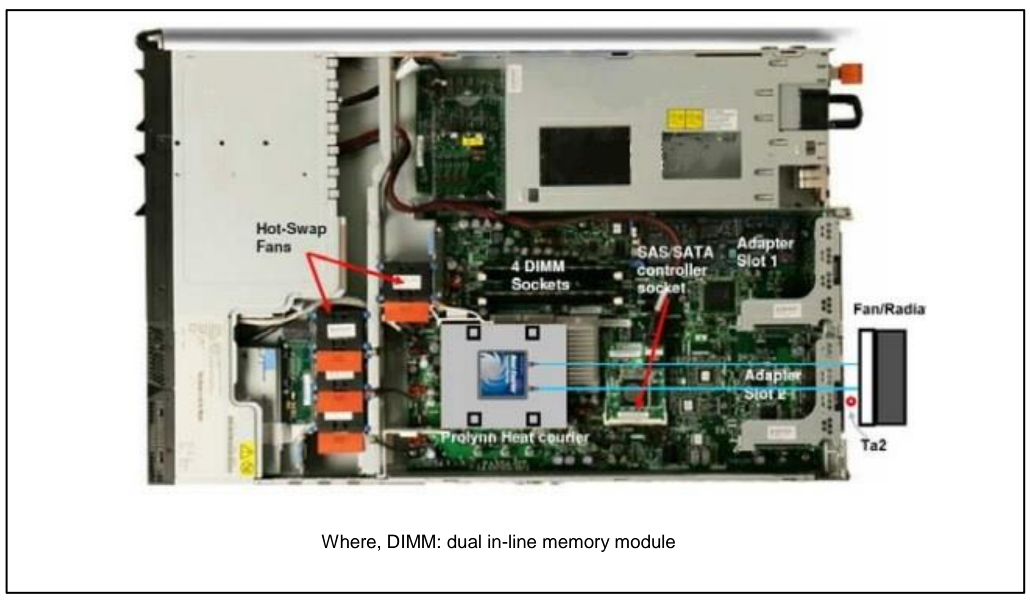

Figure 2.22: The liquid cooling system configuration

The air direct cooling and liquid cooling test results show that 46.5 ^{o}C is the difference between the air temperature to maximum CPU core temperature for IBM's original direct air cooling (with the CPU running at 100% loading). But for the liquid cooling, with the heat sink fan speed of 2200rpm, the temperature was 24.8 ^{o}C. The noise level obtained was 59.5 and 49.5 dB respectively. The speed of the heat sink fan of the liquid cooling system was reduced to 1080 rpm. The difference of the temperature between the core and the air temperature was increased to 28.4 ^{o}C, with the noise level minimized to 36.5 dB. The power consumed by the liquid cooling system was 7 W while the direct air cooling power was 37 W. These statistics showed the benefit of the liquid cooling system, since the cooling performance was high with the decreased noise and decreased power usage as compared to the direct air cooling system.

2.8.3 Direct contact with immersion

The idea of immersed cooling technique is to immerse server which has the electronic components in dielectric liquid. Where, the dielectric liquid is liquid contact direct to electronics to cool them without electrical discharge. The immersion cooling is a useful method that provides an inert environment which able to keep high dense electronic enclosure with uniform temperature. In addition, there is no fan required for immersed cooling like the traditional data centre cooling technique. So, the noise will be less. One of the best advantages of using immersed cooling technique is elimination of CRAC, Chiller and raised floor which can reduce the data centre infrastructure by 50% [68]. Table 2.1 list a comparison of infrastructure requirements of air cooling verses immersion. This technique

has been used for more than 50 years ago relying on dielectric liquid which are effective for cooling high value electronics [69].

Table 2.1: Immersed cooling verses the air cooling

	Air Cooling	Immersion
CRAC	Required	No
Chiller	Required	No
Hot/Cold Aisle	Required	No
Raised Floor	Required	No
Pipework	Required	Required

The Figure 2.23 demonstrates a concept based on the fact that the electronics can be cooled by immersion in semi open baths. When saying 'semi', one is referring to the idea of the bath being closed when access is not required. They can operate at atmospheric pressures.

In this arrangement, the server or the node plugs were attached to the backplane in the tank's bottom, as opposed to the bottom of the rack. This is half filled with the volatile dielectric fluid. The tower water or the water that is being used for the comfort heating is ideally used to cool the vapour condenser. If desired, the water is avoided, as the vapour flows passively through an outdoor natural draft cooling tower to give its heat passively to the outdoor air.

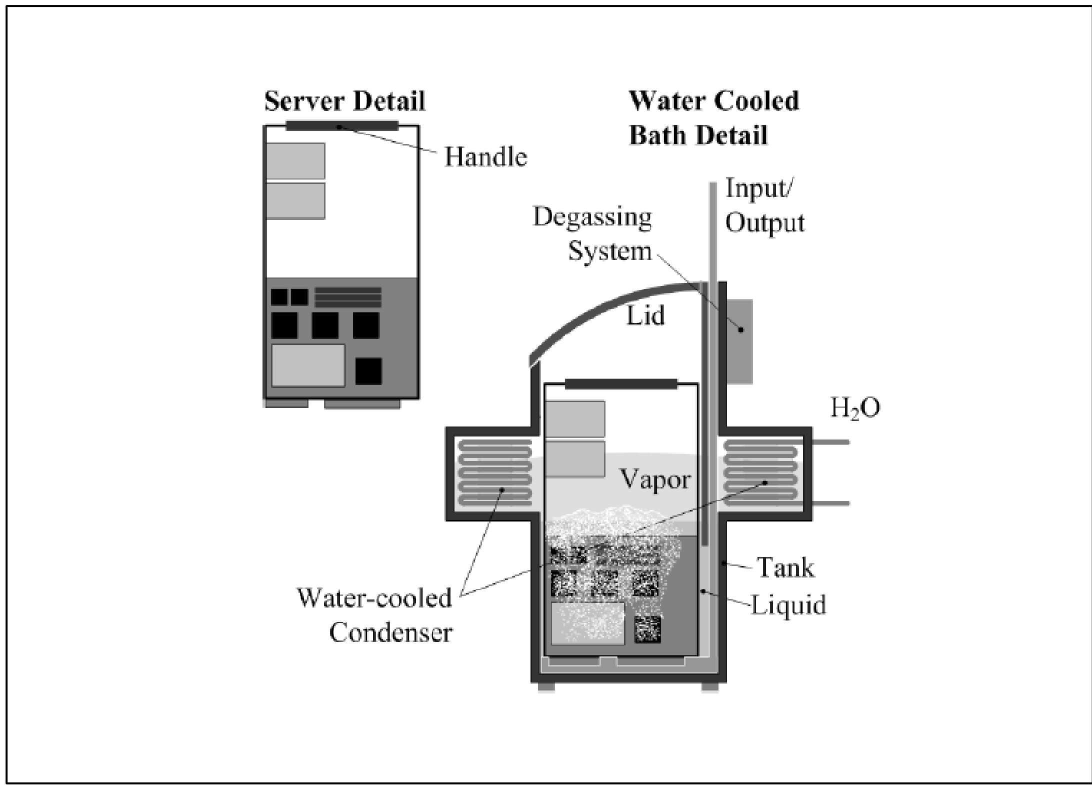

Figure 2.23: Data centre immersion concept [70]

The power needed for the cooling by the liquids is less compared to the traditional systems. The construction of facilities can be made considerably convenient through the reduction of floor space requirements, negating the requirement for an air conditioning infrastructure such as the plenum. In addition the cost can also be controlled when there will be no need for elevated ceilings, etc.

The commonly used liquid technologies are complicated system of cold plates, pumps, plumbing and valves that are required. These systems need engineering supervision and in addition are prone to mechanical failures. The consumption of natural resources is also an issue.

The advantages of the immersion cooling method in Figure 2.23, as the following:

- The design is simplified and the environmental effects are reduced by the elimination of the node level and the rack level liquid cooling hardware.
- All the devices are maintained at the same temperature.

Icoetope [71] is UK Company working on developing immersed cooling technologies, where the electronics are immersed in liquid which is (Hydrofluoroether) HFE 7300. The basic concept is to immerse the server in sealed enclosure as shown in Figure 2.24. Part (a) in the Figure 2.24 shows the cross section of Icoetope server and part (b) presents the server configuration in the rack. The heat transfers from the IT equipment, which convects the heat from the electronics inside the server and is cooled by the water heat exchanger on the opposite side. The second heat exchanger takes the heat from the server to the third heat exchanger in the rack. Then, the output warm water from the third heat exchanger can be used for heating other purposes such as rooms or water. The icoetope required just 80 watt to dissipate the heat from 20 Kilowatts [68].

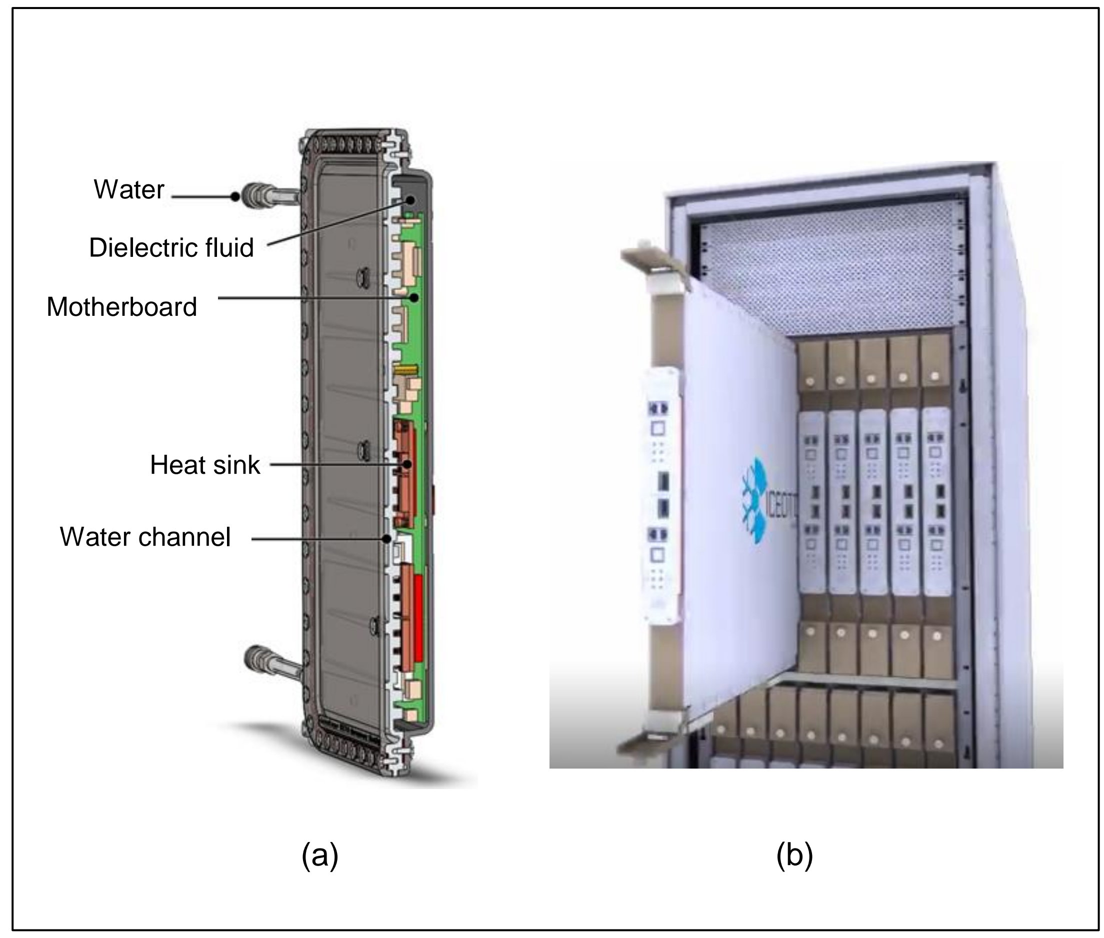

Figure 2.24: Cross section Iceotope cooling module [72]

2.9 Summary

The data centre is a huge warehouse that contains racks in rows layout. Each rack has a number of servers that consist of IT equipment. There is an increase in the number of data centres due to the growing demand for digital services. This has led to an increase in data centre power consumption. As of 2008, data centre cooling has a major share (30%) of data centre power consumption. Therefore, a reduction in data centre power consumption can be achieved by more efficient cooling approaches. The main methods of cooling data centres are air and liquid cooling methods. In case of data centre use the air cooling technique there some aspects needs

to be considered to improve the data centre air cooling method such as hot aisle and cold aisle layout, aisle containment, blanking panels, plenum and vents location. The data centre liquid cooling methods are back door heat exchanger, indirect contact liquid cooling (cold plate) and direct contact liquid cooling (immersed server). The back door heat exchanger method works by attached air water heat exchanger on the back of the rack, the cold water passes through piper and the fan push the air through the pipes to cool the servers inside the rack. The cold plate consists of good thermal conductivity material for substrate that placed on the heat source such as CPU in the server. The water in the cold plate passes via pipe inside the cold plate to dissipate the heat. The last liquid cooling method is immersed server weather the servers immersed in rack, which and be called semi bath, or immersed server in sealed enclosure.

CHAPTER 3:

MATHEMATICAL MODELLING AND SIMULATION OF LIQUID COOLING OF MICROELECTRONICS

3.1 Introduction

This chapter describes the mathematical and Computational Fluid Dynamics (CFD) modelling for models that were solved in the next chapters (4, 5 and 6). An introduction to Computational Fluid Dynamics and process of solving a simulation model is presented in this chapter. The boundary conditions for simulating the immersed server model are described. The fluid behaviour, whether it is laminar or turbulence, used for the immersed server model is explained. The turbulence model that could be implemented to solve the turbulent flow is shown with its equations.

3.2 Introduction of Computational Fluid Dynamics (CFD)

Computational fluid dynamics (CFD) assesses an Engineering system through a computer based simulation, which solves the equations for the fluid flows, heat transfer and the relevant chemical reactions [73].

The CFD is an emerging field that is a combination of fluid mechanics and computer science. Mathematical equations can be formulated to determine the physical characteristics of the fluid motion, commonly in the form of partial differential equations that include the continuity, momentum and energy governing equations. Advanced computer programming languages are used by scientists to convert these mathematical equations into computer software and programmes such as, COMSOL, ANSYS, OpenFOAM.

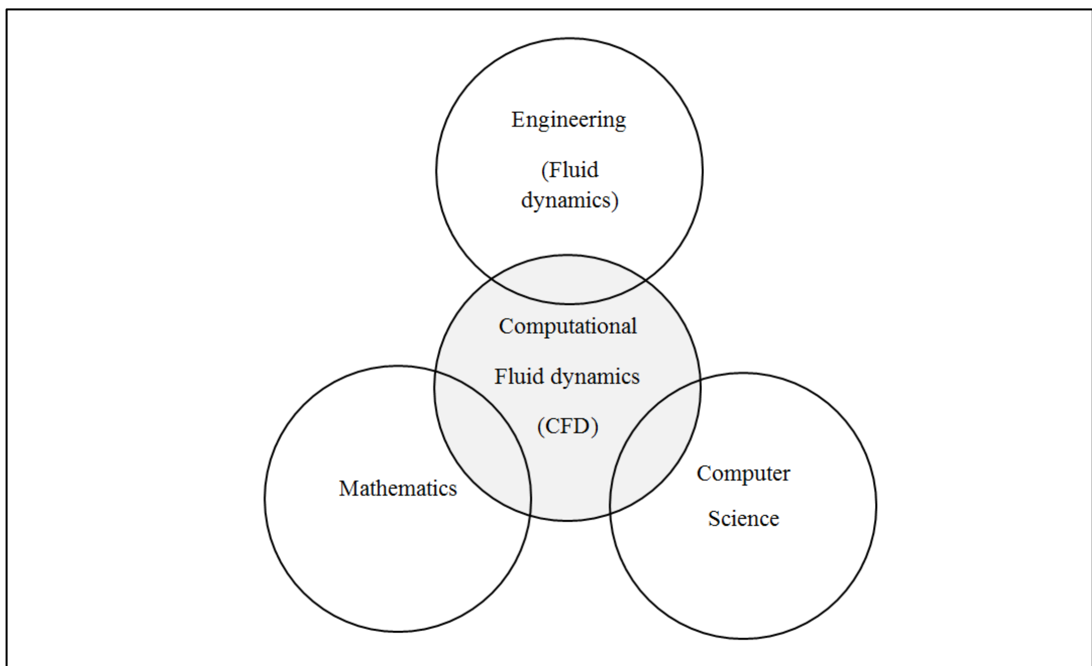

Figure 3.1: CFD combinations [74].

CFD is widely used in engineering, for example environmental engineering, biomedical engineering, aerospace and more recently it has been use for modelling air flow through electronics data centres [74].

There are three major elements, according to Versteeg and Malasakara [73] in the CFD code, these are:

1. A pre-processor.
2. Solver.
3. Post-processor.

Pre-processor is a path to enter the characteristics of a specific liquid flow into the CFD software, which is then transformed into a more suited form for the numerical algorithm (solver). An operator friendly interface is required for the user activities at the pre-processing stage, these include:

1. Geometry definition.
2. Mesh generation.
3. To select the model properties such as the chemical and physical properties.
4. Defined the fluid/physical properties.
5. To specify the adequate boundary conditions for the solution domain.

In terms of the solver, there are three most commonly used ways to formulate a numerical approximation in order to solve a single or a set of partial differential equations governing the fluid motion. These are: finite volume, finite element and the finite differences. They allow the reduction of the continuum problem described by partial differential equations into a discrete algebraic analogue that is valid at all nodes within a solution domain.

For the post-processor step, the CFD software creates a huge amount of data, which when analysed has rendered many benefits from the recent advances in the abilities of the graphical workstation. The visualization software tools now accompany the leading commercial CFD packages aids the user in understanding the fluid flow its associated geometry. These may include:

1. Views of the mesh/ grid display.
2. Vector plots.
3. Surface plots of 2D and 3D.
4. Animations of the flow.
5. Line and shaded counter plots.
6. Colour output.
7. Particle tracking.
8. View manipulation (scaling, rotation, translation, etc.)

3.2.1 Finite element method

The Finite Element Method (FEM) is numerical method which is used to approximate the solution over specific element. Through this element, various properties continuously change by interaction between any two adjacent elements. In general, FEM is good for the problems where the solid domain affects the fluid flow and heat transfer patterns [75].

For any physical phenomena, the governing equations are in the form of partial differential equations PDEs. These forms of equations are not recognised by numerical solution technique. For that, the FEM uses conversion of PDEs to meaningful algebraic form. The algebraic forms of governing equations are discretized over the entire domain.

COMSOL is based on FEM, and apply its techniques for many heat transfer and fluid flow application. For examples, in the cooling of electronic components, there is obvious interaction between the hot surface and the coolant. In addition, it can be used for various phase change problems and cooling of electrical motor [76].

3.3 Data Centre Modelling Using CFD

The CFD can be used for a data centre to predict the fluid flow in different levels such as room level, rack level or chip level. A reliable data simulation will help the designers locate the potentially risky hot spots and lead to adequate solutions for the cooling systems. It will also allow the investigation of the next generation data centre building design.

The design of the new facilities can be validated by accurate data centre fluid flow and heat transfer CFD modelling, for energy efficiency. This is the most cost effective method to reduce energy consumption of data centres.

It was in year 2000 that the results were published for the first time for the data centre airflow modelling. There have been various modelling investigations done with the application of CFD to evaluate the characteristics of the data centre air flow and heat transfer [77].

3.4 Boundary conditions

The boundary conditions are essential part that used in formulating the governing equation. The boundaries conditions are chosen to represent the flow are realistically as possible and have a big influence in the flow [78]. The inlet, outlet, wall and symmetry are explained in next sections.

3.4.1 Inlet and outlet

The water channel in cold plate on top of the immersed server in chapter 6 and 7 has inlet and outlet boundary conditions. In general, the inlet boundary conditions describe the velocity, flow rate, pressure and the temperature. The inlet used in this thesis for the water channel in server cold plate. The water in cold plate is flow in circle cross section channel. The velocity or flow rate at the inlet boundary conditions defined as fully developed flow. The fluid is became a fully developed after a distance from the entrance, which called entrance length (L_{entr}) as shown in Figure 3.2. The laminar profile is reached at great entrance length, so the L_{entr} should be significantly larger than 0.06ReD [79].

$$L_{entr} >>> 0.06ReD$$

Where the D is the inlet diameter and Re is the Reynolds number.

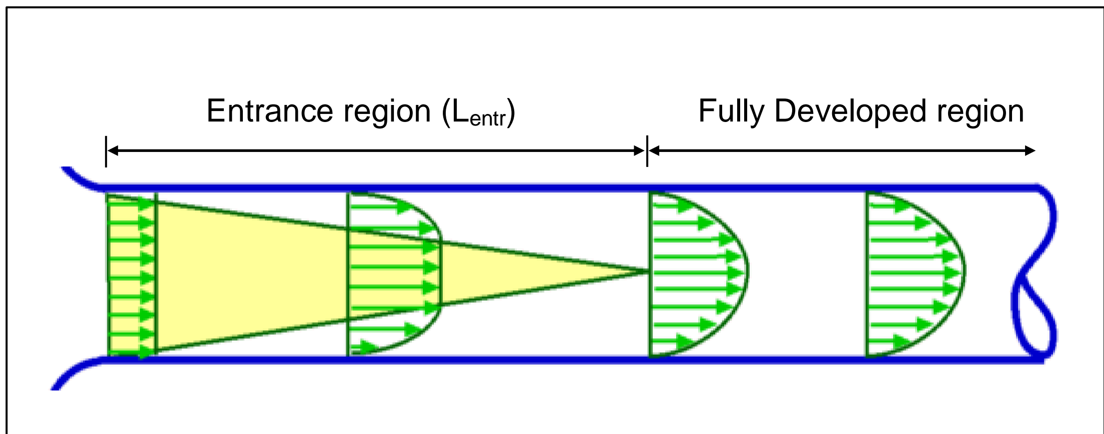

Figure 3.2: the velocity developed layer in pipe [80]

The boundary conditions of the outlet can be defined as pressure or velocity for the fluid flow. The outflow is suitable boundary conditions at outlet boundary for convection heat transfer domain. The equation that used in outflow heat transfer is

$$-\boldsymbol{n}.(-\lambda\nabla T) = 0 \tag{3.1}$$

Where, λ is the fluid thermal conductivity and n is normal vector.

3.4.2 Walls

Walls are the most common boundary in the simulation model. The velocity is zero at stationary walls for no slip condition. However, calculating the velocity near to the wall for turbulent flow is difficult because the chaotic nature of turbulent in small scale. There are two approaches to solve the turbulence flow near to the wall. The first approach is solving all the flow-stream from the wall to fluid. This required boundary layer with high density mesh adjacent the wall. The second approach is called wall function [81] , this approach is based on bridge the gap between the wall and turbulent

flow by employed analytical solution. The wall function starts the computational domain from the wall at distance δ_w as shown in Figure 3.3.

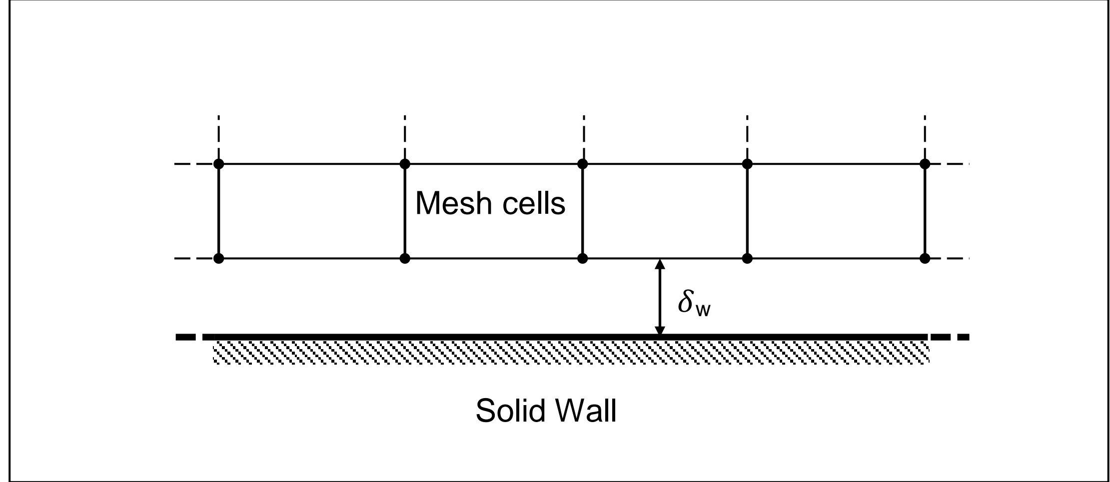

Figure 3.3:The distance between computational domain and the wall $\delta_{w.}$ [82]

The accuracy of the solution is affected by the wall lift off which automatically calculated from [82, 83]

$$\delta_w^+ = \frac{\rho u_\tau \delta_w}{\mu} \tag{3.2}$$

Where, ρ is the fluid density, δ_w is the distance between the wall and the computational domain mesh, μ is the fluid dynamic viscosity and u_τ is the friction velocity and it can be found from [82, 83],

$$u_\tau = C_\mu^{\frac{1}{4}} \sqrt{\kappa} \tag{3.3}$$

Where κ is Karman constant and it is equal to 0.41 for wall lift off. C_μ is an empirical constant which is equal to 0.09.The δ_w^+ is changes along the wall and must be checked to make sure it does not affect the solution accuracy. The value of wall lift off (δ_w^+) is 11.06 ≤ δ_w^+ ≤ 300 and it should be as close as possible to 11.06 for better accuracy [82-84]

3.4.3 Symmetry

The symmetry as boundary condition contains two boundary conditions the first one is heat symmetry and the second one is flow symmetry. The boundary for heat symmetry makes the boundary condition same as Thermal Insulation. In another word, there is no heat flux going across the heat symmetry. The equation that used for heat symmetry is:

$$-\boldsymbol{n}.(-\lambda\nabla T) = 0 \quad (3.4)$$

Where, λ is the fluid thermal conductivity and n is normal vector.

The symmetry flow boundary condition is used to define the symmetry boundary for the fluid flow only. The equations that solve the symmetry flow boundary condition are:

$$\boldsymbol{u}.\boldsymbol{n} = \boldsymbol{0} \quad (3.5)$$

$$\boldsymbol{K} - (\boldsymbol{K}.\boldsymbol{n}).\boldsymbol{n} = \boldsymbol{0} \quad (3.6)$$

$$\boldsymbol{K} = \mu(\nabla\boldsymbol{u} + (\nabla\boldsymbol{u})^T).\boldsymbol{n} \quad (3.7)$$

Where, u is velocity, μ is dynamic viscosity, n normal vector and K is viscos stress vector on the symmetry boundary.

3.4.4 Conjugate heat transfer

The heat transfer between the solid and fluid simultaneously is known as conjugate heat transfer. The convection heat transfer dominates in fluids, whereas the conduction heat transfer is dominant in solids. Figure 3.4 present a diagram to show the conjugate heat between solid and fluid. On the wall between the solid and fluid there are two temperatures, one for the fluid T_f and the other for the solid T_s. In conjugate heat there is no need to use heat transfer coefficient because the temperatures will be equalized, i.e.

T_s= T_f and the heat flux in wall between the solid and fluid is continue which is described by Fourier's law

$$-n.(-\lambda_s \nabla T_s) = -n.\left(-\lambda_f \nabla T_f\right) \quad (3.8)$$

Where, λ_s is the solid thermal conductivity, λ_f thermal conductivity of fluid.

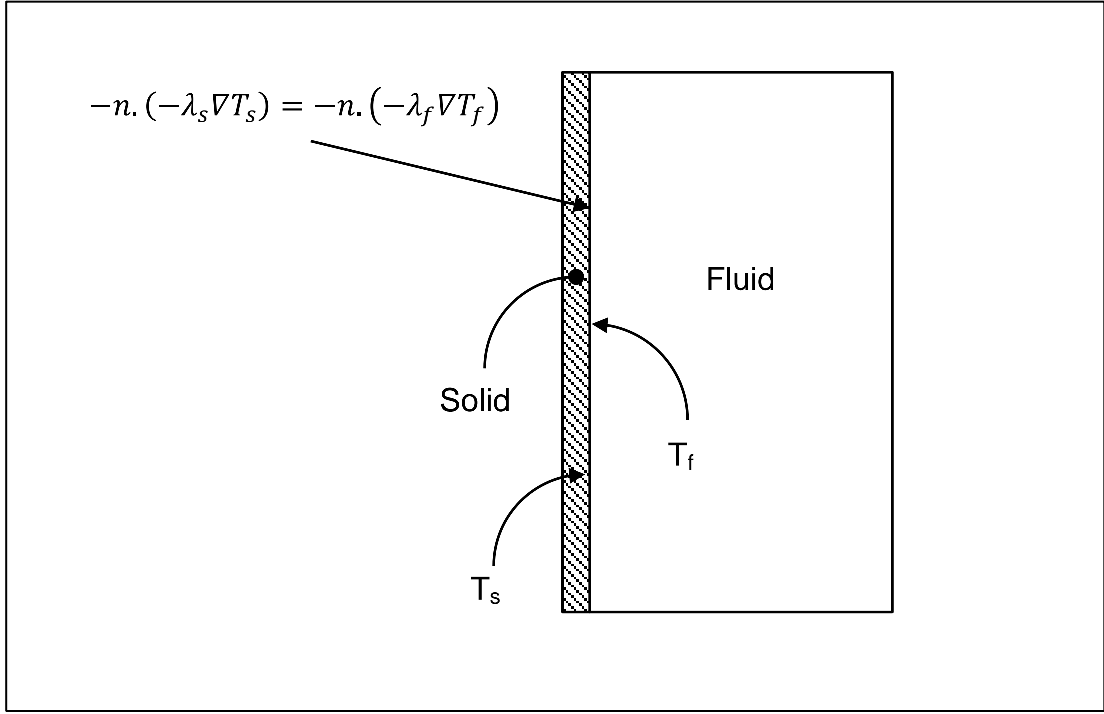

Figure 3.4: Diagram showing the conjugate heat transfer for solid and fluid domains.

3.5 Laminar flow modelling

The classic example that present the laminar flow is fluid flow between two plates as shown in Figure 3.5 where one plate is fixed and one is moving and the laminar layer moves over the other laminar layer without disorder each other [85].

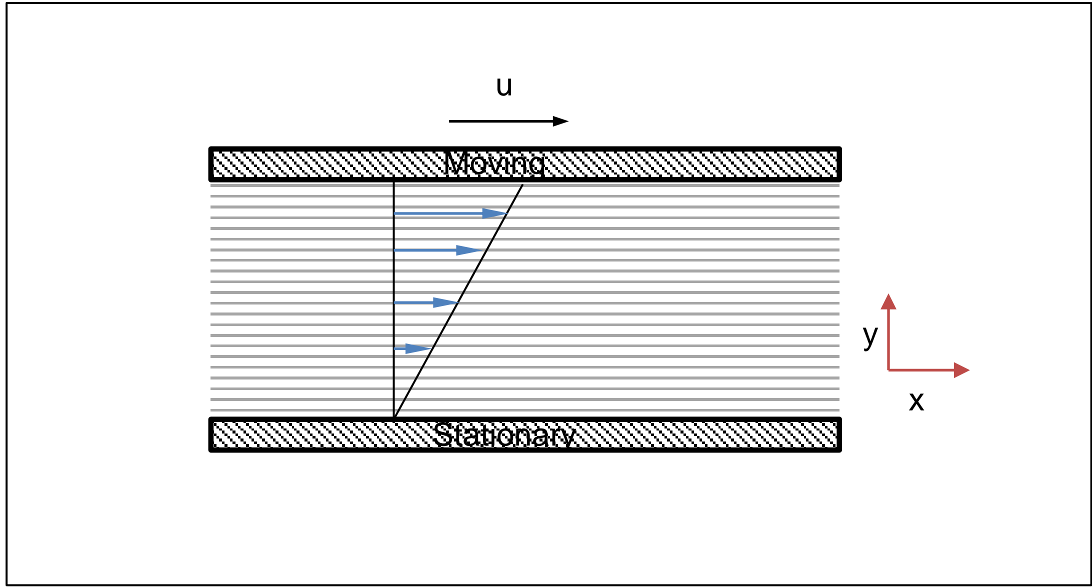

Figure 3.5: Laminar flow between two plates one moving while the other is stationary [85].

The flow status should be defined whether it is laminar or turbulent before starting to solve the model in CFD. There are two characters that indicate the flow is laminar or turbulent. The first one use for forced convection is Reynolds number (Re). It is dimensionless combination of four parameters and it is the inertia force divided the viscous force [86]:

$$\mathrm{Re} = \frac{\rho u \mathrm{D}}{\mu} \tag{3.9}$$

Where, D is pipe diameter, ρ is fluid density, μ is fluid viscosity and u is mean fluid velocity. In case of the pipe the flow behaviour is laminar when the Re≤ 2300 [86].The Re of water channel of cold plate in chapter 6 is equal to 276 which is smaller than 2300 so the fluid is laminar.

In natural convection the Rayleigh number (Ra) could use to indicate that the flow is laminar or turbulent. Ra is the ratio of buoyancy to viscous forces [87], where the constant difference temperature $\Delta T = (T_h - T_c)$

$$Ra = \frac{c_p \rho^2 g \beta \Delta T L^3}{\mu \lambda} \tag{3.10}$$

Where, C_p is specific heat, λ is thermal conductivity, β is coefficient of thermal expansion, μ is dynamic viscosity, ρ is fluid density, L is characteristic length.

Fluid flow behaviour of rectangle enclosure shown in Figure 3.6 has been investigated for a Prandtl number (Pr) range from 1 to 20 and the rectangular aspect ratio $\left(\frac{L}{W}\right)$ between 1 and 40 for different T_1 and T_2. The results from this study shown in Figure 3.7 show that the fluid in rectangular enclosure is a laminar when Ra ≤ 10^6 and the fluid became turbulent at Ra ≥ 10^7 [15]. The immersed server in chapter 5 and chapter 6 has a Pr = 18 and the aspect ratio is 13 and Ra is found to be 10^8, which is within the range of the study so the fluid flow behaviour is turbulent as the Ra greater than 10^7.

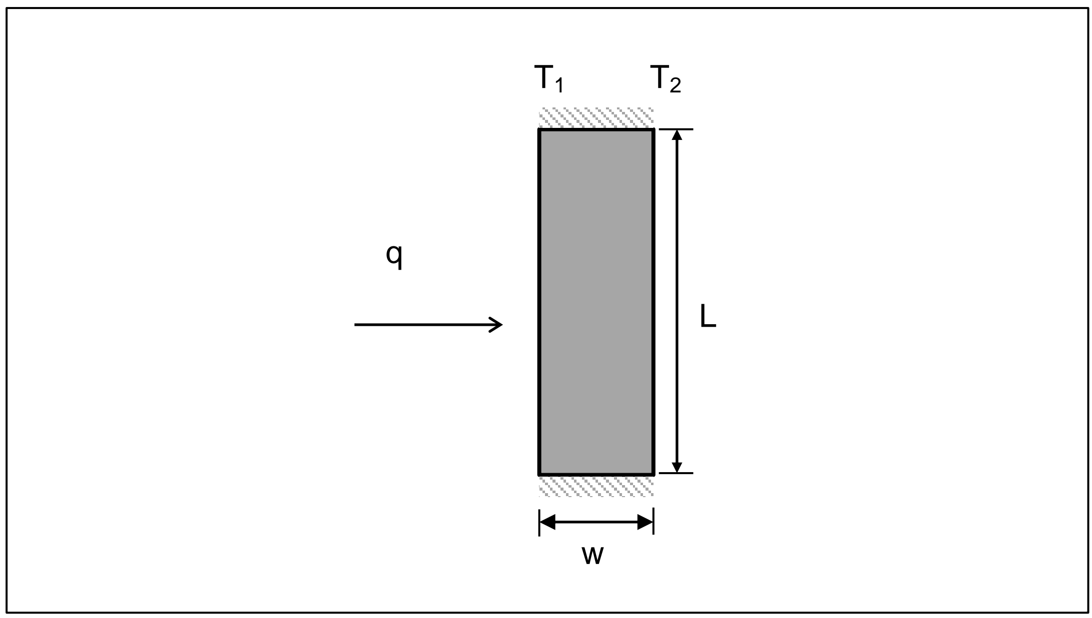

Figure 3.6: Rectangular enclosure geometry [15]

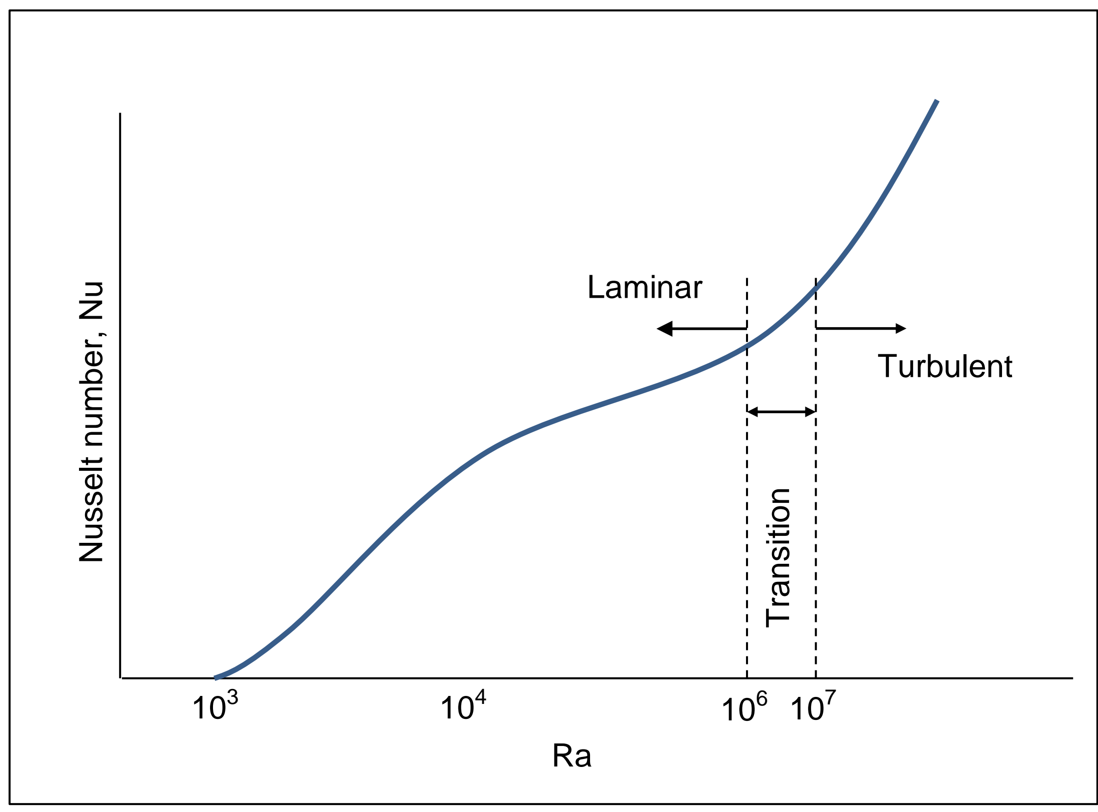

Figure 3.7: Fluid behaviour of Natural convection fluid flow in rectangular enclosure [15]

3.6 Turbulence modelling

The random of flow motion and chaotic lead to disorder in fluid stream line for laminar flow, this phenomena known as turbulent flow [78] as shown in Figure 3.8. Therefore, Turbulent is not suitable to use for laminar and it will not provide a correct solution so solving a turbulent model should not use a laminar solver to solve the model.

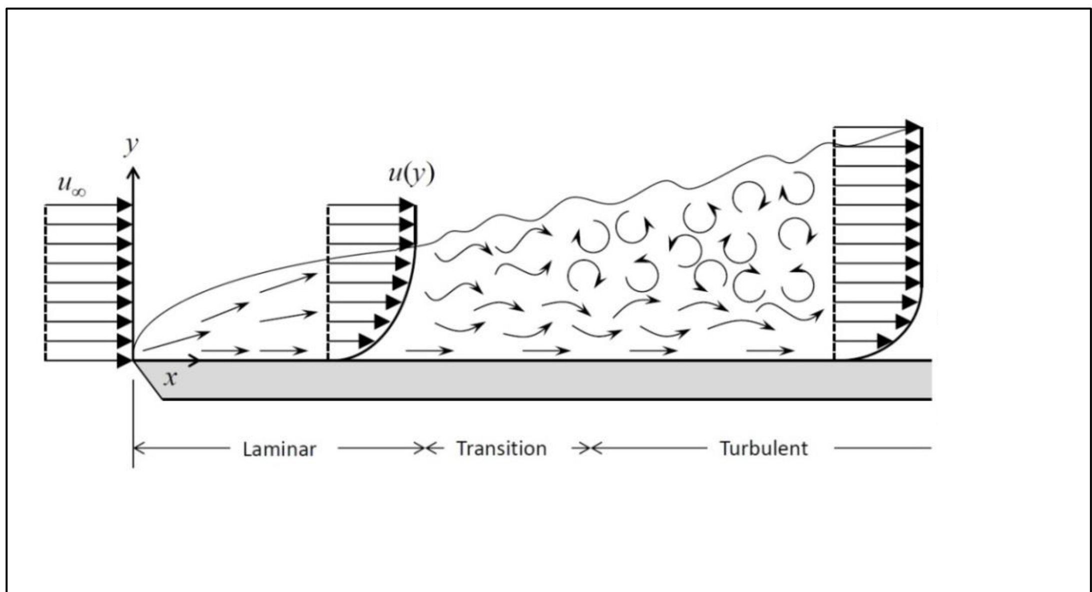

Figure 3.8: The fluid behaviour of Turbulent and laminar flow [84]

High flow rate, surfaces roughness or low viscous force of the system causes the turbulence. The rotation of the flow in turbulent flow creates eddies. Eddies have a different velocity and length. The inertia force generates large eddies. The phenomena known as vortex stretching produces transport eddies in the flow. The large eddies form small eddies because of this phenomena. The eddies became smaller and smaller until it became diminutive, then the viscose effect became important [88].

There are some methods that can be used to simulate turbulent such as Large Eddy Simulation (LES), Direct Numerical Simulation (DNS) and Reynolds Average Navier-Stokes (RANS). Large Eddy Simulation (LES) is a simulation technique that is used to solve turbulent flow based on explicit large eddies with small eddies captured based on applying subgrid-scale models. Direct Numerical Simulation (DNS) is very expensive and requires very large computers to do a simulation for most problems because the mesh grid size used to solve Navier-Stokes equation should be smaller than smallest scale of turbulence [89]. Reynolds Average Navier-Stokes (RANS) that used in COMSOL is explained in next section.

3.6.1 Turbulent flow – RANS

The most common method to solve turbulent flow is Reynolds averaged Navier stoke (RANS) equation which allows with certain degree of accuracy to capture turbulent using elements which are much larger scale by averaging what is happening through the element rather capturing localize fluctuating. So the way this is done is that variables are divided into two components one is an average component which is like integral average components which give this smooth behaviour and the other is fluctuating and it actually express Navier stoke equation in two different velocities [73].

$$\boldsymbol{U} = \boldsymbol{u} + \boldsymbol{u}' \tag{3.11}$$

Where, **u** is an average velocity vector, $\mathbf{u}'$ is velocity fluctuations vector, **U** is the unfiltered velocity. The Navier stoke equation for incompressible flow can be expressed as [73]:

Continuity equation

$$\rho \nabla . \boldsymbol{u} = 0 \tag{3.12}$$

Reynolds Averaged Momentum equation

$$\rho \frac{\partial \boldsymbol{u}}{\partial t} + \rho\, (\boldsymbol{u}. \nabla)\boldsymbol{u} + \boldsymbol{\nabla}. \overline{(\boldsymbol{\rho u' \otimes u'})} = \nabla . [-p\boldsymbol{I} + \mu(\nabla \boldsymbol{u} + (\nabla \boldsymbol{u})^T)] + \boldsymbol{F} \tag{3.13}$$

Where, **F** is the force term, which can for example account for gravity or buoyancy. $\boldsymbol{\nabla}. \overline{(\boldsymbol{\rho u' \otimes u'})}$ is Reynolds stress tensor and $\otimes$ is the outer vector product.

The Eddy Viscosity Model for RANS is

$$\boldsymbol{\nabla}. \overline{(\boldsymbol{\rho}\mathbf{u}' \otimes \mathbf{u}')} = \mu_T(\nabla \mathbf{u} + \nabla \mathbf{u}^T) - \frac{2}{3}\delta k I \tag{3.14}$$

To find out the value of k extra turbulences models need to be calculated which are defined in next sections.

3.6.2 K-ε turbulence model

One of the early turbulent models that used is k-ε and it is established by Launder and Spalding [90]. There are two unknown in k-ε model, the turbulent kinetic energy (k) and the turbulent dissipation rate (ε). This introduces two additional equations to calculated two additional unknowns. The additional equations that need to be solve with Reynolds Averaged Navier-Stokes (RANS) equations are,

Transport equation for the turbulent kinetic energy, k:

$$\rho \frac{\partial k}{\partial t} + \rho \boldsymbol{u}. \boldsymbol{\nabla} k = \nabla . \left[\left(\mu + \frac{\mu_T}{\sigma_k}\right) \nabla k\right] + p_k - \rho\varepsilon \tag{3.15}$$

Transport equation for the turbulent dissipation rate, ε:

$$\rho\frac{\partial\varepsilon}{\partial t}+\rho\boldsymbol{u}.\boldsymbol{\nabla}\varepsilon=\nabla.\left[\left(\mu+\frac{\mu_T}{\sigma_\varepsilon}\right)\nabla\varepsilon\right]+C_{e1}\frac{\varepsilon}{k}P_k-C_{e2}\rho\frac{\varepsilon^2}{k} \tag{3.16}$$

The production term can be obtained from

$$p_k=\mu_T\left[\nabla\boldsymbol{u}:(\nabla\boldsymbol{u}+(\nabla\boldsymbol{u})^T)-\frac{2}{3}(\nabla.\boldsymbol{u})^2\right]-\frac{2}{3}\rho k\nabla.\boldsymbol{u} \tag{3.17}$$

The turbulent dynamic viscosity can be defined as

$$\mu_T=\rho C_\mu\frac{k^2}{\varepsilon} \tag{3.18}$$

Where, **u** is average velocity, $\mathbf{u}^T$ is average velocity transport, μ_T is turbulent viscosity, ρ density, σ_ε is Prandtl number of ε and σ_k is Prandtl number of k. The empirical turbulent model constant parameters:

σ_k = 1, σ_e = 1.3, C_{e1}= 1.44 and C_{e2}= 1.92

The turbulent model k-ε have been used to model accurately a range of industrial applications [78]. The However, using turbulent model k-ε in cases have rotating flow or non-circular ducts provide inaccurate results [78]. Cho et al. [53] used the turbulent model k-ε in data centre to find the temperature filed because k-ε is a good turbulent model to use for open and large spaces.

3.6.3 k-ω turbulence model

The K-ω is developed by Wilcox [81] . It solves specific dissipation rate (ω) and turbulent kinetic energy (k). Turbulent dynamic viscosity is

$$\mu_T=\rho\frac{k}{\omega} \tag{3.19}$$

Transport equation for the turbulent kinetic energy, k:

$$\rho \frac{\partial k}{\partial t} + \rho \boldsymbol{u}.\boldsymbol{\nabla} k = \nabla.[(\mu + \mu_T \sigma_k^*)\nabla k] + p_k - \rho \beta_o^* k \omega \tag{3.20}$$

Transport equation for the turbulent specific dissipation rate, ω:

$$\rho \frac{\partial \omega}{\partial t} + \rho \boldsymbol{u}.\boldsymbol{\nabla} \omega = \nabla.[(\mu + \mu_T \sigma)\nabla \omega] + \alpha \frac{\omega}{k} p_k - \rho \beta_0 \omega^2 \tag{3.21}$$

The production term can be obtained from

$$p_k = \mu_T \left[\nabla \boldsymbol{u}: (\nabla \boldsymbol{u} + (\nabla \boldsymbol{u})^T) - \frac{2}{3}(\nabla.\boldsymbol{u})^2\right] - \frac{2}{3}\rho k \nabla.\boldsymbol{u} \tag{3.22}$$

Where the constant parameters,

$$\alpha = \frac{13}{25}, \quad \sigma_k^* = \frac{1}{2}, \quad \sigma_\omega = \frac{1}{2}, \quad \beta_0 = \frac{9}{125}, \quad \beta_0^* = \frac{9}{100}$$

The fluid behaviour inside the immersed server is turbulent which has same physics as fluid flow inside cavity where the temperature difference governing the fluid. Rundle [91] has developed a turbulence simulation model of cavity to compare it with experiment results to find out the best turbulence model that provides a solution close to experiment and the study concluded that the k-ω provides a superior results compare to other turbulence models. Another study by Zitzmann [92] has investigated a different number of turbulent models for a turbulent natural convection in square cavity and the results show that using k-ω can provide a good agreement with experiment. In addition, Amounallah [93] studied a number of turbulence model for a turbulent flow in cavity with one wavy wall and the results showed that the k-ω provide the best prediction compare to experiment. Based on these studies the k-ω is promising choice to solve the turbulent flow inside immersed sever for this thesis.

3.6.4 Low Reynolds Number k-ε turbulence model

The Low Reynolds Number k-ε turbulence model use if the accuracy of k-ε turbulence model is not good enough. The Low Reynolds Number k-ε turbulence model calculated the area near to the wall.

The Low Reynolds Number k-ε turbulence model introduce the damping function to the turbulence transport equations [94]

Transport equation for the turbulent kinetic energy, k:

$$\rho\frac{\partial k}{\partial t}+\rho\boldsymbol{u}.\boldsymbol{\nabla}k=\nabla.\left[\left(\mu_D+\frac{\mu_T}{\sigma_k}\right)\nabla k\right]+p_k-\rho\varepsilon \quad (3.23)$$

Transport equation for the turbulent dissipation rate, ε:

$$\rho\frac{\partial \varepsilon}{\partial t}+\rho\boldsymbol{u}.\boldsymbol{\nabla}\varepsilon=\nabla.\left[\left(\mu_D+\frac{\mu_T}{\sigma_\varepsilon}\right)\nabla \varepsilon\right]+C_{\varepsilon1}\frac{\varepsilon}{k}p_k-f_\varepsilon C_{\varepsilon2}\rho\frac{\varepsilon^2}{k} \quad (3.24)$$

The production term can be defined as

$$p_k=\mu_T\left[\nabla\boldsymbol{u}:(\nabla\boldsymbol{u}+(\nabla\boldsymbol{u})^T)-\frac{2}{3}(\nabla.\boldsymbol{u})^2\right]-\frac{2}{3}\rho k\nabla.\boldsymbol{u} \quad (3.25)$$

The turbulent dynamic viscosity can be defined as

$$\mu_T=\rho f_\mu C_\mu\frac{k^2}{\varepsilon} \quad (3.26)$$

$$f_\mu=\left(1-e^{-\frac{l}{14}}\right)^2.\left(1+\frac{5}{R_t^{3/4}}e^{-\left(\frac{R_t}{200}\right)^2}\right) \quad (3.27)$$

$$f_\varepsilon=\left(1-e^{-\frac{l}{3.1}}\right)^2.\left(1-0.3e^{-\left(\frac{R_t}{6.5}\right)^2}\right) \quad (3.28)$$

$$l=\frac{(\rho u_\varepsilon l_w)}{\mu}\ ,R_t=\frac{\rho k^2}{\mu\varepsilon}\ ,u_\varepsilon=\left(\frac{\mu\varepsilon}{\rho}\right)^{\frac{1}{4}}$$

The turbulent model constant parameters

$$C_{\varepsilon1} = 1.5\ , C_{\varepsilon2} = 1.9\ , C_{\mu} = 0.09\ , \sigma_k = 1.4\ , \sigma_{\varepsilon} = 1.4$$

Where, l_w is the distance to near wall, **u** is average velocity, μ_T is turbulent viscosity, ρ density, σ_ε is Prandtl number of ε and σ_k is Prandtl number of k.

3.7 Summary

This chapter provided an introduction of CFD and the main steps of solving a simulation model of validations and immersed server that are solved in next chapters. The flow of fluid in immersed server is turbulent because Rayleigh number Ra > 10^7, however the flow of fluid in the cold plate is laminar as Re< 2300. This chapter demonstrated the mathematical modelling that used to solve a simulation model with turbulence model or laminar. The different turbulence models that could be used in COMSOL for simulating turbulent flow model are presented, based on the literature, the turbulent model k-ω is recommended for solving turbulent fluid flow in immersed server for this thesis. The boundary conditions such as inlet, outlet, walls, symmetry and coupling a conjugate heat are showed.

CHAPTER 4: VALIDATION OF MODEL AND SIMULATION

4.1 Introduction

This chapter validates different cases to evaluate the capability of the CFD package COMSOL for modelling buoyancy driven flows and cold plates with a view to select an accurate and appropriate approach to solve the heat transfer within immersed servers with water jackets. The first case is designed to have a hot temperature (T_h) in the left wall while the right wall is cold (T_c) in square cavity, occasionally referred to as the double glazing problem. This difference in temperature creates buoyancy driven flow inside the square cavity. The second case is comparing square cavity with the different fluid such as water and dielectric liquids (e.g. hydrofluoroether HFE 7300) with different software packages like COMSOL and Fluent. The third validation is done for a published numerical model with 3 heat sources where the fluid is laminar. The fourth section is a validation of previous experimental work for finned enclosures. The last section is, a simulation model validated against experimental data for cold plates.

4.2 Natural convection flows in enclosure

In this section, the bench mark of buoyancy flow in square cavity posed by De Vahl Davis [95, 96] is simulated using COMSOL. Convection phenomena induced by body forces have been the subject of extensive research efforts. The reliable computation of buoyant flow is important in some engineering sectors, for example, ventilation and cooling of electronic equipment. The buoyancy-driven flow considered here is the natural convection in a square cavity that is produced from the difference in temperatures between the two vertical walls. Convection currents are generated due to the body forces acting on a fluid in which there is a density gradient. The density gradient is, in turn, often generated by temperature differences and the buoyancy force is due to gravity [97].

Many studies exist that have solved the buoyancy driven flow in a square cavity. De Vahl Davis [96] compared thirty seven contributions of this problem and proposed accurate solutions, which is considered as a benchmark. The simulation model of buoyancy driven flow in square cavity in COMSOL was provided by John Kame [98] in order to compare it with the benchmark buoyancy flow posed by De Vahl Davis [95]. The non-dimensional square cavity shown in Figure 4.1 considers the two-dimensional flow with $\Delta x = \Delta y = 1$ and the right wall is $T_c= 0$ and the left wall is $T_h=1$. The upper and lower walls are insulated. The flow is driven by the temperature differences which in turn affects the density of fluid. In the area near the hot wall fluid density decreases, creating an upward direction of movement. Whereas the fluid density near the opposite cold wall decreases and creates a downward direction of movement. In general a circular

movement is created inside the cavity, the direction is governed by the walls' temperature variation as shown in Figure 4.1.

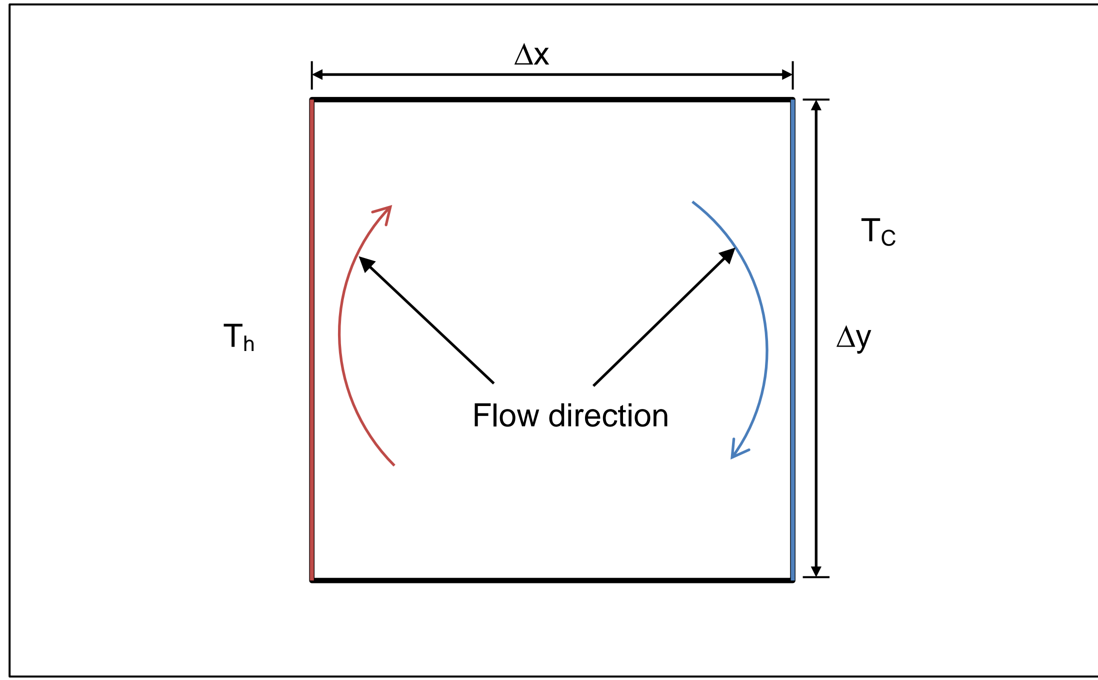

Figure 4.1: Geometry of square cavity

4.2.1 Mathematical formulation

The flow in this square cavity is laminar and assumed to be incompressible. So, the continuity equation, which in the Cartesian directions is given by

$$\frac{\partial u}{\partial x} + \frac{\partial v}{\partial y} = 0 \tag{4.1}$$

The momentum equation with a Boussinesq buoyancy approximation can be applied,

X-direction

$$\rho \frac{\partial u}{\partial t} + \rho \left[u \frac{\partial u}{\partial x} + v \frac{\partial u}{\partial y} + w \frac{\partial u}{\partial z} \right]$$

$$= -\frac{\partial p}{\partial x} + \mu \left[\frac{\partial^2 u}{\partial x^2} + \frac{\partial^2 u}{\partial y^2} + \frac{\partial^2 u}{\partial z^2} \right] + \rho g_x \beta \, (T - T_o) \quad (4.2)$$

Y-direction

$$\rho \frac{\partial v}{\partial t} + \rho \left[u \frac{\partial v}{\partial x} + v \frac{\partial v}{\partial y} + w \frac{\partial v}{\partial z} \right]$$

$$= -\frac{\partial p}{\partial y} + \mu \left[\frac{\partial^2 v}{\partial x^2} + \frac{\partial^2 v}{\partial y^2} + \frac{\partial^2 v}{\partial z^2} \right] + \rho g_y \beta \, (T - T_o) \quad (4.3)$$

Z-direction

$$\rho \frac{\partial w}{\partial t} + \rho \left[u \frac{\partial w}{\partial x} + u \frac{\partial w}{\partial y} + w \frac{\partial w}{\partial z} \right]$$

$$= -\frac{\partial p}{\partial z} + \mu \left[\frac{\partial^2 w}{\partial x^2} + \frac{\partial^2 w}{\partial y^2} + \frac{\partial^2 w}{\partial z^2} \right] + \rho g_z \beta \, (T - T_o) \quad (4.4)$$

Here, the flow is steady state

$$\frac{\partial u}{\partial t} = \frac{\partial v}{\partial t} = \frac{\partial w}{\partial t} = 0$$

$g_x = g_z = 0$ Because no gravity acceleration in *x* and *z* directions

Then, equation will be,

$$\rho \left[u \frac{\partial v}{\partial x} + v \frac{\partial v}{\partial y} \right] = -\frac{\partial p}{\partial y} + \mu \left[\frac{\partial^2 v}{\partial x^2} + \frac{\partial^2 v}{\partial y^2} \right] + \underbrace{\rho g_y \beta \, (T - T_o)}_{\text{Body force}} \quad (4.5)$$

The energy equation

$$\rho c_p \left[\frac{\partial T}{\partial t} + u \frac{\partial T}{\partial x} + v \frac{\partial T}{\partial y} \right] = k \left[\frac{\partial^2 T}{\partial x^2} + \frac{\partial^2 T}{\partial y^2} \right] \quad (4.6)$$

The non-dimensionalisation of governing equation requires the following non-dimensional quantities

$$x' = \frac{x}{L} \quad or\ x = x'L$$

$$y' = \frac{y}{L} \quad or\ y = y'L$$

$$v' = \frac{\rho L}{\mu} v \quad or\ v = \frac{\mu}{\rho L} v'$$

$$u' = \frac{\rho L}{\mu} u \quad or\ u = \frac{\mu}{\rho L} u'$$

$$p' = \frac{\rho L^2}{\mu^2} p \quad or\ p = \frac{\mu^2}{\rho L^2} p'$$

$$T' = \frac{T - T_c}{T_h - T_c} \quad or\ \ T = T'(T_h - T_c) + T_c$$

$$T'_o = \frac{T_o - T_c}{T_h - T_c} \quad or\ T_o = T'_o(T_h - T_c) + T_c$$

Where, L is the length of the square cavity, v' is non-dimensional velocity in Y direction, p' is non-dimensional pressure, u' is non-dimensional velocity in X direction, T_c is the temperature of right wall, x' is non-dimensional X coordinate, T_h is the temperature of left wall, y' is non-dimensional Y coordinate, T' is non-dimensional represent temperature, T'_o is non-dimensional reference temperature.

Now substitute non dimensional quantities into continuity equation (4.1)

$$\frac{\mu}{\rho L} \frac{1}{L} \left[\frac{\partial u'}{\partial x'} + \frac{\partial v'}{\partial y'} \right] = 0 \tag{4.7}$$

Multiply equation (4.7) into $\frac{\mu}{\rho L}\frac{1}{L}$ the non-dimensional form of continuity equation is

$$\left[\frac{\partial u'}{\partial x'}+\frac{\partial v'}{\partial y'}\right]=0 \tag{4.8}$$

Now substitute non-dimensional quantities into momentum equation with a Boussinesq buoyancy approximation (4.5)

$$\rho\left[\frac{\mu}{\rho L}u'\frac{\mu}{\rho L}\frac{1}{L}\frac{\partial v'}{\partial x'}+\frac{\mu}{\rho L}v'\frac{\mu}{\rho L}\frac{1}{L}\frac{\partial v'}{\partial y'}\right]$$
$$=-\frac{\mu^2}{\rho L^2}\frac{1}{L}\frac{\partial p'}{\partial y'}+\mu\left[\frac{\mu}{\rho L}\frac{1}{L^2}\frac{\partial^2 v'}{\partial x'^2}+\frac{\mu}{\rho L}\frac{1}{L^2}\frac{\partial^2 v'}{\partial y'^2}\right]$$
$$+\rho g_y\beta\left(T'(T_h-T_c)+T_c-T'_o(T_h-T_c)-T_c\right) \tag{4.9}$$

Rewrite the equation (4.9)

$$\frac{\mu^2}{\rho L^3}\left[u'\frac{\partial v'}{\partial x'}+v'\frac{\partial v'}{\partial y'}\right]$$
$$=-\frac{\mu^2}{\rho L^3}\frac{\partial p'}{\partial y'}+\frac{\mu^2}{\rho L^3}\left[\frac{\partial^2 v'}{\partial x'^2}+\frac{\partial^2 v'}{\partial y'^2}\right]+\rho g_y\beta(T'$$
$$-T'_o)(T_h-T_c) \tag{4.10}$$

Multiply the equation (4.10) into $\frac{\rho L^3}{\mu^2}$

$$\left[u'\frac{\partial v'}{\partial x'}+v'\frac{\partial v'}{\partial y'}\right]$$
$$=-\frac{\partial p'}{\partial y'}+\left[\frac{\partial^2 v'}{\partial x'^2}+\frac{\partial^2 v'}{\partial y'^2}\right]+\frac{\rho^2 g\beta(T_h-T_c)L^3}{\mu^2}(T'-T'_o) \tag{4.11}$$

Here, Rayleigh number (Ra)

$$Ra=\frac{c_p\rho^2 g\beta T L^3}{\mu k} \tag{4.12}$$

(‘*Ra is the ratio of buoyancy to viscous forces* [87], *where the constant difference temperature* T = $(T_h - T_c)$’

And Prandtl number (Pr)

$$Pr = \frac{\mu c_p}{k} = \frac{\nu}{\alpha} \tag{4.13}$$

(‘*Pr is Ratio of two diffusion coefficients, i.e. viscous versus thermal diffusion’* [87])

Where, C_p is specific heat, *k* is thermal conductivity, *β* is thermal expansion coefficient, μ is dynamic viscosity, ρ is density, ν is kinematic viscosity and α is thermal diffusivity.

Now, dividing Rayleigh number in equation (4.12) by Prandtl number in equation (4.13)

$$\frac{R_a}{P_r} = \frac{\frac{c_p \rho^2 g \beta T L^3}{\mu k}}{\frac{\mu c_p}{k}} = \frac{\rho^2 g \beta \, T L^3}{\mu^2}$$

Then, the equation (4.11) will be

$$\left[u' \frac{\partial v'}{\partial x'} + v' \frac{\partial v'}{\partial y'}\right] = -\frac{\partial p'}{\partial y'} + \left[\frac{\partial v'^2}{\partial x'^2} + \frac{\partial v'^2}{\partial y'^2}\right] + \frac{R_a}{P_r}(T' - T'_o) \tag{4.14}$$

There for the body force in *Y* direction is

$$F_y = \frac{R_a}{P_r}(T' - T'_o) \tag{4.15}$$

Where, F_y is force in *Y* direction that produce the body force of the fluid which depend mainly on the temperature difference $(T' - T'_o)$ and Rayleigh number. The temperature differential produces the density variation that

drives the buoyant flow. Ra varies values for 1000, 10000 and 100000 as used in study by De Vahl Davis [95] .

Where

$$T = T'(T_h - T_c) + T_c \tag{4.16}$$

Then the first differential equation of T

$$\frac{\partial T}{\partial x} = \frac{(T_h - T_c)}{L}\frac{\partial T'}{\partial x'} \tag{4.17}$$

The second differential equation of T is

$$\frac{\partial^2 T}{\partial x^2} = \frac{(T_h - T_c)}{L^2}\frac{\partial^2 T'}{\partial x'^2} \tag{4.18}$$

Now substitute the non-dimensional form of u, v, y x and equations 4.17 and 4.18 into the energy equation 4.6

$$\rho c_p \frac{\mu}{\rho L}\frac{(T_h - T_c)}{L}\left[u'\frac{\partial T'}{\partial x'} + v'\frac{\partial T'}{\partial y'}\right] = k\frac{(T_h - T_c)}{L^2}\left[\frac{\partial^2 T'}{\partial x'^2} + \frac{\partial^2 T'}{\partial y'^2}\right] \tag{4.19}$$

Now, rearrange equation 4.19

$$\frac{c_p \mu}{k}\left[u'\frac{\partial T'}{\partial x'} + v'\frac{\partial T'}{\partial y'}\right] = \left[\frac{\partial^2 T'}{\partial x'^2} + \frac{\partial^2 T'}{\partial y'^2}\right] \tag{4.20}$$

Where $P_r = \frac{\mu c_p}{k}$, the non-dimensional energy equation will be

$$P_r\left[u'\frac{\partial T'}{\partial x'} + v'\frac{\partial T'}{\partial y'}\right] = \left[\frac{\partial^2 T'}{\partial x'^2} + \frac{\partial^2 T'}{\partial y'^2}\right] \tag{4.21}$$

Because the equations in COMSOL are assumed to be in dimensional form, to match with the non-dimensional form equations, it is required to set the fluid properties as

$C_p = Pr$

$\mu = k = \rho = 1$

The non-dimensional variables are T, *p* and u

4.2.2 Building model using COMSOL

This section is showing an example of how the natural convection model is built using COMSOL. Building a model in COMSOL generally goes through three main steps. The first one is creating the geometry, then defined the physics for the model and coupled them. Finally choosing the solver whether it is steady state or time dependent. Figure 4.2 shows the model build in COMSOL for natural convection and its interface features. The process essentially follows the three steps of computational modelling, namely *pre-processing*, identified as 1, 2 and 3 in Figure 4.2. Then the *solving* stage involves defining the solver parameters, identified as 4 in Figure 4.2 and the solving process reports to 8. At the end of the solution process the *post-processing* of the results is via 5 and 7 in Figure 4.2. The area identified as 6 in Figure 4.2 is where options are selected and is used in all three steps.

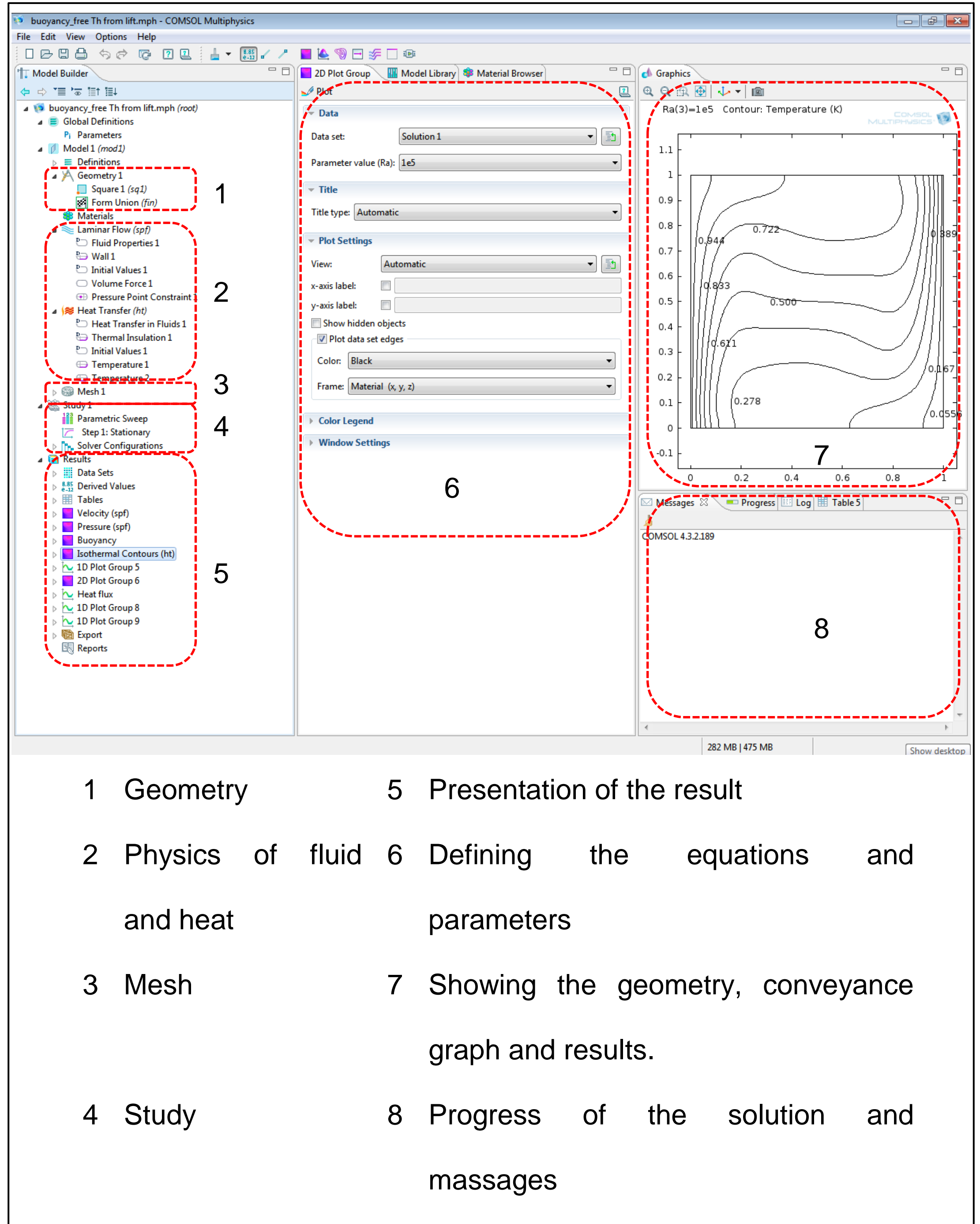

Figure 4.2: COMSOL interface for the Natural convection model

4.2.3 Results

With different value of Ra the results from Table 4.1 show that the contour of stream lines and temperature of the validation are very close to the results from the benchmark De Vahl Davis [95].

Table 4.1: Comparison of temperature contours inside the cavity between present study (right) and De Vahl Davis

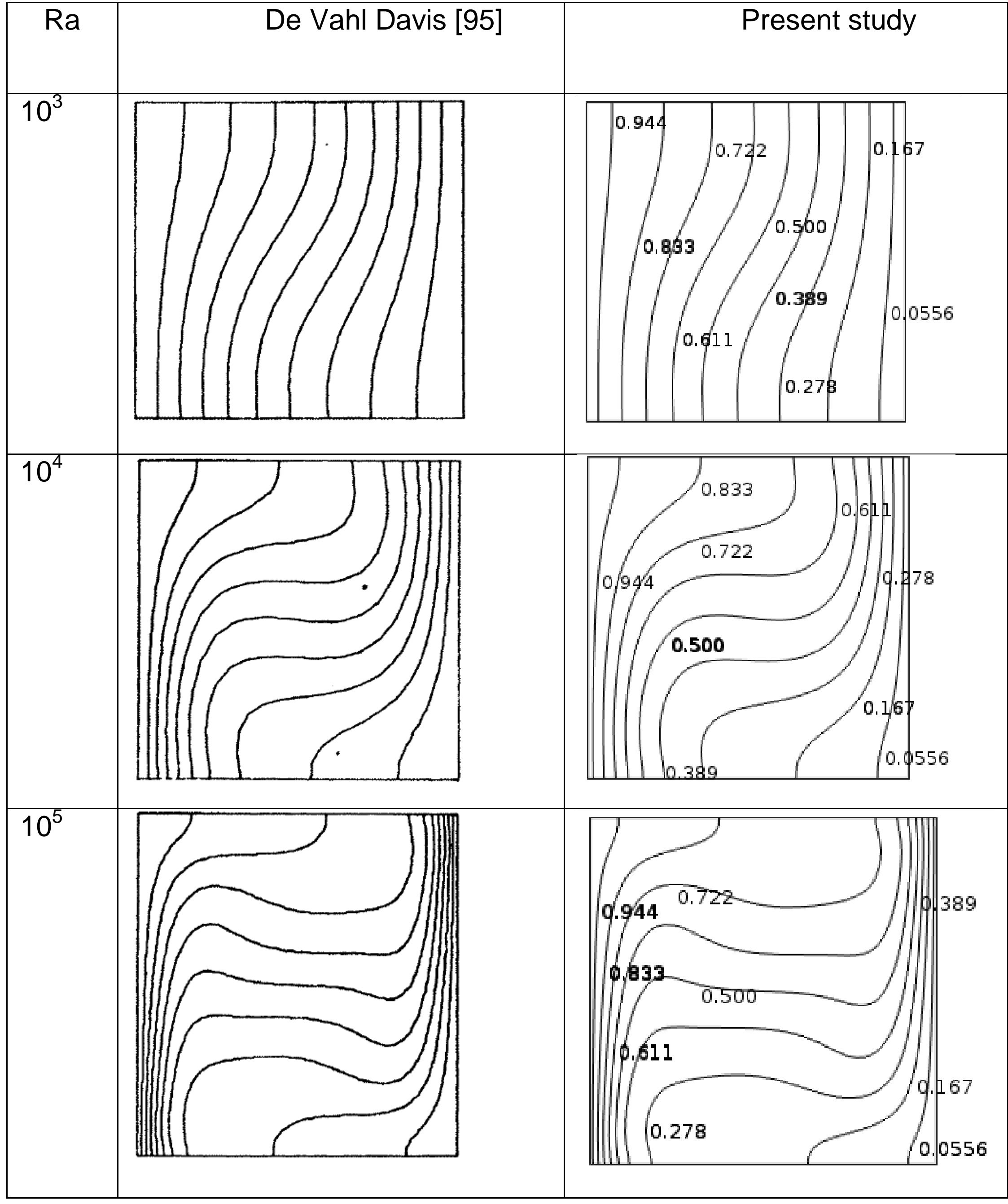

Figure 4.3 shows the velocity of u' at X direction for different Ra. The velocity is taken on the cut line in middle of the cavity. Where cut line is a line that is taken at x= 0.5. The results show that the velocity magnitude increases with increase of Ra. The velocity in the middle of the cavity is zero due to fluid circulation.

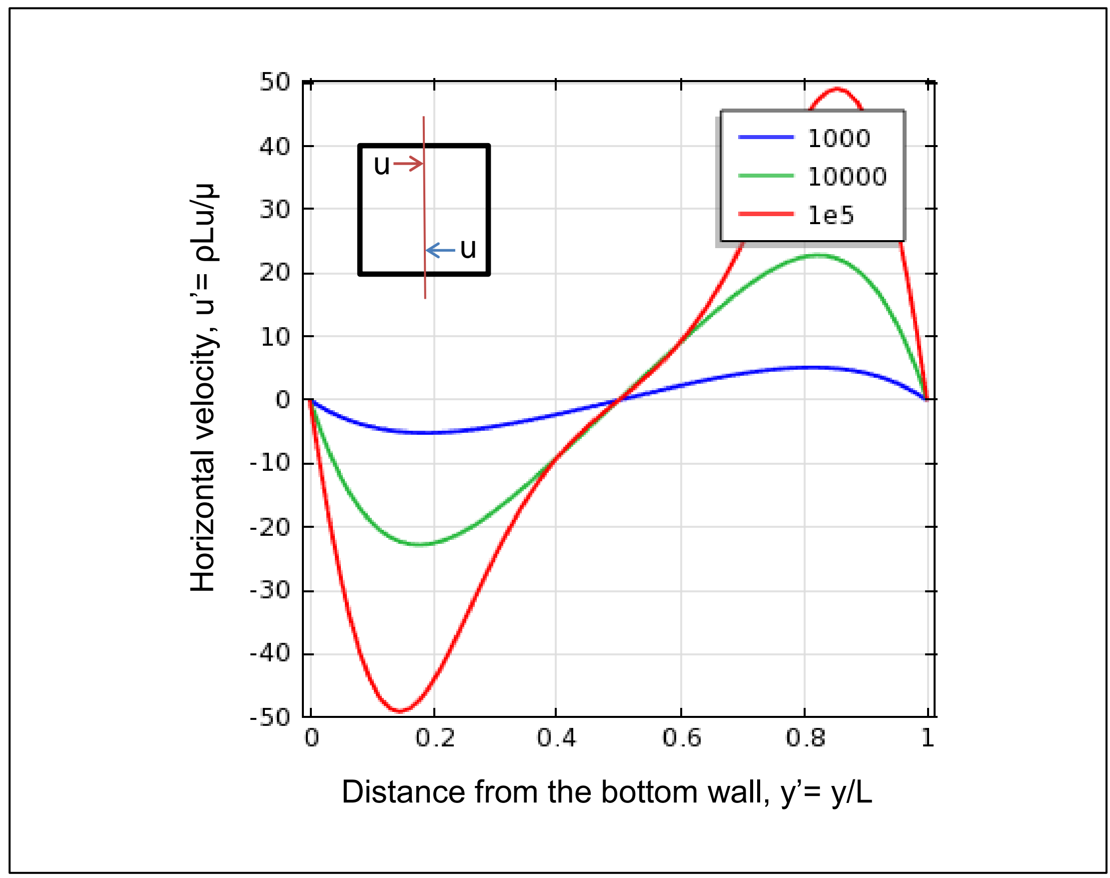

Figure 4.3: Horizontal velocity (u') at x= 0.5 for different Ra, the diagram in the corner is showing the cut line in the square cavity at x=0.5 and the horizontal velocity in X direction (u')

The cut line is taken in the middle of Y axis to present the velocity at Y direction (v') as shown Figure 4.4. The negative velocity means fluid is going down which is close to the cold wall. The results show that the velocity in Y

direction (v’) is greater than the velocity in X direction (u’), this due to that in Y direction the fluid is close to the hot and cold walls.

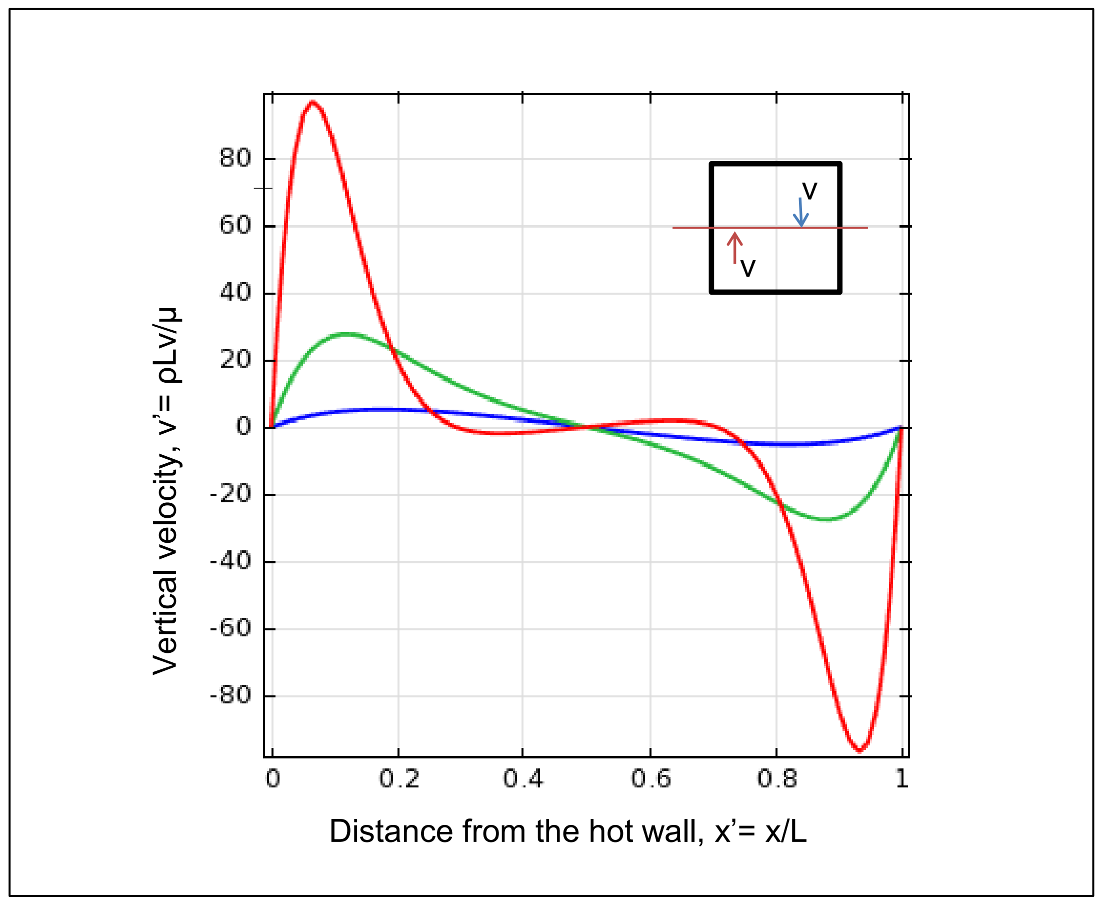

Figure 4.4: Vertical velocity (v’) at y= 0.5 for different Ra, the diagram in the corner is showing the cut line in the square cavity at y= 0.5 and the vertical velocity in Y direction (v’)

Table 4.2 shows numerical comparison between the present study and the benchmark De Vahl Davis [95]. The non-dimensional way adopted in this study is slightly different from the method that used in [95]. Therefore, in Table 4.2 the maximum velocities in both X and Y directions (u_{max}, v_{max}) are multiplied by Pr for the present study. The result shows a very good agreement between the present study and De Vahl Davis [95], where the average error between the present study and De Vahl Davis [95] for u_{max} is

0.17% and for the v_{max} is 0.14%. The average error is the sum of errors for the u_{max} or v_{max} at Ra equals to 10^5, 10^4 and 10^3 and divide them on three.

Where u_{max} is the maximum velocity in X direction, y is the is value of Y at u_{max} across line in the middle of X, v_{max} is the maximum velocity in Y direction, x is value of X at v_{max} across line in the middle of Y.

Table 4.2: Numerical comparison between present validation and De Vahl Davis [95]

Study	Parameters	Ra		
		10^5	10^4	10^3
Present validation	u_{max}	49.07	22.8	5.132
	$P_r .u_{max}$	34.84	16.19	3.644
	Y	0.854	0.822	0.806
	v_{max}	96.82	27.6	5.203
	$P_r. v_{max}$	68.74	19.59	3.694
	X	0.066	0.116	0.176
De Vahl Davis [95]	u_{max}	34.73	16.18	3.649
	Y	0.855	0.823	0.813
	v_{max}	68.59	19.62	3.697
	X	0.066	0.119	0.178

4.3 Comparison of natural convection in square cavity using different CFD packages

The work in this section is for comparing 2 different packages of CFD which has well-known name such as COMSOL and Fluent [99] . COMSOL is based on finite element method while Fluent works on finite volume. The comparison is done for 2D natural convection in square cavity. It is a subtle problem as the flow driven by varying the density with temperature so getting a good agreement will prove that COMSOL is good tool to simulate a model of server immersed cooling. The square cavity fills with two different liquid which are water and a hydrofluoroether HFE 7300 (dielectric).

To model natural convection is a square cavity where the length and height is L and the aspect ratio is 1, the left wall is a constant hot temperature (T_h) and the cold temperature on right wall is (T_c). The different between the temperatures ($\Delta T = T_h - T_c$) is kept constant at 30 ^oC and the variation of Rayleigh number (Ra) is based on cavity length (L). So cavity length is chosen as shown in Table 4.3 for the two liquids where the model Ra is less than 10^6. As the flow behaviour will be transient where Ra> 10^6 and the solver convergence became difficult with steady state [100].

Table 4.3: Square cavity length of different liquids

L (m)	$1X10^{-3}$	$2X10^{-3}$
Ra Water	$4.8X10^{2}$	$3.8X10^{3}$
Ra HFE	$1.6X10^{4}$	$1.3X10^{5}$

The thermal properties of water and HFE 7300 are shown in Table 4.4. These properties are used in same values for each CFD package.

Table 4.4: Thermal properties of water and HFE 7300

	Density	Specific Heat	Thermal conductivity	Dynamic Viscosity
expression	ρ	Cp	K	μ
unit	kg/m^3	J/(kg.K)	W/(m.K)	Pa.s (kg/m.s)
Water	$9.97X10^{2}$	$4.18X10^{3}$	$5.96\ X10^{-1}$	$8.9\ X10^{-4}$
HFE 7300	$1.59X10^{3}$	$1.14\ X10^{3}$	$6.9\ X10^{-2}$	$1.13\ X10^{-3}$
	Kinematic viscosity	Thermal diffusivity	Thermal expansion coefficient	
expression	v	α	β	
unit	$m^2.s$	$m^2.s$	$1/^oC$	
Water	$8.93\ X10^{-7}$	$1.43\ X10^{-7}$	$2.07\ X10^{-4}$	
HFE 7300	$7.1\ X10^{-7}$	$3.8\ X10^{-8}$	$1.51\ X10^{-3}$	

4.3.1 Mesh sensitivity study

The study of the effect of the mesh density on the CFD solution is performed for the HFE 7300 at Ra= $1.3X10^5$ which is the highest Ra in this comparison. The results of mesh sensitivity are shown in Table 4.5. The mesh study is carried out by observing the maximum velocity (u_{max}) in middle of square cavity at x-axis direction. The mesh used was 1600 elements to solve the simulations model for COMSOL and Fluent.

Table 4.5: u_{max} in middle of square cavity in y direction of different number of elements

Number of elements	u_{max} at y cut line	Y at the u_{max}
100	7.93E-04	$1.61x10^{-3}$
400	7.74E-04	$1.63x10^{-3}$
900	7.59E-04	$1.68x10^{-3}$
1600	7.58E-04	$1.7x10^{-3}$
2500	7.58E-04	$1.7x10^{-3}$
3600	7.58E-04	$1.7x10^{-3}$

4.3.2 CFD packages comparison results

COMSOL and Fluent CFD packages are used to solve a square cavity filled with two different liquids. The liquids filled in the square cavity were HFE 7300 and water (at separate models). Maximum velocity (u_{max}) is measured for each CFD package with the different liquids in order to compare between them.

Figure 4.5 shows u_{max} in x direction for HFE 7300 at the cavity length $1x10^{-3}$ m. This has been taken from cut line in the centre of the cavity where X-direction/2 at Y-axis. The u_{max} along centre line of COMSOL and Fluent are indistinguishable. In addition, the u_{max} for all CFD packages are matches too for HFE 7300 for the square cavity length $2x10^{-3}$ m as shown in Figure 4.6.

The u_{max} along the cut line in the centre of square cavity for water is presented in Figure 4.7. This at the square cavity length $1x10^{-3}$ m and the u_{max} for COMSOL and Fluent are indistinguishable. Moreover, the u_{max} for the different CFD packages are matches at square cavity length $2x10^{-3}$ m as illustrated in Figure 4.8. It can be noted that the HFE 7300 in the square cavity is faster than the water because the HFE 7300 has higher thermal expansion coefficient. The comparison results in this section concluded that there is no significant difference between of prediction the various packages for theses problem.

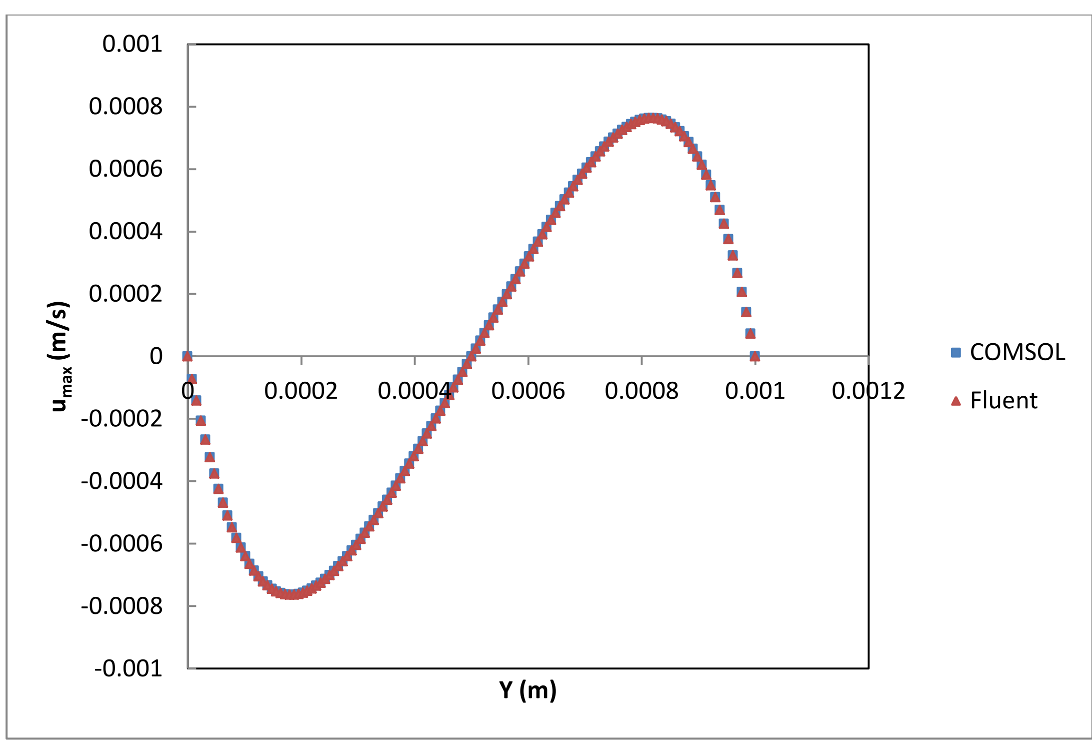

Figure 4.5: u_{max} in x-direction for HFE 7300 at $L=1x10^{-3}$ m

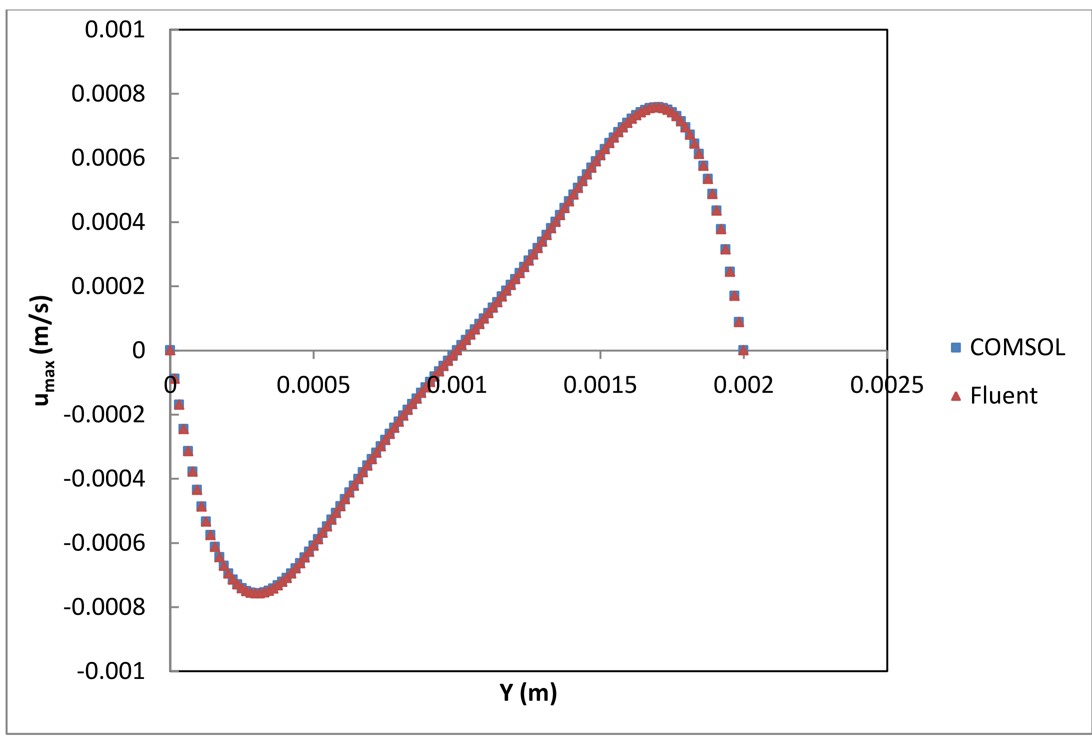

Figure 4.6: u_{max} in x-direction for HFE 7300 at $L=2x10^{-3}$ m

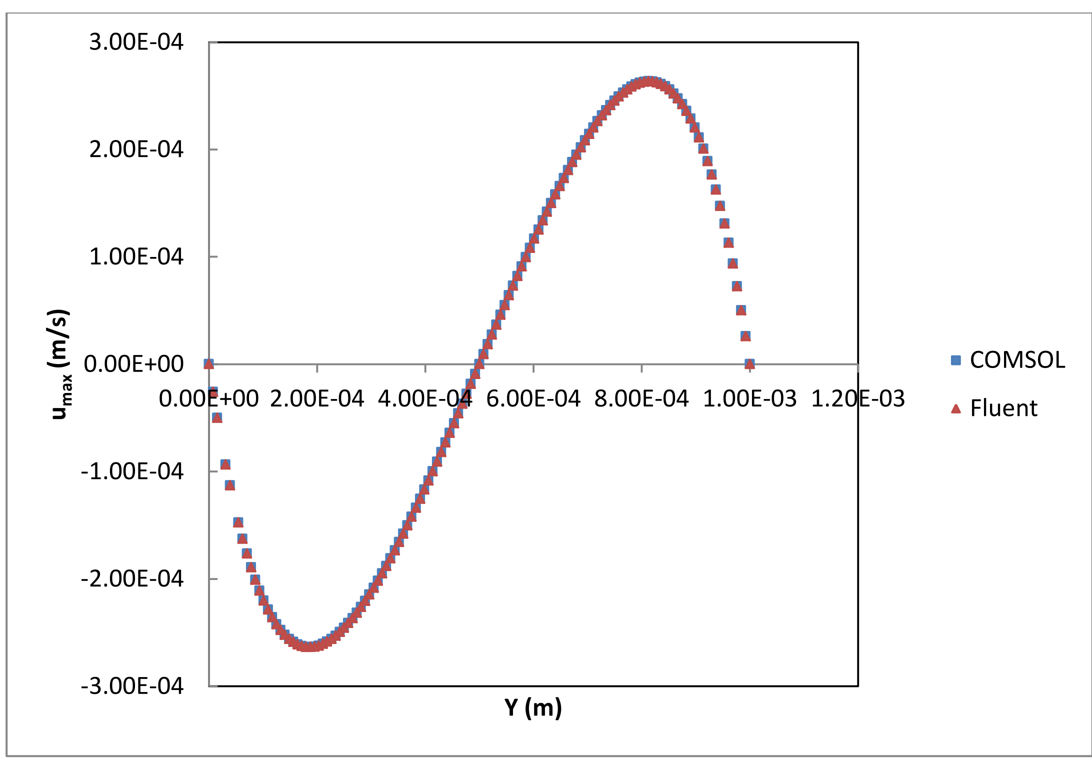

Figure 4.7: u_{max} in x-direction for water at L=1x10^{-3} m

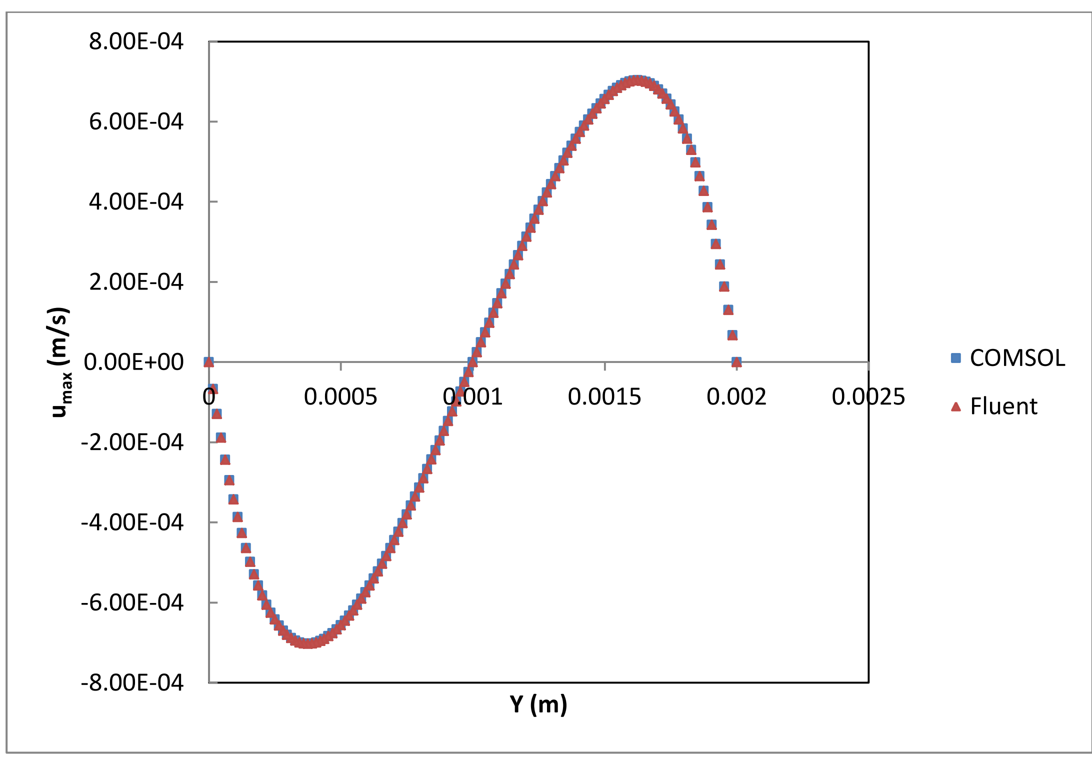

Figure 4.8: u_{max} in x-direction for water at L=2x10^{-3} m

4.4 Validation of numerical solution of heat source on enclosure

In this section the validation attention is turned to conjugate heat transfer (conduction and convection) with a heat source and rectangular model. Liu and Phan-thien [16] investigated a non-dimensional rectangular enclosure with heat being generated by three semiconductor chips as shown in Figure 4.9. Three uniform chips attached on the substrate, the distance between the chips is S_1, S_2, S_3 and S_4. S_1 is the space between the bottom walls to centre of the bottom chip, S_2 is the space from the centre of first chip to the centre of second chip, S_3 is the space between the centre of the second chip to the centre of the third chip and S_4 is the difference between the centre of the third chip to top wall. The dimension of the chip is 0.5L $\times$ L and the dimensions of substrate are 0.25L $\times$ 7L and the rectangular dimensions are 4L $\times$ 7L. The system in this study is cooled by vertical wall placed on the opposite side of the chips and the temperature in this wall is constant T_c. The other walls are assumed to be insulated. The simulation model in this study was 2D.

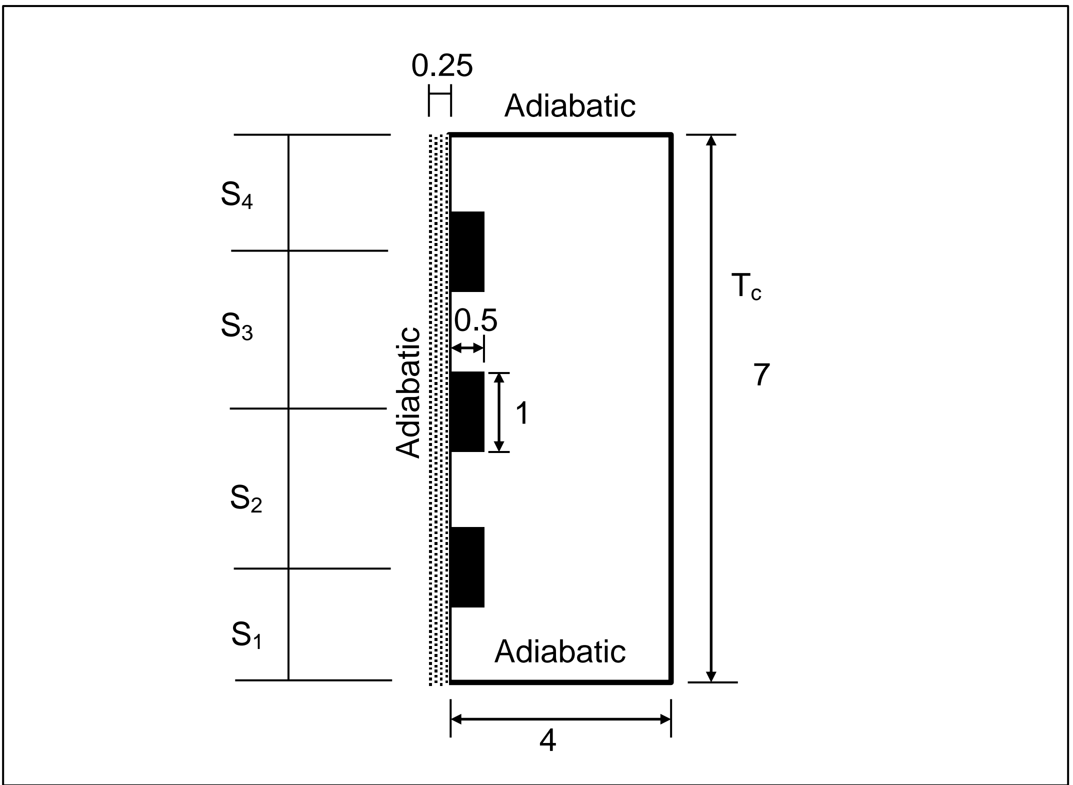

Figure 4.9: Schematic diagram of non-dimensional simulation model of three chips in an enclosure

The flow in this study is laminar and assumed to be incompressible. So, the continuity equation, which in the Cartesian directions is given by

$$\frac{\partial u}{\partial x}+\frac{\partial v}{\partial y}=0 \tag{4.22}$$

The momentum equation

X-direction

$$\rho\frac{\partial u}{\partial t}+\rho\left[u\frac{\partial u}{\partial x}+v\frac{\partial u}{\partial y}+w\frac{\partial u}{\partial z}\right]$$

$$=-\frac{\partial p}{\partial x}+\mu\left[\frac{\partial^2 u}{\partial x^2}+\frac{\partial^2 u}{\partial y^2}+\frac{\partial^2 u}{\partial z^2}\right]+\rho g_x\beta\,(T-T_c) \tag{4.23}$$

Y-direction

$$\rho\frac{\partial v}{\partial t}+\rho\left[u\frac{\partial v}{\partial x}+\ v\frac{\partial v}{\partial y}+w\frac{\partial v}{\partial z}\right]$$
$$=-\frac{\partial p}{\partial y}+\mu\left[\frac{\partial^2 v}{\partial x^2}+\ \frac{\partial^2 v}{\partial y^2}+\frac{\partial^2 v}{\partial z^2}\right]+\rho g_y\beta\ (T-T_c) \qquad (4.24)$$

Z-direction

$$\rho\frac{\partial w}{\partial t}+\rho\left[u\frac{\partial w}{\partial x}+\ u\frac{\partial w}{\partial y}+w\frac{\partial w}{\partial z}\right]$$
$$=-\frac{\partial p}{\partial z}+\mu\left[\frac{\partial^2 w}{\partial x^2}+\ \frac{\partial^2 w}{\partial y^2}+\frac{\partial^2 w}{\partial z^2}\right]+\rho g_z\beta\ (T-T_c) \qquad (4.25)$$

Here, the flow is steady state

$$\frac{\partial u}{\partial t}=\frac{\partial v}{\partial t}=\frac{\partial w}{\partial t}=0$$

$g_x=g_z=0$ Because no gravity acceleration in *x* and *z* directions

Then, equation will be,

$$\rho\left[u\frac{\partial v}{\partial x}+\ v\frac{\partial v}{\partial y}\right]=-\frac{\partial p}{\partial y}+\mu\left[\frac{\partial^2 v}{\partial x^2}+\ \frac{\partial^2 v}{\partial y^2}\right]+\rho g_y\beta\ (T-T_c) \qquad (4.26)$$

The energy equation

$$\rho c_p\left[\frac{\partial T}{\partial t}+u\frac{\partial T}{\partial x}+v\frac{\partial T}{\partial y}\right]=k\left[\frac{\partial^2 T}{\partial x^2}+\ \frac{\partial^2 T}{\partial y^2}\right] \qquad (4.27)$$

Non-dimensional quantities of the governing equation of the model in this section are as follow:

$$x'=\frac{x}{L} \quad or\ x=x'L$$

$$y'=\frac{y}{L} \quad or\ y=y'L$$

$$v' = \frac{L}{\alpha\sqrt{R_a P_r}} v \quad or\ v = \frac{v' \alpha\sqrt{R_a P_r}}{L}$$

$$u' = \frac{L}{\alpha\sqrt{R_a P_r}} u \quad or\ u = \frac{u' \alpha\sqrt{R_a P_r}}{L}$$

$$p' = \frac{\alpha^2 \rho R_a P_r L^2}{L^2} p \quad or\ p = \frac{L^2}{\alpha^2 \rho R_a P_r} p'$$

$$(T_h - T_c) = \frac{q_v L^2}{k_f}$$

$$T' = \frac{T - T_c}{T_h - T_c} \quad or\ \ T = T'(T_h - T_c) + T_c$$

$$T' = \frac{T - T_c}{T_h - T_c}\ = \frac{(T - T_c)k_f}{q_v L^2}$$

Where, L is the length of the chip, v' is non-dimensional velocity in Y direction, p' is non-dimensional pressure, u' is non-dimensional velocity in X direction, T_c is the temperature of right wall, x' is non-dimensional X coordinate,q_v is the heat flux per unit volume, y' is non-dimensional Y coordinate, T' is non-dimensional represent temperature, k_f is thermal conductivity of fluid, Ra is Rayleigh number, Pr is Prandtl number, α is thermal diffusivity.

The non-dimensional fluid domain governing equation can be expressed:

Non-dimensional continuity equation:

$$\frac{\partial u'}{\partial x'} + \frac{\partial v'}{\partial y'} = 0 \tag{4.28}$$

Now substitute non-dimensional quantities into momentum equation (4.26)

$$\rho\left[\frac{\alpha\sqrt{R_aP_r}}{L}\right]\left[\frac{\frac{\alpha\sqrt{R_aP_r}}{L}}{L}\right]\left[u\frac{\partial v'}{\partial x'}+v\frac{\partial v'}{\partial y'}\right]=$$

(4.29)

$$-\rho\left[\frac{\alpha^2R_aP_r}{L^2}\frac{1}{L}\right]\frac{\partial p'}{\partial y'}+\left[\frac{\alpha\sqrt{R_aP_r}/L}{L^2}\right]\mu\left[\frac{\partial^2 v'}{\partial x'^2}+\frac{\partial^2 v'}{\partial y'^2}\right]+\left[\frac{\rho g_y\beta L^2T'q_v}{k_f}\right]\left[\frac{\vartheta}{\vartheta}\right]$$

Multiply by

$$\frac{L^3}{\rho\alpha^2R_aP_r}$$

Where on the body force term

$$\left[\frac{q_vg_y\beta L^5}{k\alpha\vartheta}\right]\left[\frac{1}{R_aP_r}\right]\left[\frac{\vartheta}{\alpha}\right]T' = T'$$

The non-dimensional equation of the momentum equation is

$$\left[u'\frac{\partial v'}{\partial x'}+v'\frac{\partial v'}{\partial y'}\right]=-\frac{\partial p'}{\partial y'}+\sqrt{\frac{P_r}{R_a}}\left[\frac{\partial^2 v'}{\partial x'^2}+\frac{\partial^2 v'}{\partial y'^2}\right]+T' \tag{4.30}$$

Now Non-dimensionalisation of fluid energy equation (4.27), Where

$$T = T'(T_h - T_c) + T_c \tag{4.31}$$

Then the first differential equation of T

$$\frac{\partial T}{\partial x} = \frac{(T_h - T_c)}{L}\frac{\partial T'}{\partial x'} \tag{4.32}$$

The second differential equation of T is

$$\frac{\partial^2 T}{\partial x^2} = \frac{(T_h - T_c)}{L^2}\frac{\partial^2 T'}{\partial x'^2} \tag{4.33}$$

Now substitute non-dimensional parameter of u', v', y', x' and equations 4.32 and 4.33 into energy equation 4.27

$$\rho c_p \frac{\alpha\sqrt{R_a P_r}}{L}\frac{(T_h - T_c)}{L}\left[u'\frac{\partial T'}{\partial x'} + v'\frac{\partial T'}{\partial y'}\right] = \mathrm{k_f}\frac{(T_h - T_c)}{L^2}\left[\frac{\partial^2 T'}{\partial x'^2} + \frac{\partial^2 T'}{\partial y'^2}\right] \quad (4.34)$$

Now, rearrange equation 4.34

$$\frac{\rho c_p}{\mathrm{k_f}}\alpha\sqrt{R_a P_r}\left[u'\frac{\partial T'}{\partial x'} + v'\frac{\partial T'}{\partial y'}\right] = \left[\frac{\partial^2 T'}{\partial x'^2} + \frac{\partial^2 T'}{\partial y'^2}\right] \quad (4.35)$$

Where $\alpha = \frac{\mathrm{k_f}}{\rho c_p}$ the non-dimensional energy of fluid will be

$$\sqrt{R_a P_r}\left[u'\frac{\partial T'}{\partial x'} + v'\frac{\partial T'}{\partial y'}\right] = \left[\frac{\partial^2 T'}{\partial x'^2} + \frac{\partial^2 T'}{\partial y'^2}\right] \quad (4.36)$$

Energy equation for the three chips

$$\rho \mathrm{c_p}\left[\frac{\partial T}{\partial \mathrm{t}} + u\frac{\partial T}{\partial x} + v\frac{\partial T}{\partial y}\right] = q_v + \mathrm{k_{chip}}\left[\frac{\partial^2 T}{\partial x^2} + \frac{\partial^2 T}{\partial y^2}\right] \quad (4.37)$$

Because no fluid movement and the problem is steady state

$$0 = q_v + k_{chip}\left[\frac{\partial^2 \mathrm{T}}{\partial x^2} + \frac{\partial^2 \mathrm{T}}{\partial y^2}\right] \quad (4.38)$$

Where

$$T' = \frac{\mathrm{T} - \mathrm{T_c}}{(\mathrm{T_h} - \mathrm{T_c})}$$

$$(\mathrm{T_h} - \mathrm{T_c}) = \frac{q_v\ \mathrm{L}^2}{\mathrm{k_f}}$$

So,

$$\mathrm{k_f} = \frac{q_v\ \mathrm{L}^2}{\Delta \mathrm{T}}$$

The non-dimensional Energy equation for the chip after Substitute non-dimensional quantities and equation 4.33

$$0=q_v+k_{chip}\frac{\Delta T}{L^2}\left[\frac{\partial^2 T'}{\partial x'^2}+\frac{\partial^2 T'}{\partial y'^2}\right] \tag{4.39}$$

Multiply the equation into $\frac{\mathrm{L}^2}{\Delta\mathrm{T}}$

$$0=\frac{q_v\mathrm{L}^2}{\Delta\mathrm{T}}+\mathrm{k_{chip}}\left[\frac{\partial^2 T'}{\partial x'^2}+\frac{\partial^2 T'}{\partial y'^2}\right]$$

Where

$$\frac{q_v\mathrm{L}^2}{\Delta\mathrm{T}}=\mathrm{k_f}$$

Then non-dimensional of the Energy equation for the chip is

$$0=1+\frac{\mathrm{k_{chip}}}{\mathrm{k_f}}\left[\frac{\partial^2 T'}{\partial x'^2}+\frac{\partial^2 T'}{\partial y'^2}\right] \tag{4.40}$$

Energy equation for the substrate

$$\rho c_p\left[\frac{\partial\mathrm{T}}{\partial\mathrm{t}}+\mathrm{u}\frac{\partial\mathrm{T}}{\partial\mathrm{x}}+\mathrm{v}\frac{\partial\mathrm{T}}{\partial\mathrm{y}}\right]=q_v+k_{\mathrm{s}}\left[\frac{\partial^2\mathrm{T}}{\partial\mathrm{x}^2}+\frac{\partial^2\mathrm{T}}{\partial\mathrm{y}^2}\right] \tag{4.41}$$

Because no fluid movement, no heat source and the problem is steady state

$$0=k_s\left[\frac{\partial^2\mathrm{T}}{\partial\mathrm{x}^2}+\frac{\partial^2\mathrm{T}}{\partial\mathrm{y}^2}\right] \tag{4.42}$$

The non-dimensional Energy equation for the substrate after Substitute non-dimensional quantities and equation 4.33

$$0=\mathrm{k_s}\frac{\Delta\mathrm{T}}{\mathrm{L}^2}\left[\frac{\partial^2 T'}{\partial x'^2}+\frac{\partial^2 T'}{\partial y'^2}\right]$$

Where

$$\frac{\Delta\mathrm{T}}{\mathrm{L}^2}=\frac{q_v}{\mathrm{k_f}}$$

The q_v assumed to be 1, so the non-dimensional equation of the substrate is

$$0=\frac{\mathrm{k_s}}{\mathrm{k_f}}\left[\frac{\partial^2 T'}{\partial x'^2}+\frac{\partial^2 T'}{\partial y'^2}\right] \quad (4.43)$$

Where, k_{chip} is the chip thermal conductivity, k_f is the fluid thermal conductivity, k_s is the substrate thermal conductivity.

The Rayleigh number (Ra) is defined by specifying the heat source (Chips).

$$Ra=\frac{g\beta\rho^2 q_v C_p L^5}{k_f\mu} \quad (4.44)$$

Where L is width of the chip, q_v is the heat source of the chip per unit volume, β is thermal expansion coefficient, ρ is a density, C_p is specific heat capacity, k_f is thermal conductivity and μ is the dynamic viscosity.

Liu and Phan-thien [16] used software called Fasttalk which is based on the finite element method. The simulations presented here are solved using COMSOL v4.3 using a conjugate heat transfer model to couple the conduction and convection of heat. The Ra is 1×10^5, Prandtl number (Pr) is 0.7 and from the non-dimensional governing equation the fluid thermal properties are:

$$\mu=\sqrt{\frac{\mathrm{Pr}}{Ra}} \quad (4.45)$$

$$C_p=\sqrt{RaPr} \quad (4.46)$$

The density is ρ=1.

The thermal conductivity of the solid domain

Thermal conductivity of chip $=\frac{\mathrm{K}_{chip}}{K_f}$

Thermal conductivity of Substrate $= \frac{K_s}{K_f}$

Where K_{chip}= 2.63, K_f= 0.0263 and K_s= 0.263.

The boundary conditions of this problem are

For all solid boundary

$$\boldsymbol{u} = 0 \tag{4.47}$$

For the facing the substrate

$$T' = 0 \tag{4.48}$$

For the rest of walls (adiabatic)

$$\frac{\partial T'}{\partial n} = 0 \tag{4.49}$$

The temperature continue between heat source and substrate

$$T'_{chip} = T'_s \tag{4.50}$$

The heat flux continue

$$\frac{k_{chip}}{k_f}\left(\frac{\partial T'}{\partial n}\right)_{chip} = \frac{k_s}{k_f}\left(\frac{\partial T'}{\partial n}\right)_s \tag{4.51}$$

The temperature continue between heat source and fluid

$$T'_{chip} = T'_f \tag{4.52}$$

The heat flux continue

$$\frac{k_{chip}}{k_f}\left(\frac{\partial T'}{\partial n}\right)_{chip} = \left(\frac{\partial T'}{\partial n}\right)_f \tag{4.53}$$

The temperature continue between substrate and fluid

$$T'_s = T'_f \tag{4.54}$$

The heat flux continue

$$\frac{k_s}{k_f}\left(\frac{\partial T'}{\partial n}\right)_s = \left(\frac{\partial T'}{\partial n}\right)_f \tag{4.55}$$

Figure 4.10 is showing the results of Liu and Phan-Thien and the validation results of the temperature along the substrate. This case is type1 which S_1 = 1.5, S_2= 2, S_3= 2 and S_4= 1.5. The results of model that is done by COMSOL is so close to Liu and Phan-Thien results. The average error is 2.1%, consequently validation is in good agreement with the previous study.

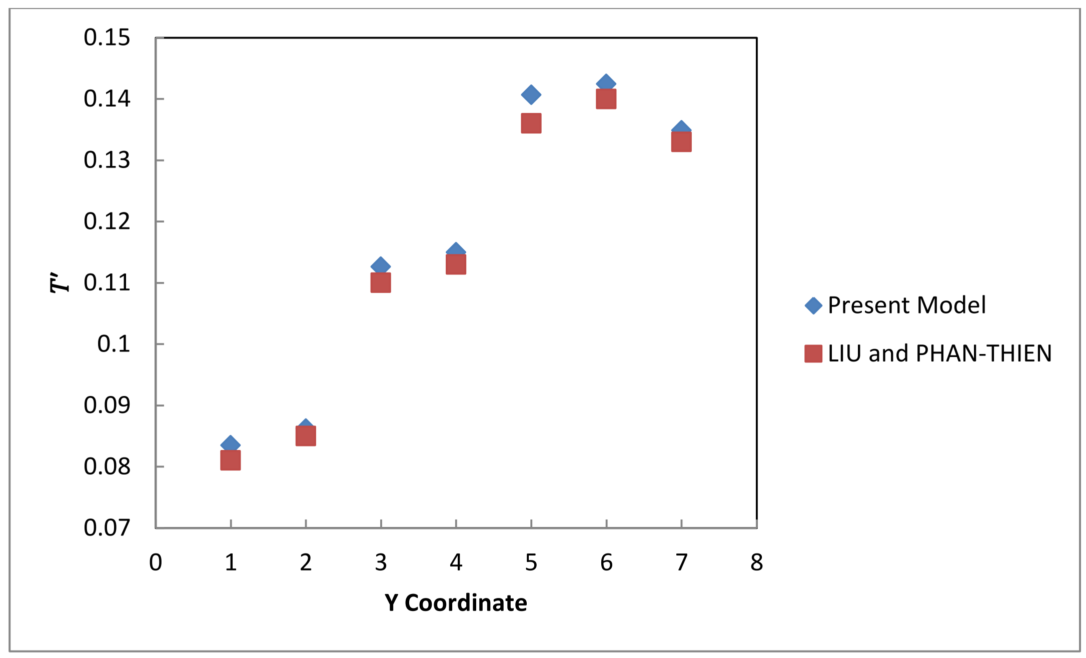

Figure 4.10: Temperature profile along substrate surface to compare simulation model and Liu and Phan-Thien results.

4.5 Turbulent finned enclosure

The model that is investigated in this thesis is an immersed server (see chapter 5). The fluid flow behaviour inside the server is turbulent as explained in chapter 5 section 5.2.2. Thus, this section validates a published experiment for finned enclosure that was developed by Nada [19] where the fluid flow is a turbulent and in this thesis too. The diagram of the experimental setup for the finned enclosure is shown in Figure 4.11. The rate of heat that is generated on the left hot plate is 500W and the heat transfer media inside the enclosure is air. The water is used as a cooling liquid on the cold plate. The orientation of the enclosure is vertical at Y axis and the height between the hot plate and cold plate is H = 40 mm, the depth of the enclosure is b = 200 mm and the width is a = 320 mm.

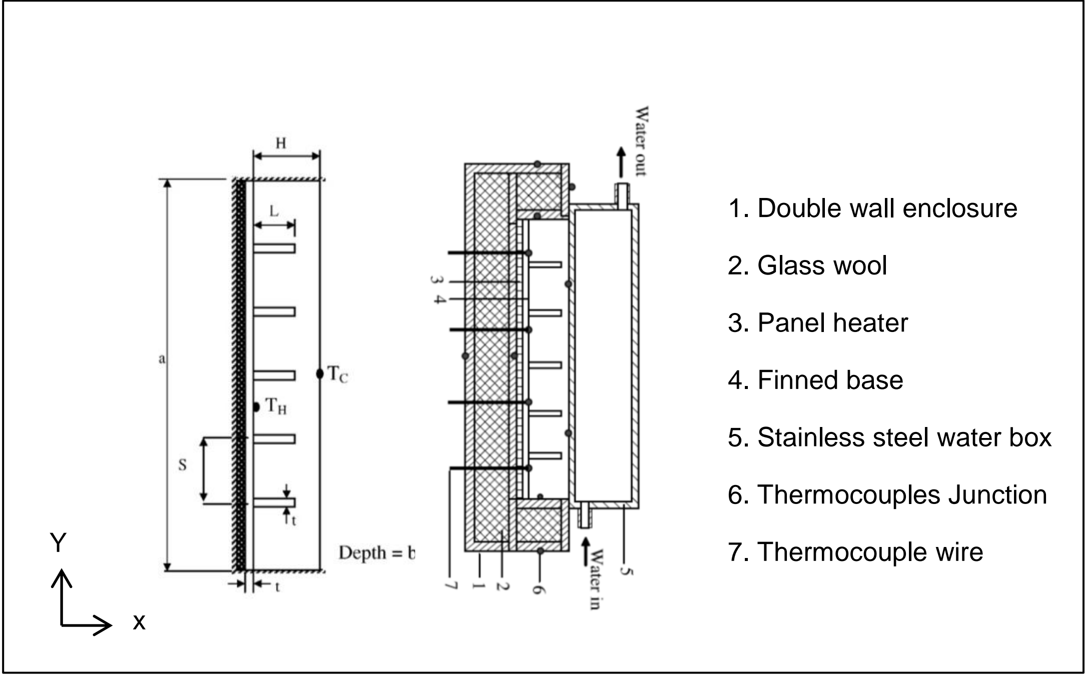

Figure 4.11: Schematic diagram of experiment setup of finned enclosure[19].

The study is performed by changing the number of fin, fin spacing (S/H) and Fin length (L/H). The empirical correlation for the heat transfer that was obtained for a vertical finned enclosure from the experiment was found to be:

$$N_u = 1.33Ra^{0.56}\left(\frac{L}{H}\right)^{0.22}\left(0.022\left(\frac{S}{H}\right)^3 - 0.096\left(\frac{S}{H}\right)^2 + 0.131\left(\frac{S}{H}\right) - 0.044\right) \tag{4.56}$$

Where, N_u is Nusselt number, L is fin length, S is the space between the fins. The simulation model of finned enclosure is presented in Figure 4.12. To compare experiment work with simulation modelling, the dimensions and properties need to be the same. The dimensions that is used in simulation

model are H= 40mm, S= 80mm and L= 20mm. thus, the ratio of fin length L/H= 0.5, the space between the fin S/H=2.

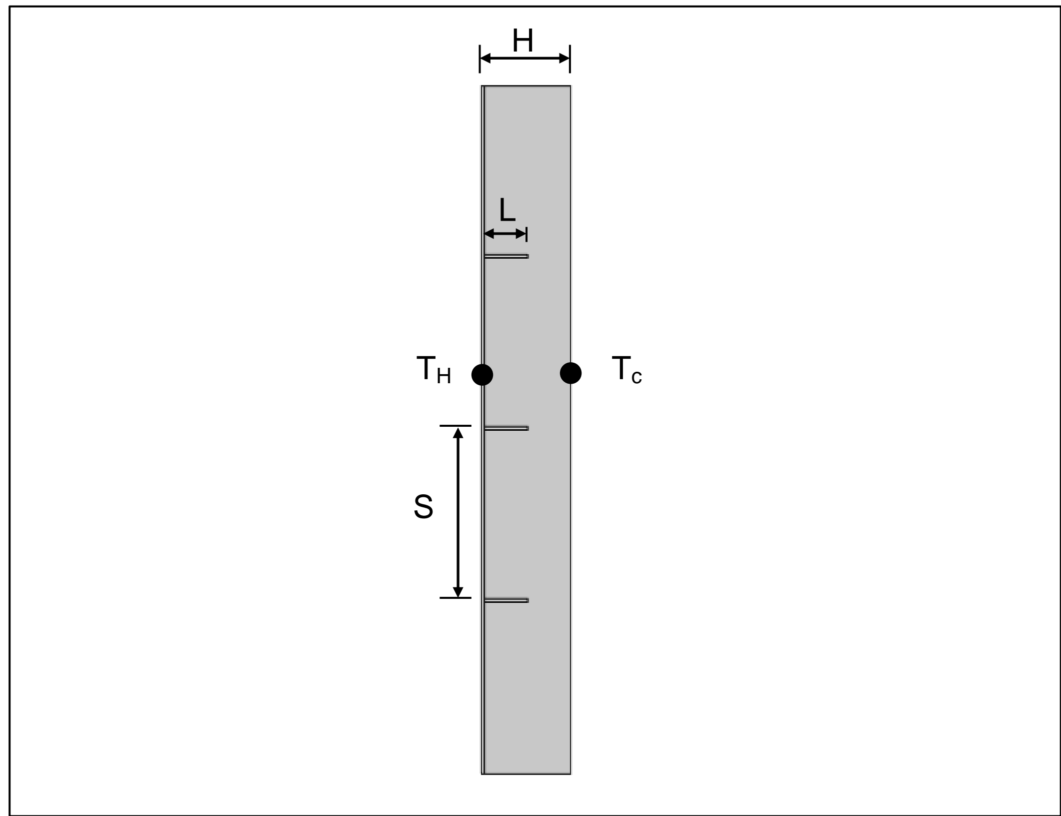

Figure 4.12: Finned enclosure of model simulation in this work where N = 3, L/H =0.5 and S/H=2

The heat flux is adjusted from 80 W to 500 W to provide Rayleigh number and T_c kept constant at 303 K. The temperature on the hot plate (T_h) is obtained from the model. Consequently, the heat transfer coefficient can be calculated from

$$h = \frac{q}{(T_H - T_c)} \tag{4.57}$$

Where the h is the heat transfer coefficient, q is the input heat flux. The Nusselt number for this study has been calculated by,

$$N_u = \frac{h\mathrm{H}}{K_f} \tag{4.58}$$

The Rayleigh number (Ra) is calculated by knowing the fluid properties and obtains the T_H from the simulation model.

$$R_a = \frac{g\beta\rho^2 C_p (T_H - T_c) H^3}{k\mu} \tag{4.59}$$

Where k is the thermal conductivity, C_p is specific heat capacity, ρ is density and β is thermal expansion coefficient for the air. The thermal fluid properties were taken at the mean temperature, which is the average of hot plate temperature and cold plate temperature.

$$T_m = \frac{T_H + T_c}{2} \tag{4.60}$$

The turbulent model that is used in the simulations is the *k*-ω, used here since it has been used for natural convection turbulent flows in enclosures and showed good agreement with experiments [93] [92] [91]. Figure 4.13 show that the simulation model is in good agreement with experiment results. The average error between simulation model and experiment result doesn't exceed 4.8%. In this study this error can be considered as adequate for numerical and experiment the validation.

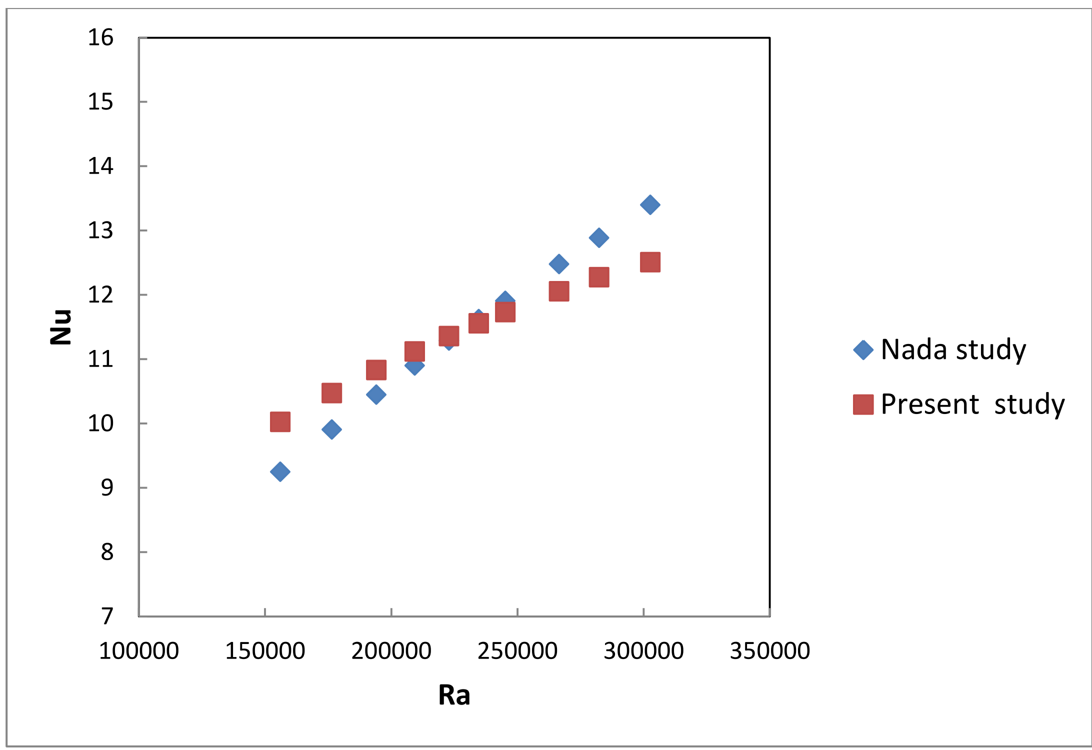

Figure 4.13: Comparison of present study model with experiment for Nusselt number.

4.6 Cold plate validation

The immersed server considered in the Chapter 6 has a water jacket that transports the heat – this is essentially a cold plate on the cold side (see Chapter 6). The previous sections have validated the aspects of natural convection. However, this section is performed to do a validation with forced convection, i.e. water pumped via a cold block. The validation in this section is for industrial cold plate designed by the AVVID THERMALLOY [101] as shown in Figure 4.14. The water in the cold plate is used as liquid coolant which passes through copper pipe. The pipe is inside the Aluminum substrate. The heat source underneath the cold plate generates 100W. The inlet water temperature is 283 K that flows to cool the heat source. All the

Aluminum block walls are considered to be insulated except the bottom. The flow rate is varying from 2 to 4 US gallons per minute (GPM).

The water passes through pipe which has different cross sectional areas as it is presented in Figure 4.15. The two cross sectional areas for the pipe are shown in Figure 15. It is difficult to model the two different pipe geometries in COMSOL due to mesh convergence. Based on the simulation analysis of the cold plate model, it was found that the cross section of the pipe has an influence on the pressure drop. In case of using circular pipe for the entire model, the pressure drop of the model is less than pressure drop of the AVVID THERMALLOY results. This is due to the difference in the area between the actual cold plate and the simulation model. On the other hand, in the case of using the semi-circle cross section pipe the pressure drop of the model is greater than the presser drop of the AVVID THERMALLOY, because the internal area of the pipe is smaller than AVVID THERMALLOY. In order to overcome this problem, an average cross sectional area was considered and used in the simulation analysis. It was seen that the pressure drop for the proposed model showed very good agreement with the AVVID THERMALLOY pressure. This gives more confidence in carrying out the simulation with the current approach.

The areas of the circular and semi-circular pipes are 38.68 mm^2 and 27.32 mm^2 respectively. According to the proposed approach, the equivalent area for the model is 33 mm^2.

The water inlet is changed based on the velocity in the simulation model. The AVVID THERMALLOY inlet is based on the flow rate. So velocity can be calculated:

$$V = \frac{4Q_{in}}{\pi D_{in}^2} \tag{4.61}$$

Where the Q_{in} is the flow rate in m^3/s and the D_{in} is the inner diameter in m.

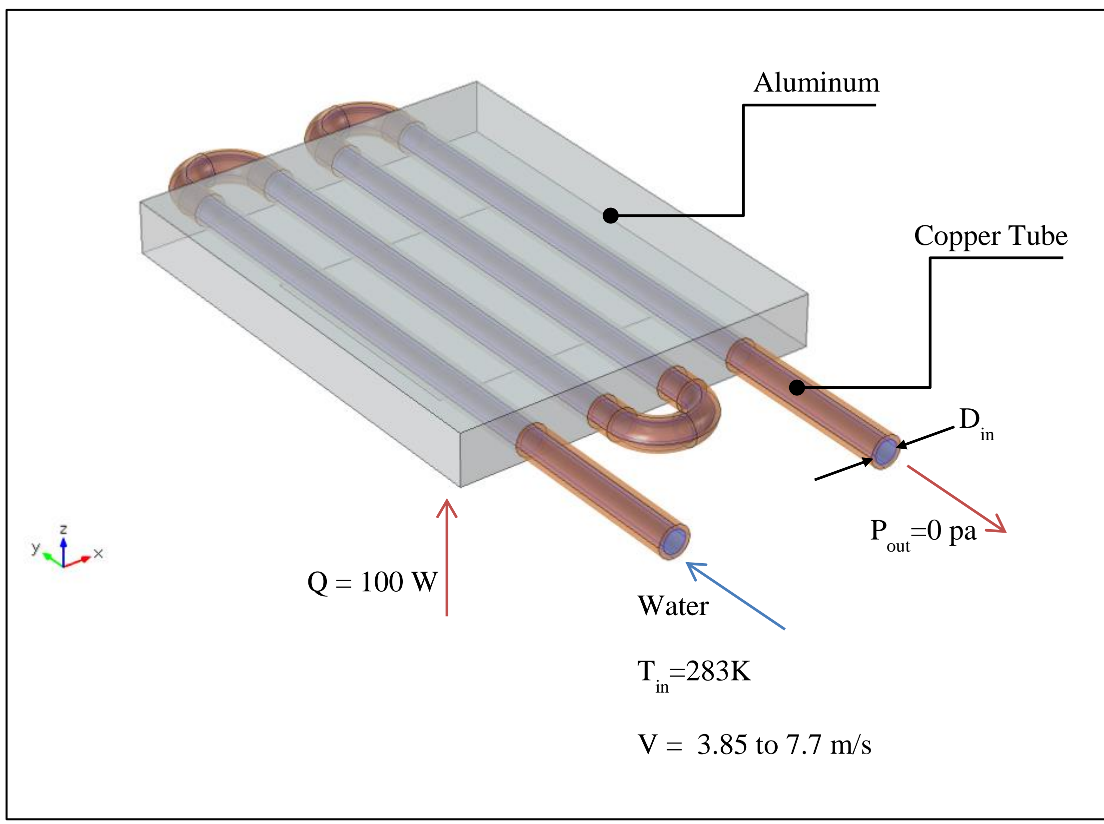

Figure 4.14: Simulation model components of validation AVVID cold plate

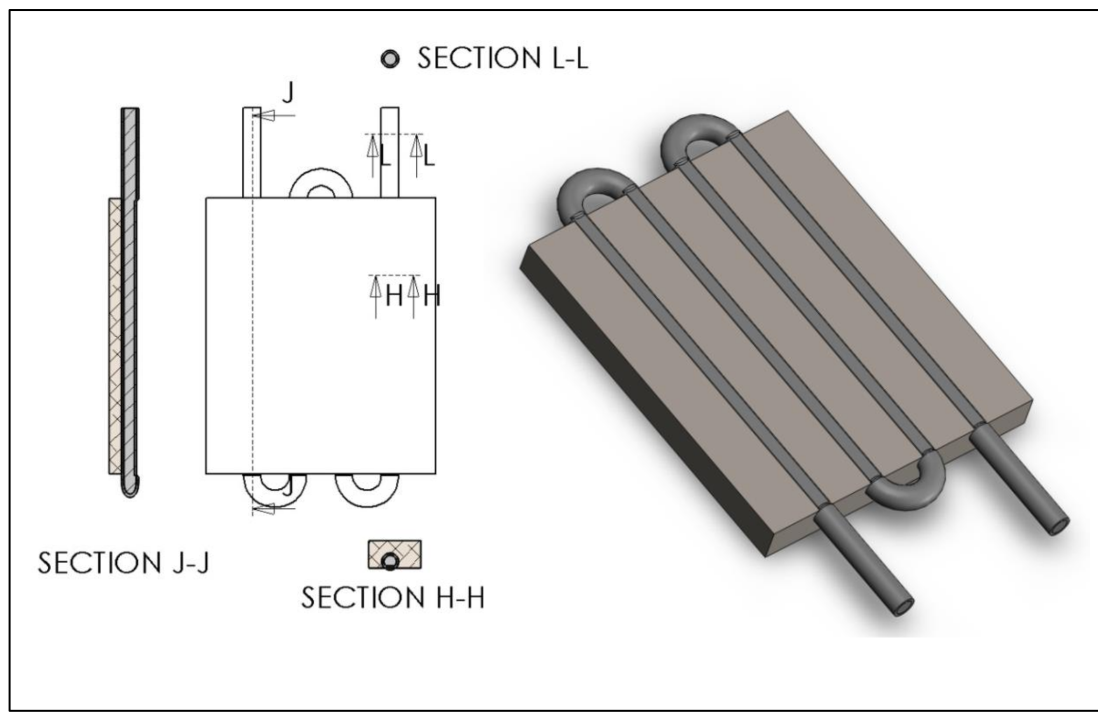

Figure 4.15: AVVID model geometry showing the different cross section of real cold plate

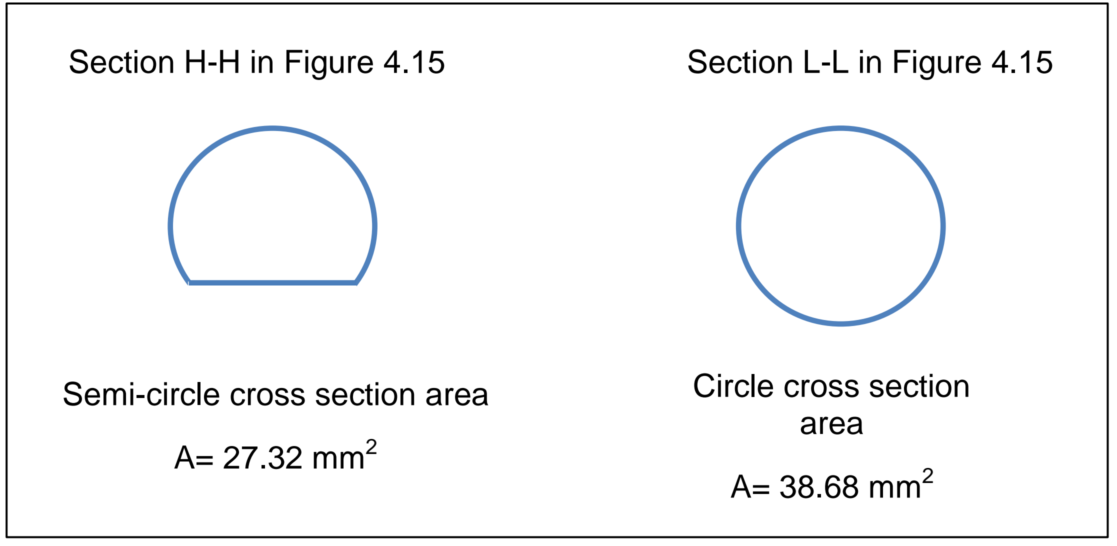

Figure 4.16: Zoom-in to different cross section areas that the water passes through in clod plate pipe

The water flow behaviour needs to be investigated to know the water flow is turbulent or laminar. The water flow behaviour inside the pipe can be determined by calculating Reynolds number which can be expressed as

$$Re = \frac{\rho V D_{in}}{\mu} \tag{4.62}$$

Here, ρ is water density (1002 Kg/m^3), V inlet water velocity for the smallest velocity value in this validation (3.85 m/s), μ is dynamic viscosity (0.001317124 Pa.s) and D_{in} the inside diameter (6.46 mm). The Reynolds number found to be 18922.3, which is sufficiently large for water flow in pipes to be treated as turbulent flow [86].

Therefore, the simulation model used a turbulent conjugate heat model to validate against the AVVID cold plate experimental data. The *k*-ε turbulent model is applied to solve the simulation of cold plate because K- ε provides better results in comparison to experiment for the flow in pipes [102] it is commonly used in industrial application due its robustness [103] [104]. The K-ε model uses the wall function near to the wall as explained in detail in chapter 3. Thus, the Wall lift off could affect the accuracy of the solution (see chapter 3 section 3.4.2), so the wall lift off needs to be checked for when using the K-ε. Table 4.6 shows a different wall lift off surfaces for a different velocity values. As the velocity increases, the values of wall lift off increases too. However, the wall lift off values in all different velocities is within the recommended range. The wall lift off values is not significantly higher than 11.06 on most of the wall (see chapter 3 section 3.4.2).

Table 4.6: Wall lift off inside the water pipe in the cold plate for different velocities

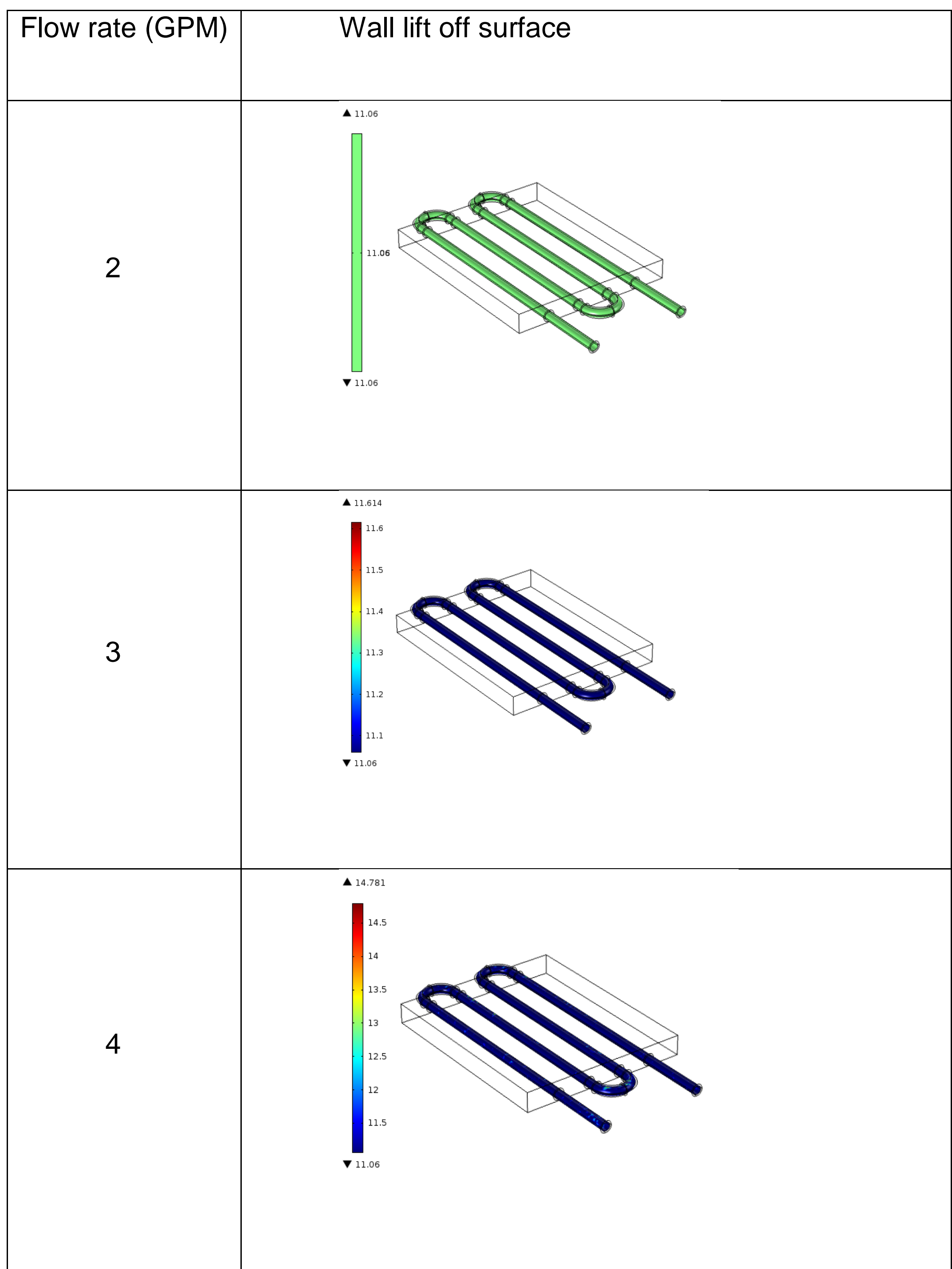

Flow rate (GPM)	Wall lift off surface
2	
3	
4	

4.6.2 Cold plate validation results

The validation of the cold plate simulation model against the AVVID experimental result is carried out by comparing pressure drop and thermal resistance versus the flow rate. Figure 4.17 shows the variation of pressure drop with flow rate for simulation model and AVVID. The flow rate is varied from 2 to 4 GPM. The average error of pressure drop between the simulation model and experiment is 3%. This proves that the results of simulation model and experiment are in good agreement.

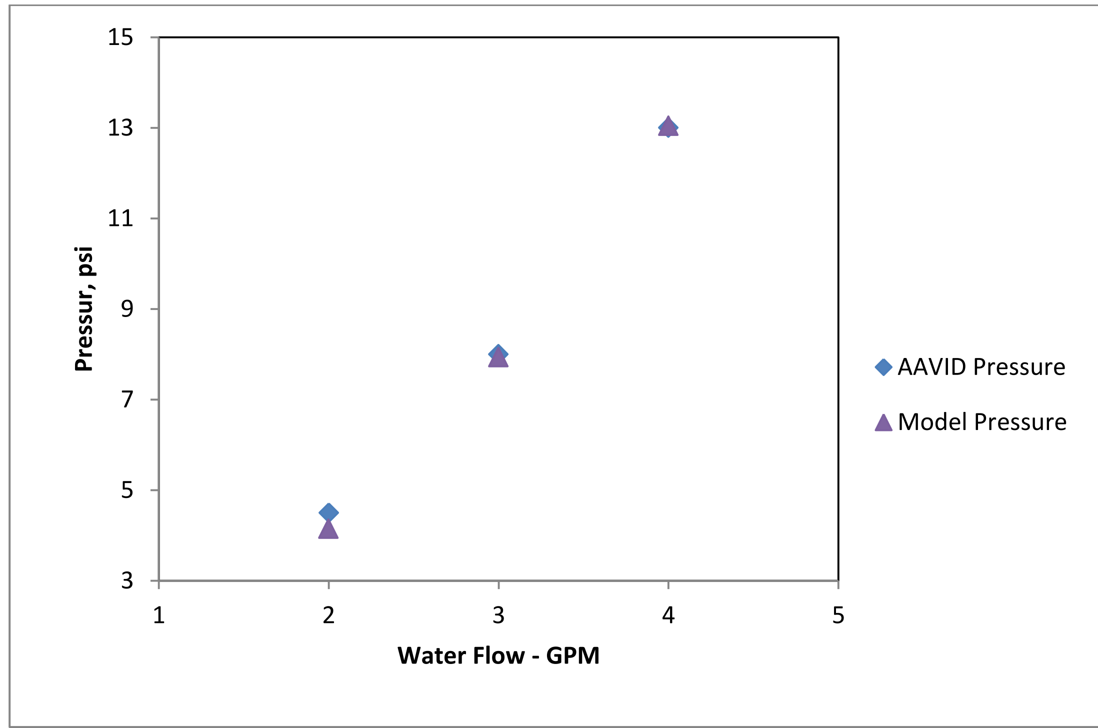

Figure 4.17: The validation of simulation model and AAVID results by varying the flow rate and measuring the pressure drop.

An alternative approach of comparing the results of simulation model with experiment in terms of the heat transfer, the thermal resistance can be used. The thermal resistance can be calculated from the following equation

$$R_s = \frac{T_{s,max} - T_{in}}{Q}$$

Where, R_s is the thermal resistance, $T_{s,max}$ is the maximum temperature for the hot surface T_{in} is the inlet temperature and Q is the total heat flux. The inlet temperature and flow rate are known, however, the maximum temperature value of the hot surface is obtained from the results of the simulations.

The variation of thermal resistance with flow rate for the simulation model and experiment are shown in Figure 4.18. The results from the figure demonstrate that the comparing the thermal resistances of the simulations with the experimental results of the cold plate yield good agreement with an average error of 3.46%.

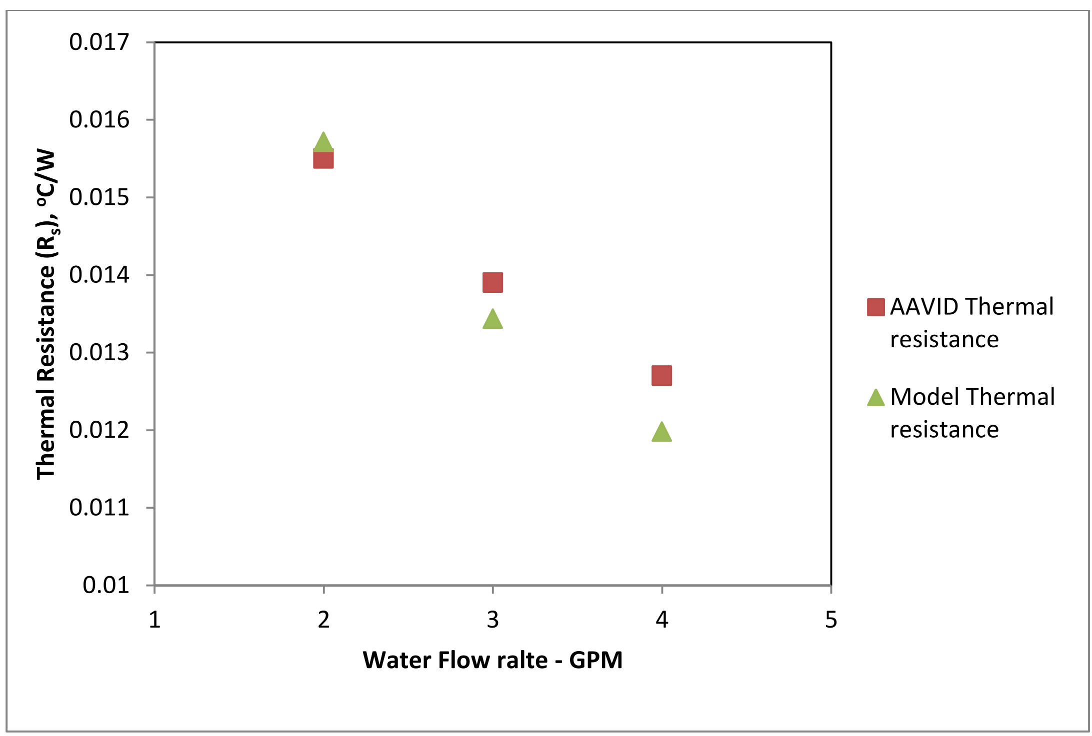

Figure 4.18: The validation of simulation model and AAVID results by varying the flow rate and measure the Thermal resistance drop

4.7 Summary

This chapter has shown validation of numerical and experiment work with simulation model using COMSOL 4.3. The aim of the validation is to build up the important components of the immersed server and ascertain whether COMSOL is an appropriate tool that can be used to create a full simulation model for the conjugate heat transfer in an immersed server. The validation started with a 2D natural convection benchmark, after that the comparison of different CFD packages such as COMSOL and Fluent were presented for the 2D natural convection problem. Then, the validation carried out of numerical model for rectangular enclosure contains three heat sources. A simulation model using COMSOL was validated with experiment work of the finned enclosure. The last section developed a simulation model of an

industrial cold plate. In summary, COMSOL is found to be an effective tool for simulating buoyancy driven flows with complex conjugate heat transfer. Good agreement is obtained with a range of buoyancy driven flows, COMSOL now will be used in the analysis of the immersed liquid server

CHAPTER 5:

OPTIMAL HEAT SINK FIN AND COLD PLATE HEIGHTS FOR LIQUID IMMERSED SERVERS OF MODEL AND SIMULATION

5.1 Introduction

In the previous chapter, the validation of the different cases shows that the Finite Element simulation package, COMSOL, is capable of simulating a turbulent naturally convecting flow where there are buoyancy driven forces on the flow.

The immersed server model is simulated in this chapter using COMSOL with a set up that is similar to the finned rectangular enclosure and heat source in enclosure. The immersed server idea is that the server is fully submerged into a dielectric liquid and the heat is removed by convection from the CPU on one side to the cold plate on the opposite side. This chapter focuses on optimising the heat transfer by looking at the heat sink

fin height (H_{fin}) and the cold plate height (H_{plate}) as shown in Figure 5.1. The objective of this study is to minimise the temperature of the top centre temperature of the CPU, which is referred to as the T_{case} value.

In this chapter a model of turbulent natural convection flow and conjugate heat transfer is developed to investigate heat transfer in a vertical sever filled with dielectric liquid. The CPU heat flux and cold plate temperature remained constant. An Optimal Latin Hypercube [105] design of experiment and Genetic Algorithm (GA) optimisation method were used. The main objective of this work is to find the optimum heat sink fin height and cold plate height in order to reduce the temperature of the T_{case}.

5.2 Modelling methodology

5.2.1 Model geometry

The model being investigated consists of slice of a server with the dimensions 400mm x 4.5mm x Height of plate as a range between (30 – 45 mm). This is because the 1U (Industrial standard naming for server height) recommends it to be 45mm. the server was modelled in vertical position. The top and bottom wall assumed to be insulated. A 45mm x 45mm CPU (100W) was used on the bottom of the heat sink to generate heat. The temperature on the cold surface or cold plate was constant at 303.15 K.

Figure 5.1 illustrates the geometry of slice server. The heat sink fin is made of copper. the heat sink base area is 90mm x 70mm and fin thickness 1.5mm and the space between the fin 3mm [8]. All the dimensions were kept constant except the two parameters; heat sink fin height (H_{fin}) and cold

plate height (H_{plate}). The side walls have symmetry boundary conditions. Using symmetry configuration reduces the computational domain and time.

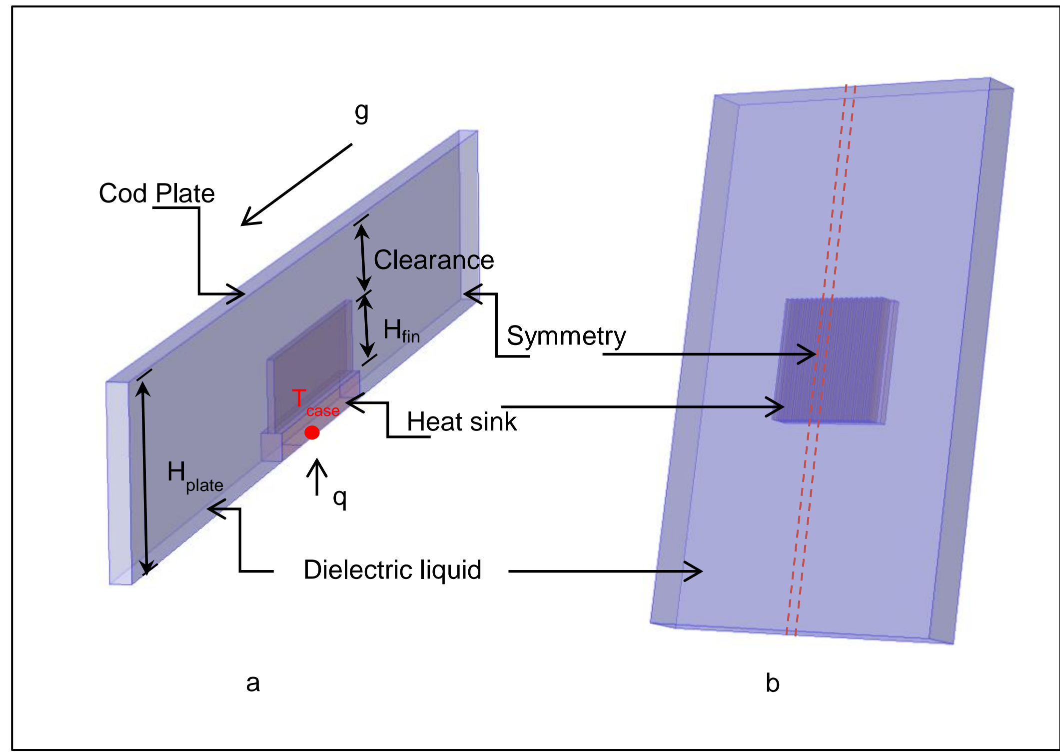

Figure 5.1: Geometry of a) Computational domain b) Server

5.2.2 Mathematical Model

The first step in solving the model is to determine whether the flow is turbulent or laminar. In case of natural convection the fluid flow classification can be determined by calculating Ra. As the heat is generated by heat flux, the Ra formula used as following:

$$Ra = \frac{g\beta(T_h - T_c)H_{plate}^3\rho^2 C_p}{\lambda\mu} \tag{5.1}$$

Where Ra is Raleigh number, T_h is the average temperature of CPU and T_c is average temperature of the cold, ρ is fluid density , C_p is specific heat capacity , λ is thermal conductivity , μ is dynamic viscosity , g is gravity force, β is thermal expansion coefficient.

The Ra value of this case is $6.4x10^8$ which is greater than 10^7 so the flow is considered to be turbulent [15]. For turbulent fluid flow in an enclosure, the reliable turbulent model is *k*-ω model as investigated in [91-93]. Therefore, this study used K-ω model.

The governing equations which represent the continuity, energy and momentum have been solved by COMSOL v4.3 for turbulent natural convection inside the immersed server model,

Continuity equation

$$\nabla.(\rho \boldsymbol{u_D}) = 0 \tag{5.2}$$

Momentum equation

$$\rho(\boldsymbol{u_D}.\nabla)\boldsymbol{u_D} = \nabla.\Big[-p\boldsymbol{I} + (\mu_D + \mu_{DT})(\nabla \boldsymbol{u_D} + (\nabla \boldsymbol{u_D})^T) - \frac{2}{3}(\mu_D + \mu_{DT})(\nabla.\boldsymbol{u_D})\boldsymbol{I} - \frac{2}{3}\rho k\boldsymbol{I}\Big] + \boldsymbol{F} \tag{5.3}$$

The body force is **F** which mainly depends on the density variation. The temperature increases the density of the fluid decreases. This drive the buoyancy force which can be expressed as:

$$\boldsymbol{F} = \rho(T)\boldsymbol{g} \tag{5.4}$$

Where the g= (0,0,g) is the gravity force in Z direction. The dielectric liquid density is given as a function of temperature [106]

$$\rho(T) = 1716.2 - 2.2T \tag{5.5}$$

The K- ω turbulent models introduce two additional variables turbulent kinetic energy, k, and specific dissipation rate, ω. The transport equation [81] which use in the CFD model are:

$$\rho(\boldsymbol{u_D}.\nabla)k = \nabla.[(\mu_D + \mu_{DT}\sigma_k^*)\nabla k] + p_k - \rho\beta_0^* k\omega \quad (5.6)$$

$$\rho(\boldsymbol{u_D}.\nabla)\omega = \nabla.[(\mu_D + \mu_{DT}\sigma_\omega)\nabla\omega] + \alpha\frac{\omega}{k}p_k - \rho\beta_0\omega^2 \quad (5.7)$$

The turbulent viscosity can be defined as

$$\mu_{DT} = \rho\frac{k}{\omega} \quad (5.8)$$

The production term can be obtained from

$$p_k = \mu_{DT}\left[\nabla\boldsymbol{u_D}:(\nabla\boldsymbol{u_D} + (\nabla\boldsymbol{u_D})^T) - \frac{2}{3}(\nabla.\boldsymbol{u_D})^2\right] - \frac{2}{3}\rho k\nabla.\boldsymbol{u_D} \quad (5.9)$$

Energy equation

$$\rho c_p\boldsymbol{u_D}\nabla T = \nabla.\left((\lambda_D + \frac{c_p\mu_{DT}}{Pr_T})\nabla T\right) \quad (5.10)$$

Where λ_D is thermal conductivity of dielectric liquid and Pr_T is turbulent Prantl Number (using Kays- Crawford)

The empirical turbulent model constant parameters

$$\alpha = \frac{13}{25}, \sigma_k^* = \frac{1}{2}, \sigma_\omega = \frac{1}{2}, \beta_0 = \frac{9}{125}, \beta_0^* = \frac{9}{100}$$

For the solid domain

$$0 = \nabla.(\lambda_{HS}\nabla T) \quad (5.11)$$

Where, the λ_{Hs} is the thermal conductivity for the heat sink which is copper.

5.2.3 Boundary conditions

The boundary conditions of the simulation model is presented in schematic diagram as shown in Figure 5.2. The boundary conditions are expressed as follows:

No slip on all solid walls,

$$\boldsymbol{u}.n = 0 \quad (5.12)$$

Except CPU and cold plate surface, all the out boundaries of the simulation model are adiabatic

$$-n.(-\lambda \nabla T) = 0 \quad (5.13)$$

Both side planes are symmetry

$$\boldsymbol{u}\,.n = 0 \quad (5.14)$$

$$\boldsymbol{\tau} - (\boldsymbol{\tau}.\mathbf{n})\mathbf{n} = 0 \quad (5.15)$$

$$\text{where } \boldsymbol{\tau} = \left[(\mu_D + \mu_{DT})(\nabla \mathbf{u}_{\boldsymbol{D}} + (\nabla \mathbf{u}_{\boldsymbol{D}})^{\mathrm{T}}) - \frac{2}{3}\rho k \mathbf{I}\right].\boldsymbol{n} \quad (5.16)$$

$$\nabla \mathrm{k}.\mathrm{n} = 0 \quad (5.17)$$

$$\nabla \omega.\mathrm{n} = 0 \quad (5.18)$$

$$-n.(-\lambda \nabla T) = 0 \quad (5.19)$$

There are conjugate heat transfer interfaces which are

Temperature interfaces between the heat sink and dielectric liquid

$$\mathrm{T}_{HS} = T_D \quad (5.20)$$

And heat flux is continuous, so that the heat lost from the heat sink is the same as the heat gained by the dielectric liquid.

$$-n.(-\lambda_{HS} \nabla T_{HS}) = -n.(-\lambda_D \nabla T_D) \quad (5.21)$$

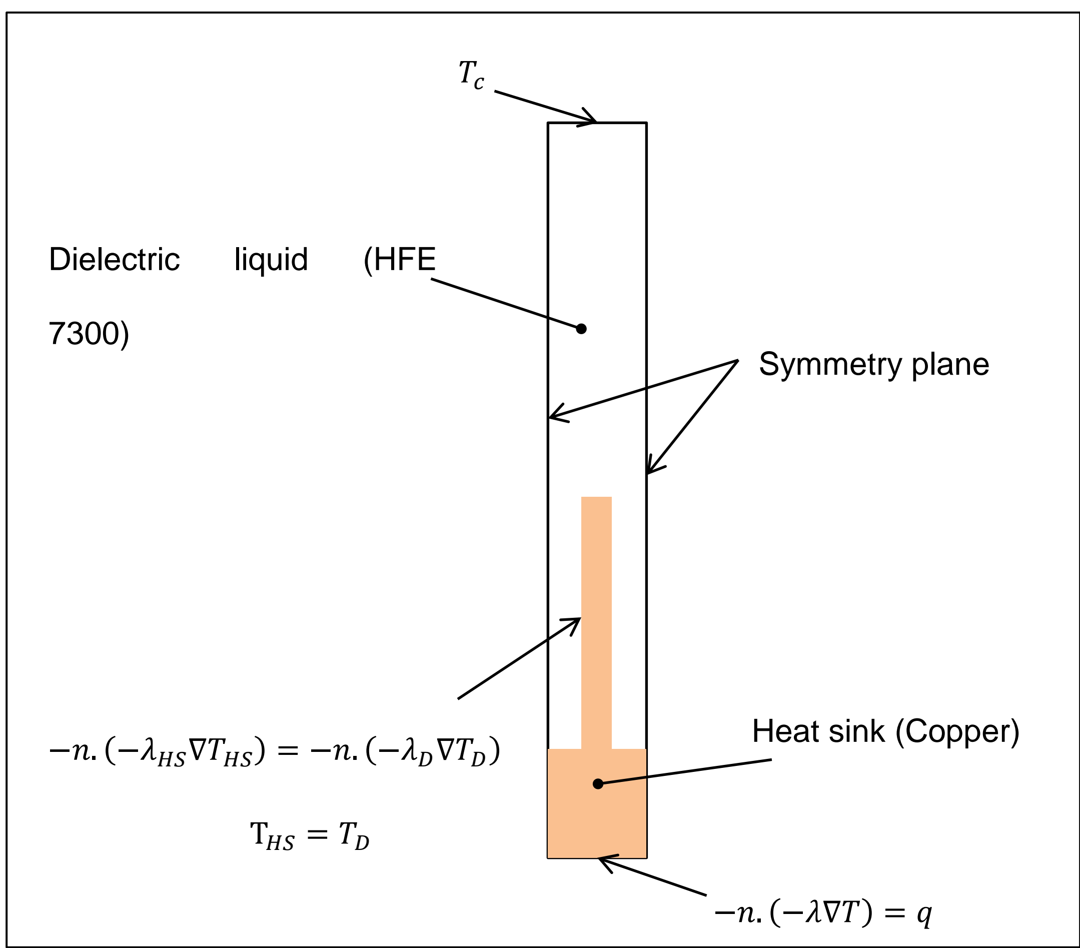

Figure 5.2: Schematic diagram of cut plane in the centre of the model to show the boundary conditions of the model and the conjugate heat

5.2.4 Heat flux calculation

The server with heat sink is shown in Figure 5.3. The heat flux is generated from the CPU with dimensions L_1x L_1 and the rest of the server on this side is insulated. However, for the symmetry model of the computational domain the heat flux extended with symmetry planes. So, the ratio between the CPU and the gap should be taken in account to calculate the heat flux [107].

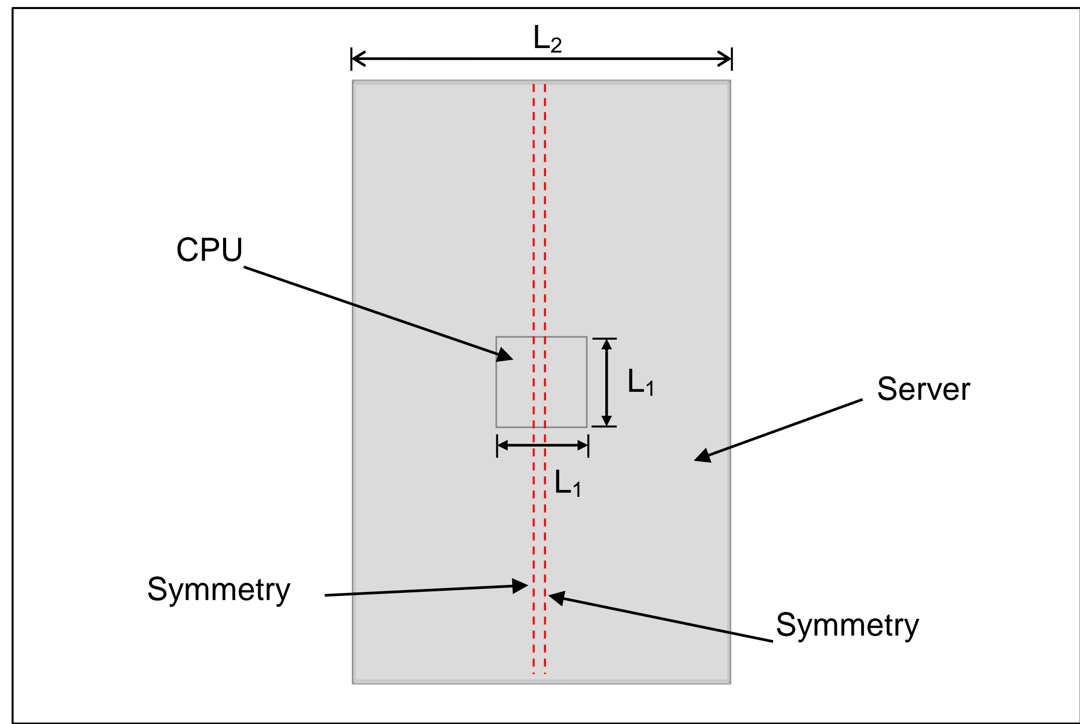

Figure 5.3: CPU and server dimensions

A comparison between the symmetry model and the full server model requires a way of calculating heat flux for the symmetry model in this chapter. The heat from CPU is 100 W and the dimensions of the CPU are 45x 45 mm (L1 xL1). For the server the dimensions are 400x 250 mm. Therefore the heat from for symmetry model and full server can be calculated as follow:

Heat flux calculation:

For symmetry

$$q_{sym} = \frac{Q}{A_{sym}} = \frac{Q}{L_1 L_2} \quad (5.22)$$

For real case 3D

$$q_{3D} = \frac{Q}{A_{3D}} = \frac{Q}{L_1 L_1} \tag{5.23}$$

$$\frac{q_{sym}}{q_{3D}} = \frac{\frac{Q}{A_{sym}}}{\frac{Q}{A_{3D}}} = \frac{\frac{Q}{L_1 L_2}}{\frac{Q}{L_1 L_1}} = \frac{L_1}{L_2} \tag{5.24}$$

$$q_{sym} = \frac{L_1}{L_2} q_{3D} \tag{5.25}$$

$$q_{3D} = \frac{Q}{L_1 L_1} = \frac{100}{0.045x0.045} = 49382.7\ \frac{w}{m^2} \tag{5.26}$$

$$q_{sym} = \frac{L_1}{L_2} q_{3D} = \frac{0.045}{0.25} 49382.7 = 8888.8\ \frac{w}{m^2} \tag{5.27}$$

Where; q_{3D} is the heat flux for the 3D model (W/m^2), q_{sym} is the heat flux for the symmetry model (W/m^2), Q is the total heat flux (W), L_1 is CPU Width and length (m), L_2 is the server width, A_{3D} is area of CPU for 3D, A_{sym} is area of CPU for symmetry.

Figure 5.4 shows the temperature along top centre of the CPU for symmetry model and full server model. The temperature of symmetry and full server models are very close. The error between the symmetry model and the full server model is 0.49%, which corresponds to a temperature difference of 2K. This error is considered to be small.

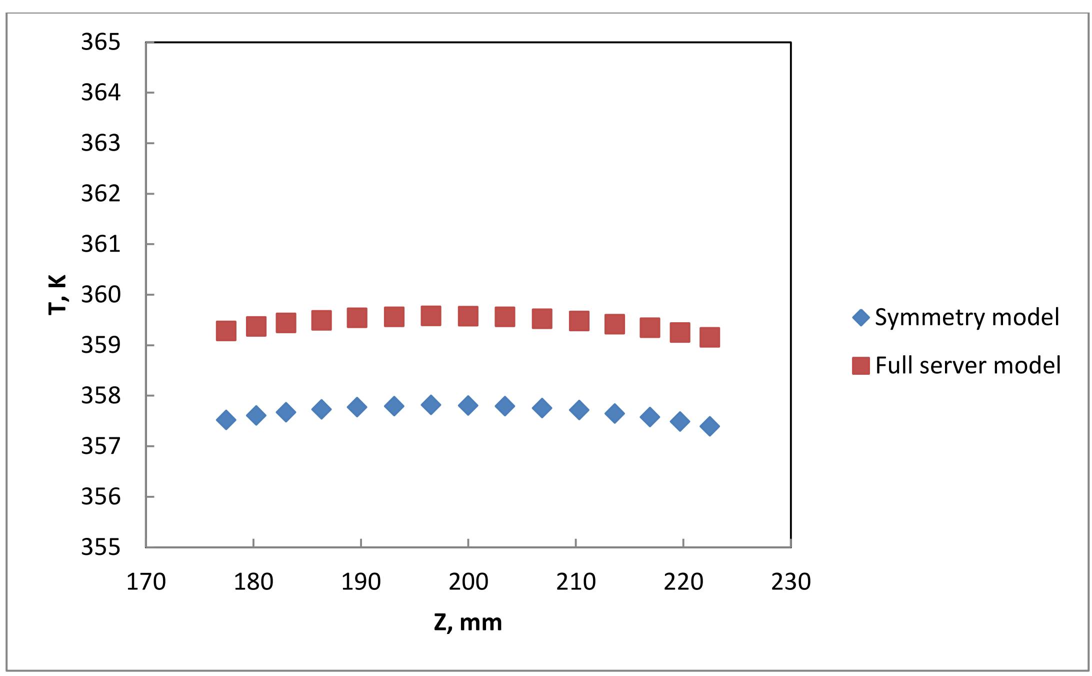

Figure 5.4: Temperature in centre of CPU along Z direction.

Although, symmetry helps to solve the problem, there are limitations of this configuration, which is not in the physics but rather limitations in the geometry, for example two staggered CPUs and also due to memory constraints, since COMSOL has large demands on random access memory.

5.2.5 The number of fins

This section is investigated the effect of the number of fins for the simulation model of symmetry. The number of fins that is used in this section is one, two and three fins as shown in Figure 5.5.

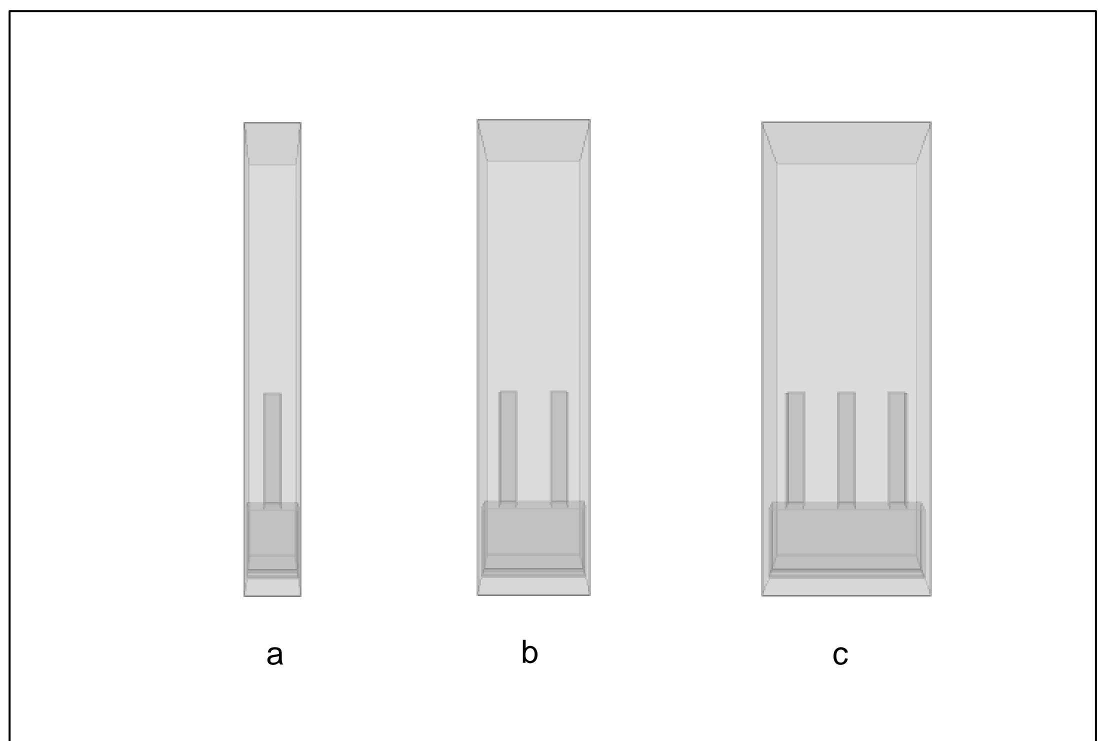

Figure 5.5: Top view of different number of fins a) one fin b) two fins c) three fins.

The results in Figure 5.6 show that the difference between the one fin, two fins and three fins are indistinguishable. However, the number of mesh is reduced by 48% from three fins to one fin model. Therefore, using one fin model is better in term of saving mesh and computational time.

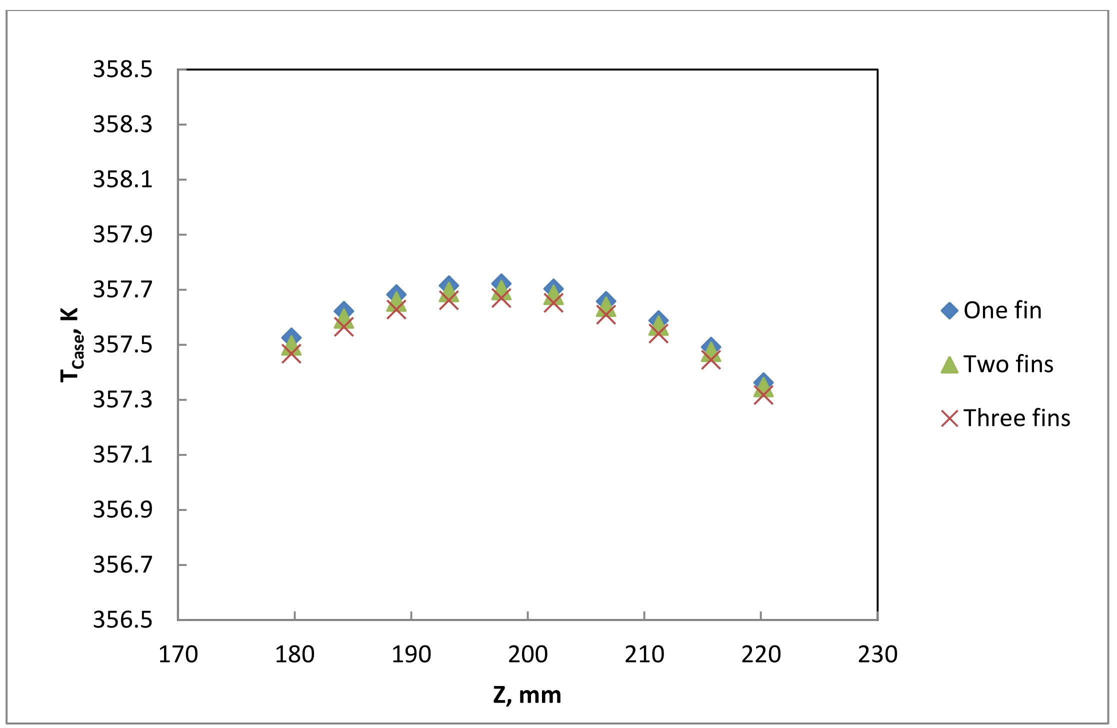

Figure 5.6: Show the temperature along Z axis in order to compare between the numbers of fins.

5.2.6 Fluid and material properties

The material of heat sink is copper and the dielectric liquid is used as coolant liquid for the server is class of HFE 7300 fluid and is manufactured by 3M [106].

Table 5.1 present the thermal properties of the HFE 7300 dielectric liquid. All the fluid thermal properties assumed to be constant except the density which is function of the temperature.

Table 5.1: Working fluid thermal properties

Properties	Abbrev.	HFE 7300 dielectric liquid
Specific heat capacity	C_p	1140 (J/kg.K)
Thermal expansion	β	1.15×10^{-3} (K^{-1})
Dynamic viscosity	μ	1.12×10^{-3} (Pa.s)
Thermal conductivity	k	6.9×10^{-2} (W/m.K)

5.2.7 Mesh sensitivity study

The mesh sensitivity study has been done to ensure that the mesh does not affect the results accuracy. The mesh consisting of 37563, 77977, 145860, 238149 and 465968 elements were used for the model simulation. The mesh accuracy depends on the temperature on the top centre of the CPU (T_{case}) which is shown in Figure 5.1.

The mesh study shows that the maximum difference temperature for T_{case} is 0.1 K between the two grids 238149 and 465968 elements. Consequently, the grid 238149 elements are considered to be used in this study in order to save memory and computational time.

Wall lift off may affect the accuracy of the results when employing the turbulent model as explained earlier in section 3.4.2, so this requires verification. The wall lift off should be between 11.06 and 300 on the walls and it is recommended that wall lift off should be as close as possible to 11.06 on most of the walls for the best accuracy [82-84]. In this study the

wall lift off value was found to be 11.06 on all the walls as shown in Figure 5.7.

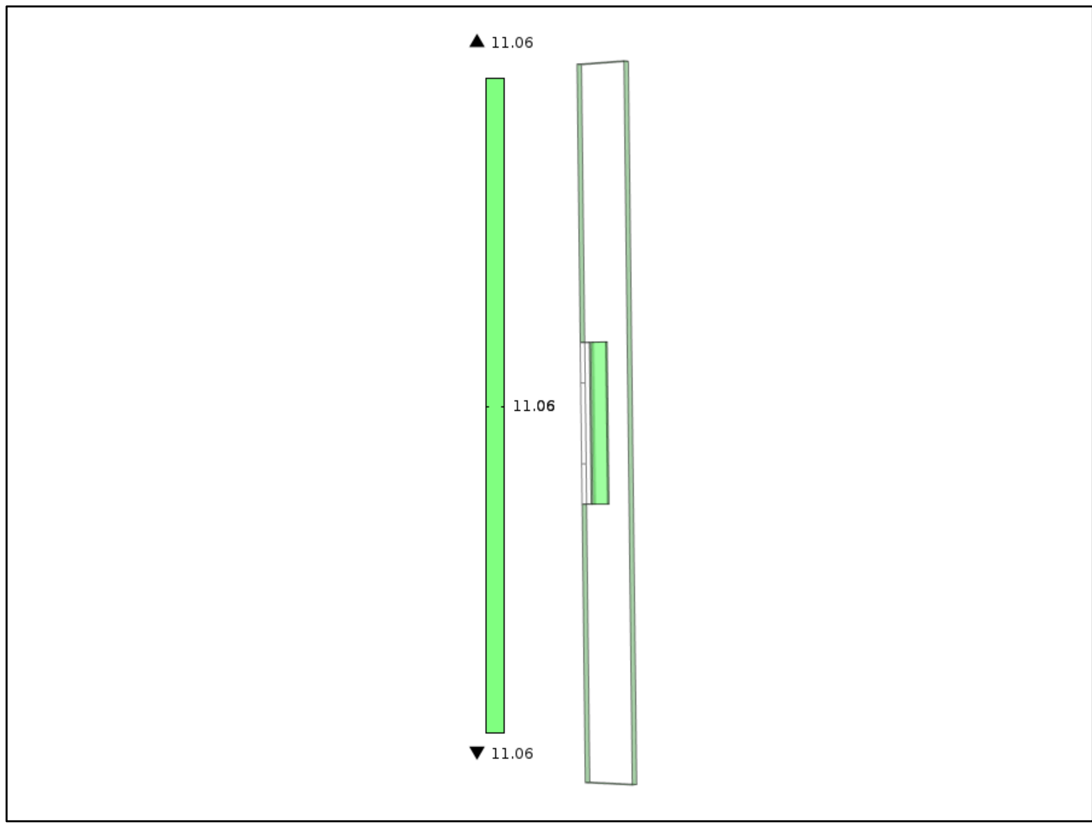

Figure 5.7. Wall lift off of the simulation model

5.3 Optimisation method

In order to improve the performance of the immersed server and reduce the temperature case, optimisation analysis was carried out in this section. In the optimisation analysis, design variables need to be selected to achieve the objective function. In this research, the heat sink fin height and the cold plate height were chosen as important parameters based on the literature [18, 19].

The study has been carried out to determine the effect of two design variables; heat sink fin height (H_{fin}) and cold plate height (H_{plate}) to minimize the T_{case}. The optimisation problem is defined as follow:

Objective function: minimize (T_{case})

Subject to: $9.5 \text{ mm} \leq H_{fin} \leq 24 \text{ mm}$

$30 \text{ mm} \leq H_{plate} \leq 44.5 \text{ mm}$

In optimisation problems, the response surface is selected form the design space that is created by the design variables. The selection points in design space are important to provide an accurate response surface which is known as the design of experiment (DoE).

An optimum Latin Hypercube [105] Design of experiment (DoE) is performed to create 30 combinations of two design variables. The 30 points are divided into 20 building points and 10 validation points. The building points will be used to find the optimum solution, while the validation points will be used to validate the response surface. The upper and lower limits of the two design variables are illustrated in above ranges. The distribution of the design space is shown in Figure 5.8.

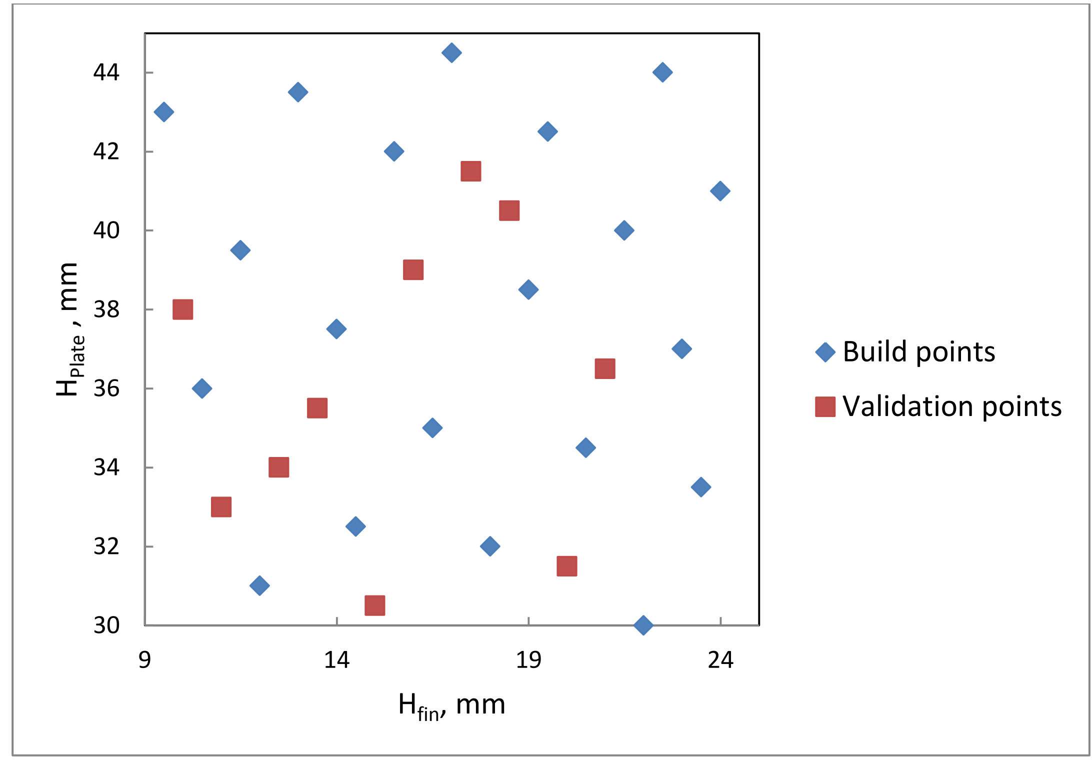

Figure 5.8: Design of experiment

5.4 Optimisation analyses

5.4.1 Unconstrained optimisation problem

COMSOL software was used to run 30 models that represent the selected 30 points distribution in the design space where 20 are building points and 10 validation points. The approximation response surface of the CPU top centre temperature, T_{case}, within the design space was performed by applying a Moving Least Squares Regression approximation method. The approximation of T_{case} for fin height and cold plate height are shown in Figure 5.9.

The validation points were used to validate that the response surface accurately and can be used to perform the optimisation analysis. Coefficient of determination (R square) is a statistical method that is used to determine

how well the response surface compares to the validation points. The range of R square value is between 0 to 1, and 1 means that the validation points are fit on the response surface. The R square for this study is 0.963 which shows that the validation points were very close to the predicted surface response which gives confidence in the surface response fit curve.

Response surface of the optimisation presented here shows that the fin height influences the T_{case} much more than cold plate height. T_{case} drops dramatically with increasing fin height. However, the T_{case} has different behaviour with variation of cold plate height. Figure 5.9 show that the lowest T_{case} value occurs at nearly highest limit of fin height which is 23.9 mm with the lowest cold plate height of 30mm. A Genetic Algorithm optimisation technique is applied using Hyperstudy v11. Table 5.2 compares the predicted T_{case} with the simulated T_{case} with acceptable error values. Also this table shows the lowest T_{case} that come from the optimum design variables.

Table 5.2: Compare between the predicted T_{case} and simulated optimum design variables.

Design variables (mm)		T_{case} (K)		
Fin height	Cold plate heigh	predicted	Simulated	Error %
23.9	30	342.3	343.15	0.25

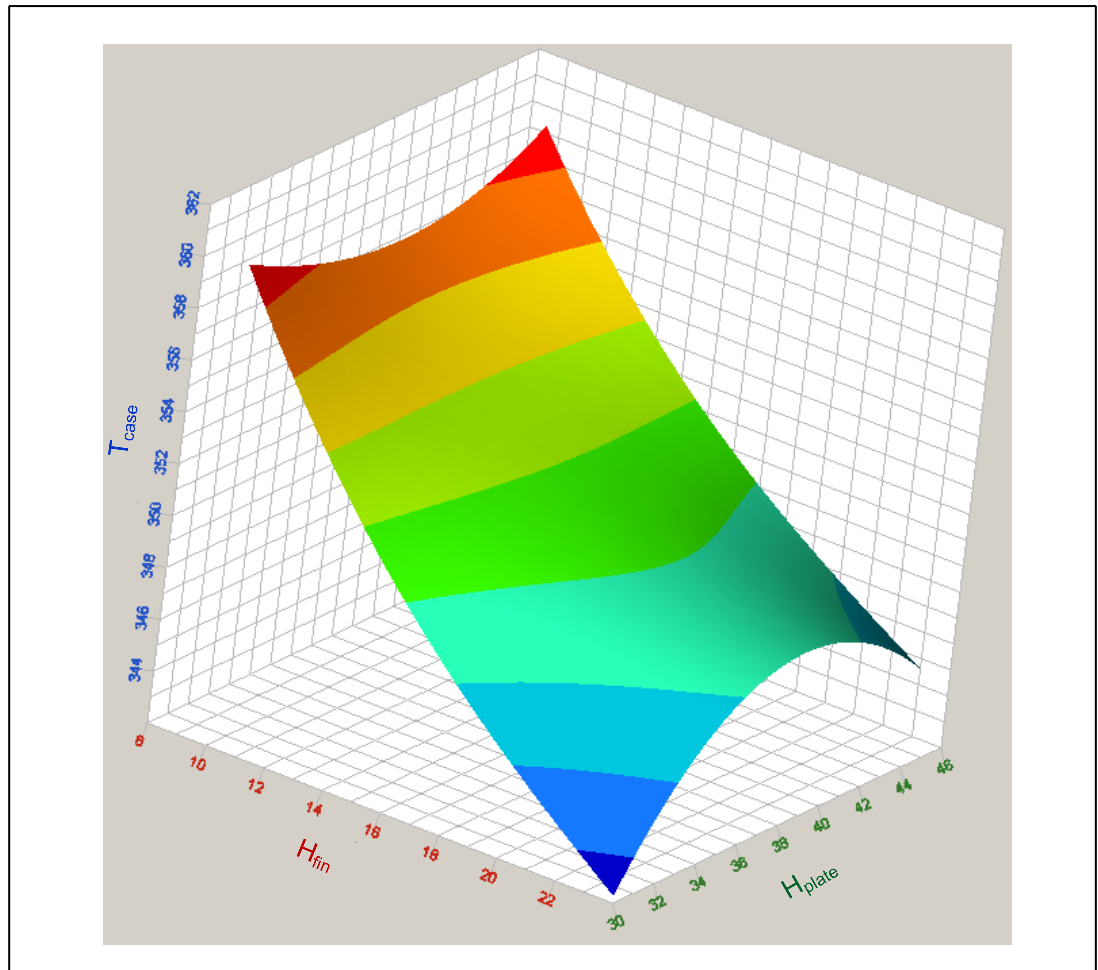

Figure 5.9. Response surface of T_{case}

5.4.2 Investigation of lowest T_{case} models

Six cases were picked from the above optimisation simulations in order to investigate how the fin height and cold plate height effects the temperature of the top centre of the CPU (T_{case}). The next sections present the effect of the temperature and velocity by changing the fin height and cold plate height. The six cases that are selected in Table 5.3 present the lowest T_{case} in this study.

Table 5.3: Lowest T_{case} cases

Case number	Fin height (mm)	plate height (mm)	Clearance parameter (mm)	T_{case} (K)
1	20	31.5	5.5	345.27
2	21.5	40	12.5	346.61
3	22	30	2	344.29
4	22.5	44	15.5	347.23
5	23.5	33.5	4	346.85
6	23.9	30	0.1	343.15

5.4.2.1 Temperature field

The effect of heat sink fin height and cold plate height on the CPU temperature is presented in along a cut line on the top of the CPU in Figure 5.10. As seen from this figure, the lowest T_{case} is case 6 which is the optimum solution that has the highest heat sink fin height which has the bigger surface area too and lowest cold plate height. It can be noticed that cold plate height H_{plate} has an influence on T_{case} for most cases, i.e. lower H_{plate} resulting in lower CPU temperature. However, in case 2 and 5 the situation is different where case 5 has H_{plate} lower than case 2 yet the T_{case} of case 5 is slightly higher than case 2. This is due to the effect of velocity

where the flow of case 2 is faster than the flow in case 5. This is explained further by explorer the velocity field in section 5.4.2.2.

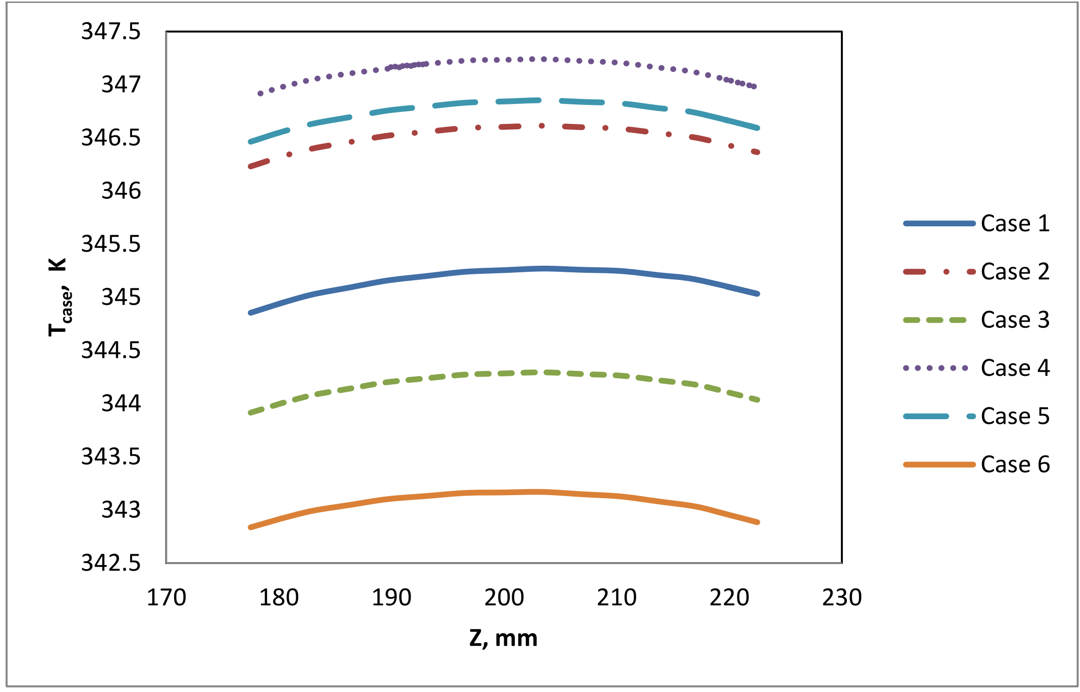

Figure 5.10. Temperature line along the top centre of the CPU in Z direction

5.4.2.2 Velocity field

Figure 5.11 shows the variation of velocity fields for all 6 cases. As seen from this figure, the velocity in all cases increases with the decreasing clearance between the fin height and cold plate height. Consequently, the lowest clearance would give the optimum value for the minimum T_{case}. The increase velocity over the cold plate increases the flow rate causing an increase of heat transfer coefficient [108]. Therefore, the T_{case} decreases due to increases in the heat transfer coefficient.

For case 5 the velocity over the cold plate and between the fins is slower than the velocity of case 2 which makes case 2 have a lower T_{case} value. The recirculation in case 5 above the heat sink fins flows in the opposite

sense to the convenction current over the heat source, this slows the the fluid velocity down and impairs the heat transfer coefficient. This recirculation occurs when the cold plate height is in the middle of cold plate height study range.

5.4.3 Constraint optimisation problem

As previously discussed, the simulation for 30 models were carried out for different fin height and plate height. The results showed that the lowest T_{case} can be obtained at highest fin. The T_{case} can be achieved for optimum value is 343.15 K. However, it is good to have a constraining in order to reduce the fin height. The lowest T_{case} in the previous section is 343.15 K and the boiling point of working fluid is 371.15 K [106]. Hence, the constraining of the T_{case} is going to be selected between 343.15 K and 371.15 K. The fin height is going to be constrained at T_{case}= 353.15 K. The constrained optimisation problem is as follow:

Objective function: Minimize (H_{fin})

Subject to: $T_{case} \leq 353.15$ K

$9.5 \text{ mm} \leq H_{fin} \leq 24$

$30\text{mm} \leq H_{plate} \leq 44.5\text{mm}$

Hyperstudy software is used to find the minimum fin height that is constrained by T_{case} = 353.15 K. It was found that the fin height and plate height is 12.5 mm and 32.5 mm respectively which provide T_{case}= 352.83 K.

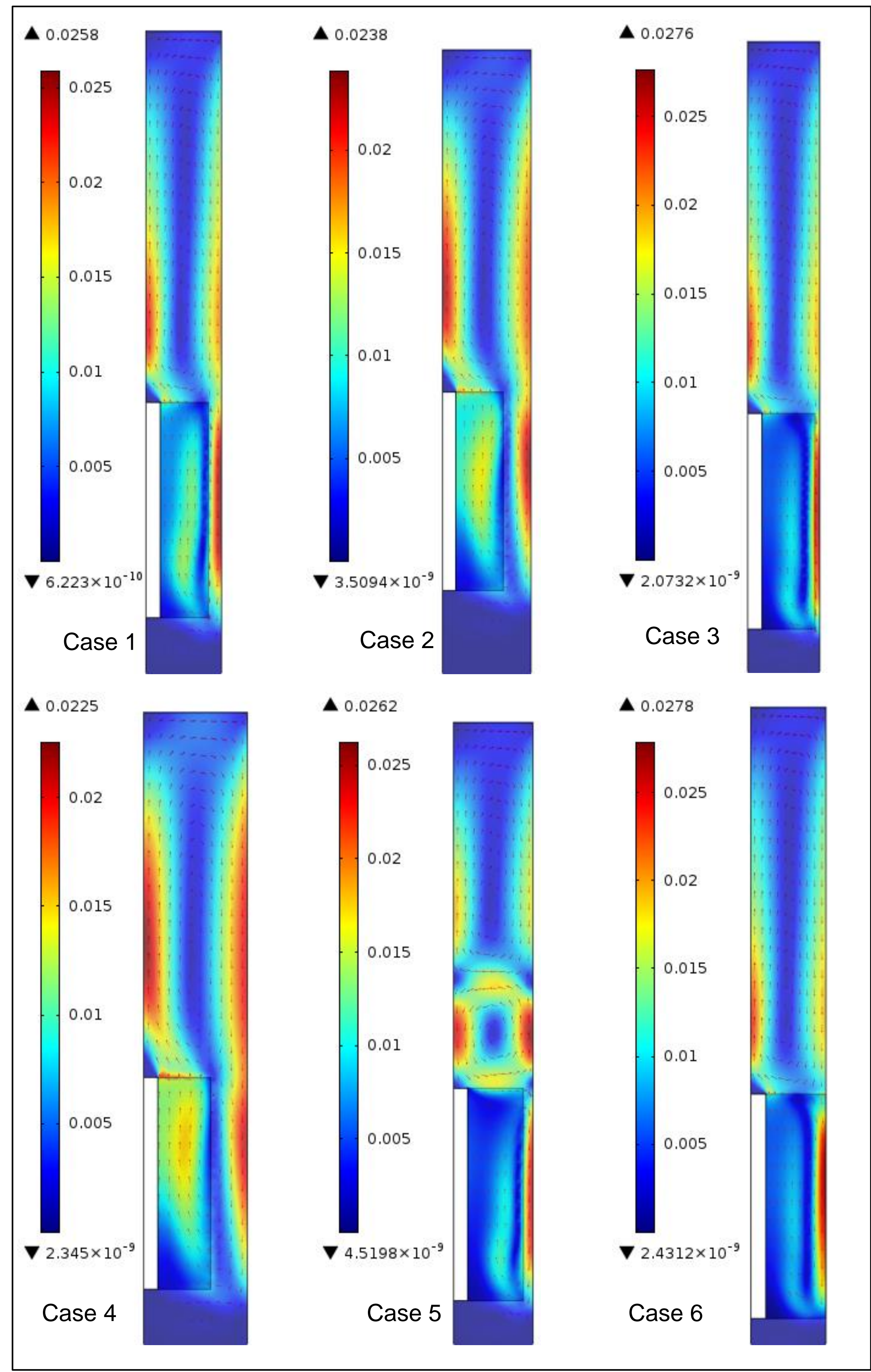

Figure 5.11: Velocity field Z component, m/s

5.5 Summary

This study has been done for fin heat sink immersed in a dielectric liquid in a server. Natural convection with conjugate heat gradient conditions for a vertical sever is solved using COMSOL v4.3. Since the flow in the server has a $Ra>10^7$, the flow is considered to be turbulent and the k-ω turbulence model is used. Mesh independency investigations were conducted to ensure that a sufficient mesh was employed in the simulations that did not affect the solution accuracy.

An optimal Latin Hypercube design of experiment was created with thirty points in design space for two design variables which are the heat sink fin height and the cold plate height. A Genetic Algorithm was used to obtain an optimum value of two parameters from thirty simulations.

Six out of thirty cases were selected to show the effect of the changing parameters on temperature and velocity. These six cases represent the lowest T_{case} of thirty cases. The heat sink fin height has a significant influence on decreasing the T_{case}. The cold plate height helps to reduce the T_{case} once it became closer to the fin.

The optimum fin height is 23.9 mm and the cold plate height is 30 mm. The value of T_{case} for this optimum solution is 343.15 K. This dropped the temperature of the T_{case} by 16.4K compared to the highest T_{case} of the thirty simulations that are performed in this study.

For the optimum solution the fin will be at nearly highest limit. So to reduce the fin height by using T_{case}= 353.15 K as constrain. The selected T_{case} is between the fluid boiling and the lowest T_{case} that has been obtained from

this study. The results showed that the T_{case}= 352.83 K can be achieved by using fin height and plate height as 12.5 mm and 32.5 mm, respectively.

The optimisation analysis carried out in the current study showed that the T_{case} could be improved by finding the optimum between Fin height and cold plate height. On the other hand, the response surfaces of the optimisation problem is not difficult to predict but this analysis can be implemented on more complicated geometries in order to find the optimum design variable to improve the thermal performance of the immersed server.

CHAPTER 6:

INVESTIGATION OF DIFFERENT BAFFLE CROSS SECTIONS FOR IMPROVING THE COOLING IN LIQUID IMMERSED SERVERS

6.1 Introduction

The effect of baffles on the immersed server is investigated in this chapter. The study is carried out for different baffles of cross sectional areas, namely square, rectangular and trapezoidal. The model simulation is explained in the next section and the comparison of the model results with heat balance equations is performed and shows good agreement. The results show that the best baffle cross sectional area is rectangular and further investigation demonstrates that the CPU and heat sink location has a big influence of improving the heat transfer performance.

6.2 Modelling of immersed server

6.2.1 Immersed server modelling

The server in this study consists of cold plate that contains a water channel, heat sink, baffles and a HFE 7300 dielectric liquid as presented in Figure 6.1. The computational domain that represented in symmetry slice of server is shown in Figure 6.2 (note: Figure 6.1 and Figure 6.2 are showing the server geometry in a horizontal orientation rather than the real vertical orientation for clarity). It consists of a CPU generating heat with dimensions of (L_1) 45mm x (w) 4.5mm. Then heat is conducted to a copper heat sink, (L_3) 90mm x (w) 4.5mm x (L_4) 18.5mm. The dimensions of the server that is filled with a dielectric liquid are (L) 400mm x (w) 4.5mm x (H) 32.5mm. The cold plate dimensions are (w) 4.5mm x (H_c) 4.5mm and the cooling liquid which is water passes through a channel with diameter of (D) 3.5mm.

The top and bottom walls of the server are assumed to be insulated. Symmetry boundary conditions are used for both sidewalls, as demonstrated in Chapter 5, thus reducing the computational time and domain.

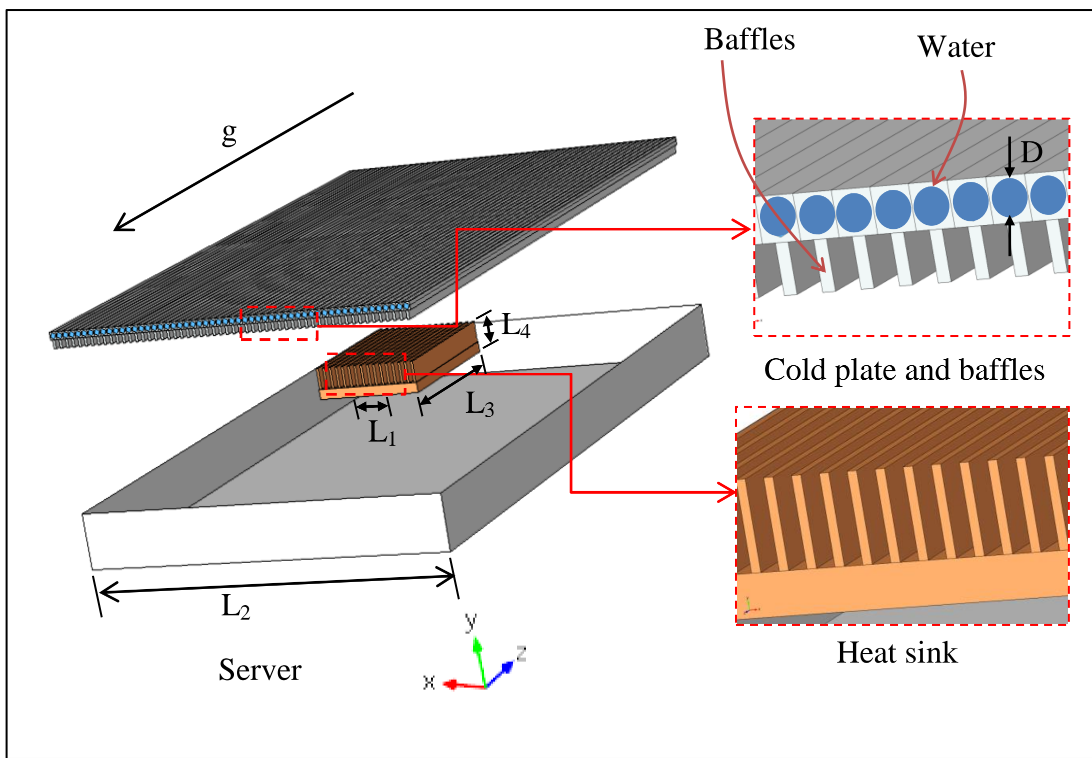

Figure 6.1: Server assembly geometry (turned to horizontal orientation for clarity) with a zoom-in to the interesting parts of the heat sink and the cold plat and baffles showing the fine details of the geometry design.

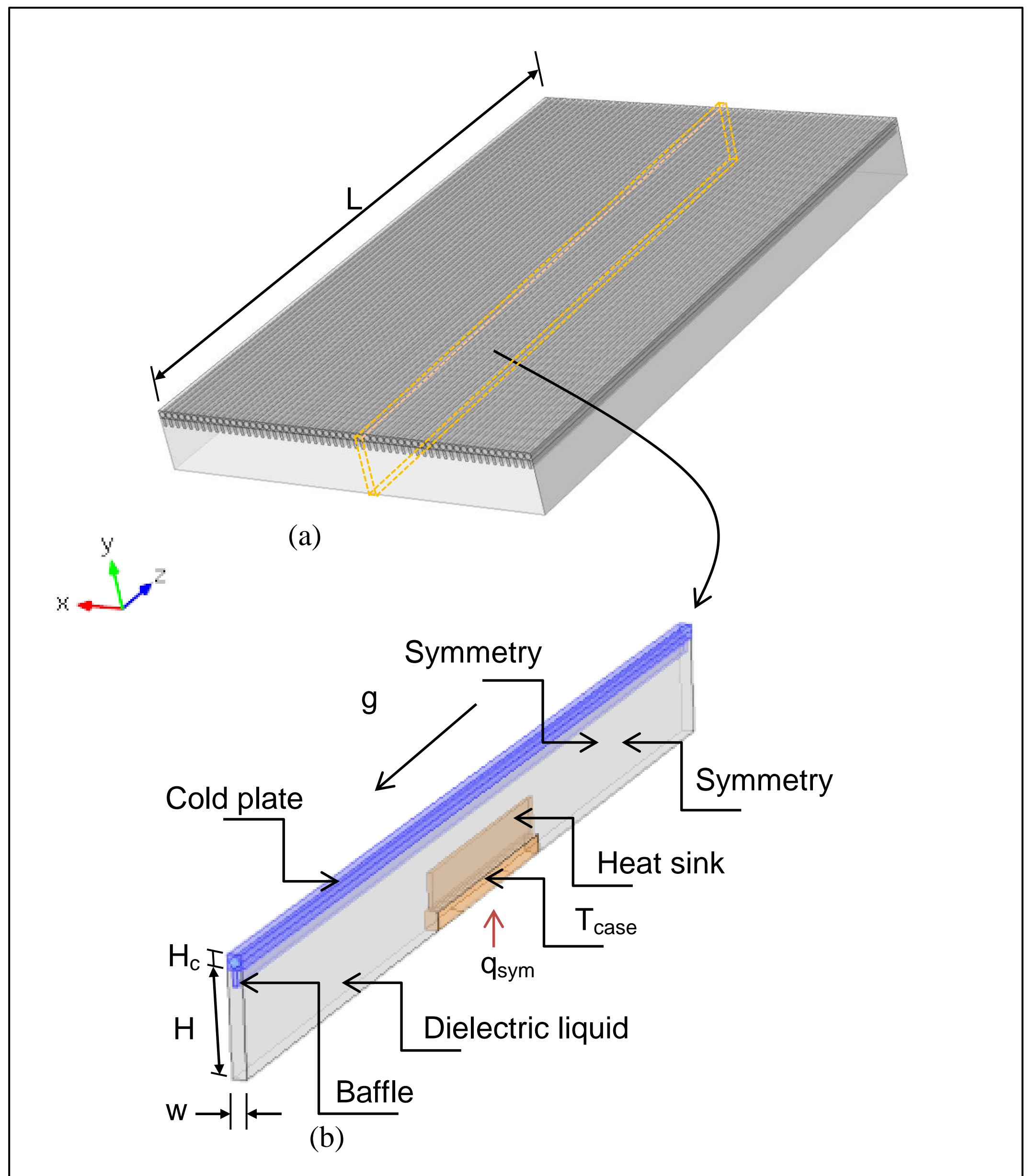

Figure 6.2: Server diagram (turned into horizontal orientation for clarity) a) Full server. b) Computational domain of the server.

The baffles are placed on the cold plate and the cross section of these baffles is displayed in Figure 6.3 and details of the parametric values are presented in Table 6.1. The baffles cross section area were kept constant 7.5 mm^2. It was kept constant to make sure all baffles have a same weight (subsequently same cost) because as density for all baffles is the same. The mass, *m,* of baffles can be calculated from:

$$m = \rho A L \tag{6.1}$$

Where A is cross section area and L is the length of baffle which is the same for all cross sections.

Table 6.1: Geometrical parameter values

Parameter	Value	Unit
t	$2.74\text{x}10^{-2}$	m
h_1	$5\ \text{x}10^{-2}$	m
w_1	$1.5\ \text{x}10^{-2}$	m
h_2	$6\ \text{x}10^{-2}$	m
b_1	$2.5\ \text{x}10^{-2}$	m
A	$1.5\ \text{x}10^{-2}$	m
b_2	$2.5\ \text{x}10^{-2}$	m
h_3	$3.75\ \text{x}10^{-2}$	m

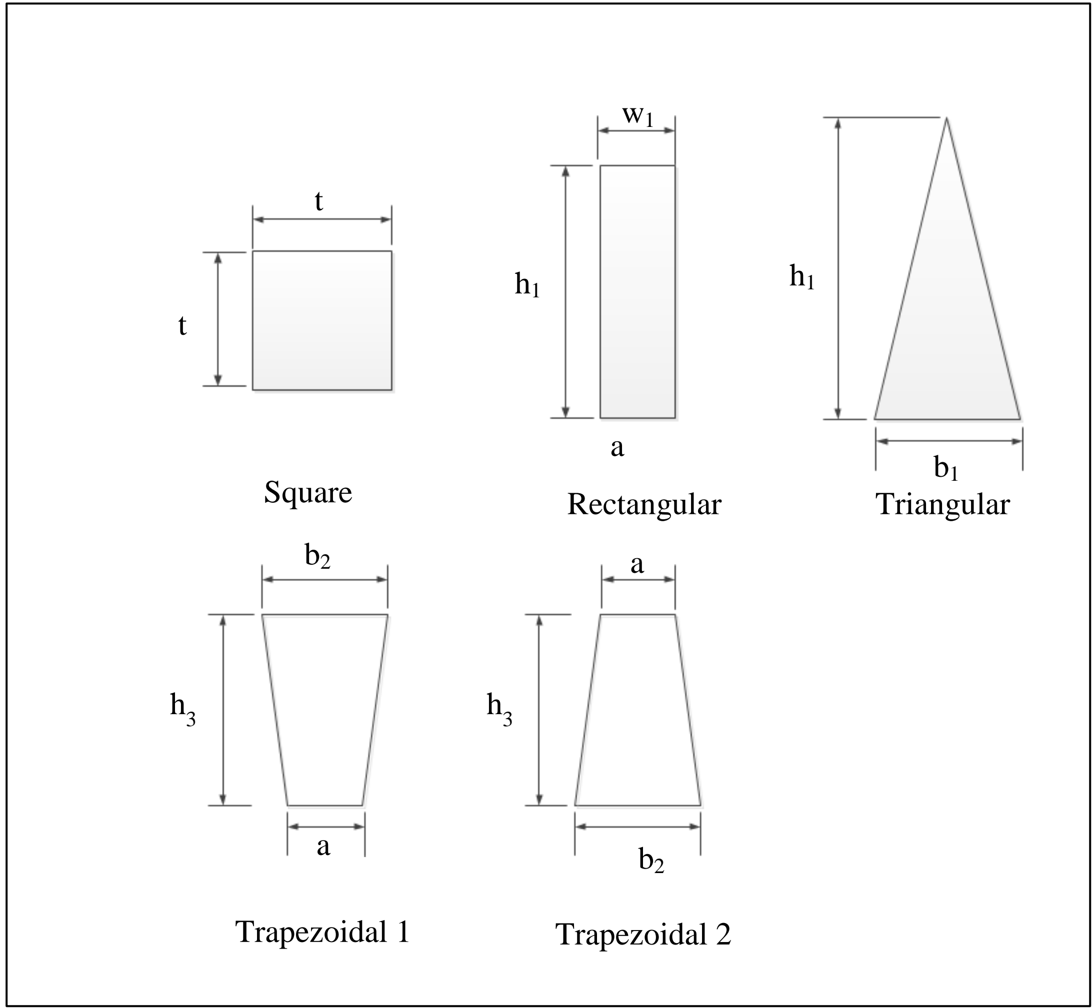

Figure 6.3: baffles different cross sections

The material of the heat sink is copper and the baffles and cold plate are made of Aluminium. The working fluids in this study are water and HFE 7300 dielectric liquid (see Table 5.1). The water is used as cooling liquid that passes through the cold plate channel. The server is filled with a hydrofluoroether (HFE 7300) dielectric liquid.

6.2.2 Mathematical formulation

In this study, the model consists of two physics of fluid flow. The dielectric liquid is moving inside the server due to the density variation which is natural convection and the other fluid is pumped (forced convection) through channels in an aluminium black of the server. Before solving the model, the fluid flow behaviour needs to be checked whether it is turbulent or laminar. For the water forced convection this could be determined by calculating Re

$$Re = \frac{\rho_w V D}{\mu_w} \tag{6.2}$$

Where D is water channel diameter (3.5×10^{-3} m), V is the average velocity (6.3×10^{-2} m/s), ρ_w (996.6 kg/m^3) and μ_w (7.96×10^{-4} pa.s) is are the density and viscosity of water, respectively. The Re is 276 at maximum flow rate in this study which equals to 6.06×10^{-7} m^3/s. Therefore, The Re < 2300 this means the fluid considered as laminar [86].

For natural convection inside the server, the dielectric fluid flow behaviour can be indicated by using Rayleigh number [16], Ra

$$Ra = \frac{g\beta\,(T_h - T_c) H^3 \rho_D^2 c_p}{\lambda_D \mu_D} \tag{6.3}$$

Where H is the server height, T_h is CPU average temperature, Tc is cold plate average temperature, g is the acceleration of gravity, c_p is Specific heat capacity, ρ_D is density, λ_D is the thermal conductivity, μ_D is viscosity, β is the thermal expansion coefficient. All these fluid thermal properties are for the HFE 7300 dielectric liquid. The Ra is equal to 1.8×10^{8} which greater than 10^7, so the fluid is considered to be turbulent [15].

Inside the server the fluid flow is turbulent and the conservation equation for mass, momentum and energy for turbulent natural convection of the dielectric liquid domain have been listed in Chapter 5 (c.f. equations (5.2) to (5.11)).

For the water channel which is a pumped laminar fluid flow,

Continuity equation

$$\nabla(\rho \boldsymbol{u_w}) = 0 \tag{6.4}$$

Momentum equation

$$\rho(\boldsymbol{u_w}.\nabla)\boldsymbol{u_w} = \nabla.\left[-p2\boldsymbol{I} + \mu_w(\nabla\boldsymbol{u_w} + (\nabla\boldsymbol{u_w})^T) - \frac{2}{3}\mu_w(\nabla.\boldsymbol{u_w})\boldsymbol{I}\right] \tag{6.5}$$

Energy equation

$$\rho c_p \boldsymbol{u_w}\nabla T = \nabla.(\lambda_w \nabla T) \tag{6.6}$$

For the solid domain around the channel flow and which is in contact with the dielectric fluid on the inside of the server, the energy equations reduce to:

$$0 = \nabla.(\lambda_{Al}\nabla T) \tag{6.7}$$

Where, the λ_{Al} is the thermal conductivity for the Aluminium block.

6.2.3 Boundary conditions

The boundary conditions of the simulation model is presented in schematic diagram as shown in Figure 6.4, which is in fact an extension of those presented in section 5.2.3. The additional boundary conditions for the modified multiphysics problem are expressed as follows:

Temperature interface between the HFE 7300 dielectric liquid and the baffle

$$T_D = T_b \tag{6.8}$$

And the heat flux

$$-n.(-\lambda_D \nabla T_D) = -n.(-\lambda_{Al} \nabla T_b) \tag{6.9}$$

Temperature interface between the baffle and water

$$\mathrm{T}_b = T_w \tag{6.10}$$

And the heat flux

$$-n.(-\lambda_{Al} \nabla T_b) = -n.(-\lambda_w \nabla T_w) \tag{6.11}$$

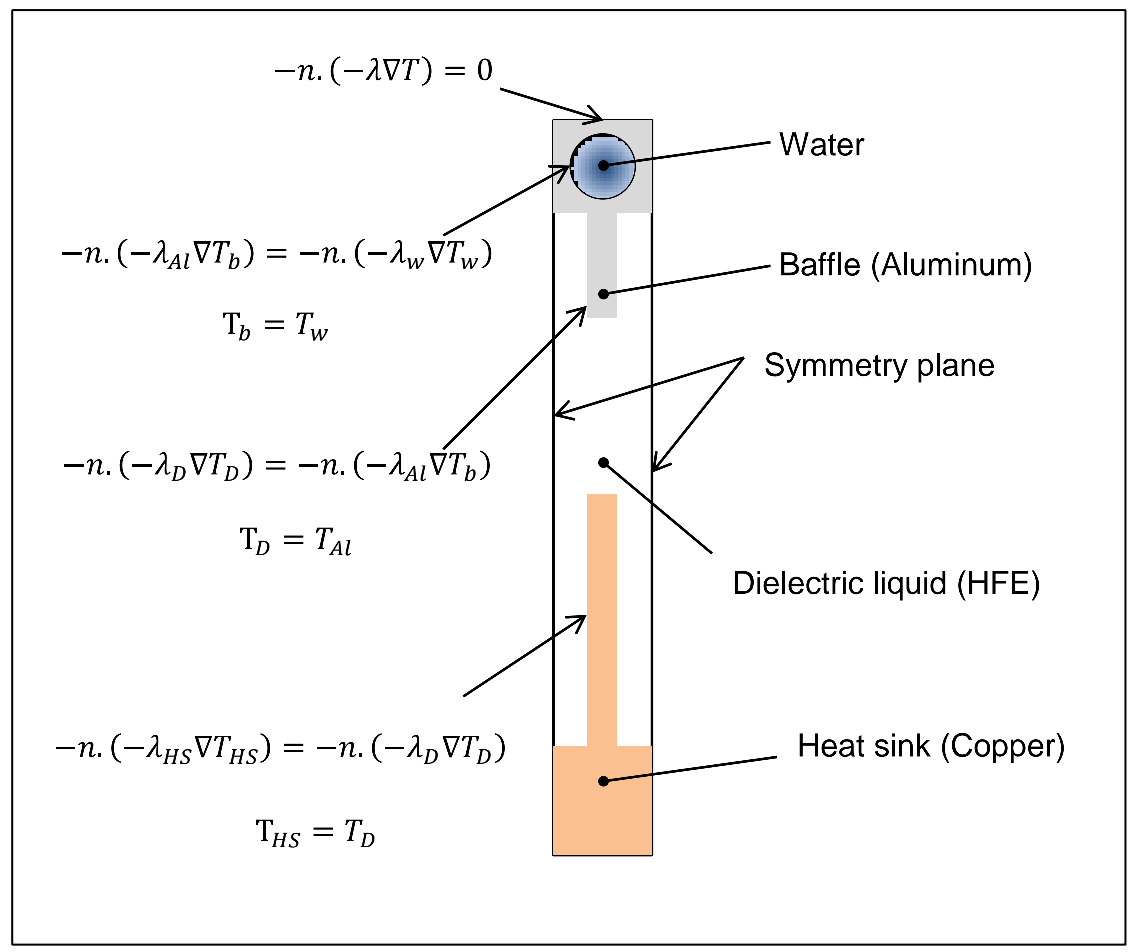

Figure 6.4: Schematic diagram of cut plane in the centre of the model to show the boundary conditions of the model and the conjugate heat

The inlet boundary of the water channel is defined as developed flow. The entrance length (L_{entr}) is required to solve the developed flow. The value of L_{entr} should be large enough to make sure that the flow does achieve a developed laminar profile. This must be considerably bigger than the 0.06ReD for laminar flow [86].

$L_{entr} >> 0.06ReD$

Where D = 3.5×10^{-3} m is the water channel diameter and Re = 276 is the Reynolds number, so L_{entr} must be greater than 5.7×10^{-2} m. However, in this study the L_{entr} is assumed to be 0.6 m based on the above equation.

Heat flux per unit area of the symmetry model (q_{sym}) in this study (see Figure 6.2) was calculated using equation (5.25)

$$q_{sym} = \frac{L_1}{L_2} q_{3D}$$

Where q_{3D} is the heat flux of the full server, L_1 is CPU width and L_2 is the server width as shown in Figure 6.1. (L_1/L_2) is the ratio between of the heat flux of the full server model and symmetry model, taking into account gap besides the CPU.

The outlet of the water in the cold plate channel has pressure defined.

$P_{out} = 0$

6.2.4 Numerical solution

The conjugate heat models are coupled and solved in one steady state solver using COMSOL multiphysics 4.3. The server with cold plate and without the baffles is used to find out the mesh sensitivity. The number of elements that is used for this study is 29321, 67845, 114439, 285756 and 541513. The T_{case} value difference between 285756 and 541513 is 0.4 K. therefore the mesh with 285756 elements is chosen to save on solution time and memory usage.

Beside the validation with numerical (Section 4.4) and experimental (Section 4.5) previous work, the analytical approach will offer a way to validate the results of computational model in this study by finding the variation of water outlet temperature (T_{out}) with changing inlet flow rate as presented in Figure 6.5. To compare the analytical with model results, the water outlet temperature can be calculated as follows:

$$\dot{Q} = \mathrm{m}\, c_p(T_{in} - T_{out}) \tag{6.12}$$

$$m = Q_{in}\rho \tag{6.13}$$

$$T_{out} = \frac{\dot{Q}}{Q_{in}\rho c_p} + T_{in} \tag{6.14}$$

Where the $\dot{Q}$ is the total heat flux, T_{in} is the inlet temperature, T_{out} is outlet temperature, Q_{in} is the water flow rate, ρ and C_p is density and specific heat of water. All the fluid properties were taken at mean temperature T_m. The results prove that the analytical and model of T_{out} and flow rate are nearly identical and the model setup is fine.

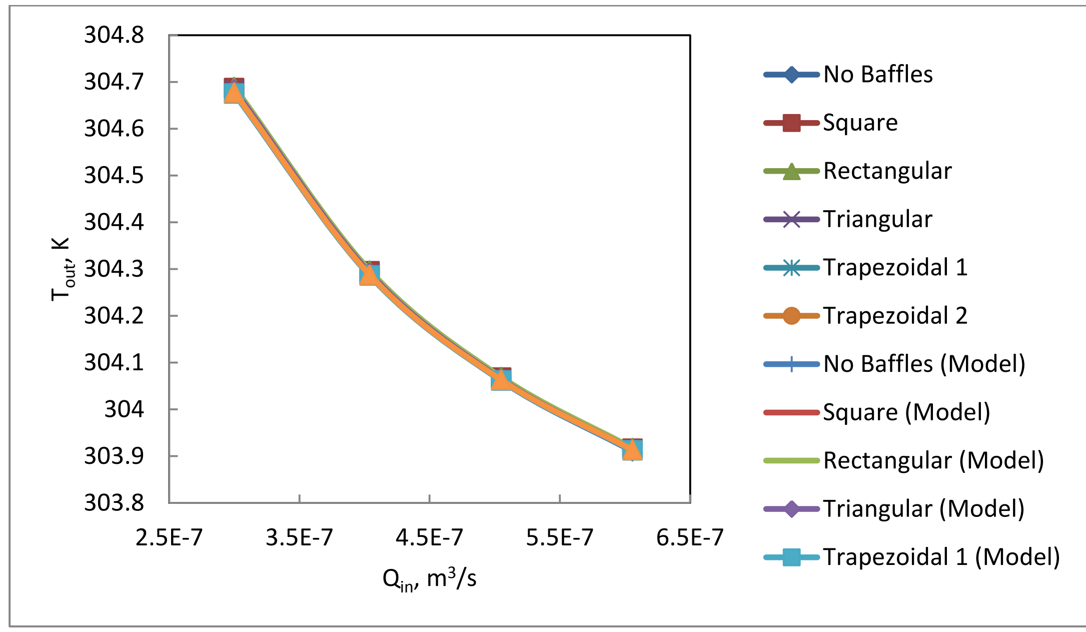

Figure 6.5: comparison of variation T_{out} with flow rate of the analytical and computational model.

6.3 Result and discussion

The model of natural convection and forced convection were carried out for the immersed server with its water jacket (similar to a cold plate) in

order to investigate the different cross sections of the baffles. The heat flux load (q_L), inlet flow rate (Q_{in}), inlet temperature (T_{in}) is varying for each baffle cross section and the parameters variation is explained in subsequent sections. The parameters of the baffles cross sectional shape that are used for this study are showed in Table 6.2.

The best heat transfer performance is obtained by investigating the geometrical parameters for each of the different baffle cross sections. In addition the best enhancement of heat transfer for the baffle cross sections is performed with different heat flux load. The simulation of different CPU locations has also been carried out to find the effect of it on the heat transfer performance.

6.3.1 Parametric study of immersed server

In a typical immersed server cooling system the parameter that can be changed is the water channel inlet temperature (T_{in}), inlet flow rate of the water channel (Q_{in}) and the load of heat flux load (q_L). This section is to find out which parameter has the largest effect on the heat transfer performance for different values of these parameters that are selected. Therefore, 64 simulations have been performed for the different parameters such as the heat flux load (q_L) varying from 70% to 100% (where the total heat flux per unit area (q_{sym}) is 8.8 kW/m^2), the flow rate (Q_{in}) varying from $3x10^{-7}$ to $6.06x10^{-7}$ m^3/s and inlet temperature is varied from 303 and 318 K. The Nusselt number (Nu) is plotted with different parameters, where the value of Nusselt number for the present study is defined by:

$$Nu = \frac{h\mathrm{H}}{\lambda_D} \tag{6.15}$$

Where the h is the heat transfer coefficient, H is the server height of the server (see Figure 6.2) and λ_D is thermal conductivity of HFE 7300 dielectric liquid.

The heat transfer coefficient is calculated first by knowing the heat flux and heat sink surface area (A_s) and then from the model the average temperature on the baffles and cold plate surface (T_c) and the average heat sink temperature (T_s) are obtained to yield a value for h as;

$$\mathrm{h} = \frac{Q}{A_S(T_S - T_c)} \tag{6.16}$$

The variation of Nu with input heat flux load (q_L) for different baffles cross sections is shown in Figure 6.6. The minimum Nu occurs for the model with no baffles for all input heat flux load. The Nu for all models increases as the input heat flux load increase. The Nu has a significant improvement when using baffles compared to no baffles. The rectangular baffle cross section can offer the highest Nu. In the case of rectangular baffle cross sections the Nu is increased by 71%.

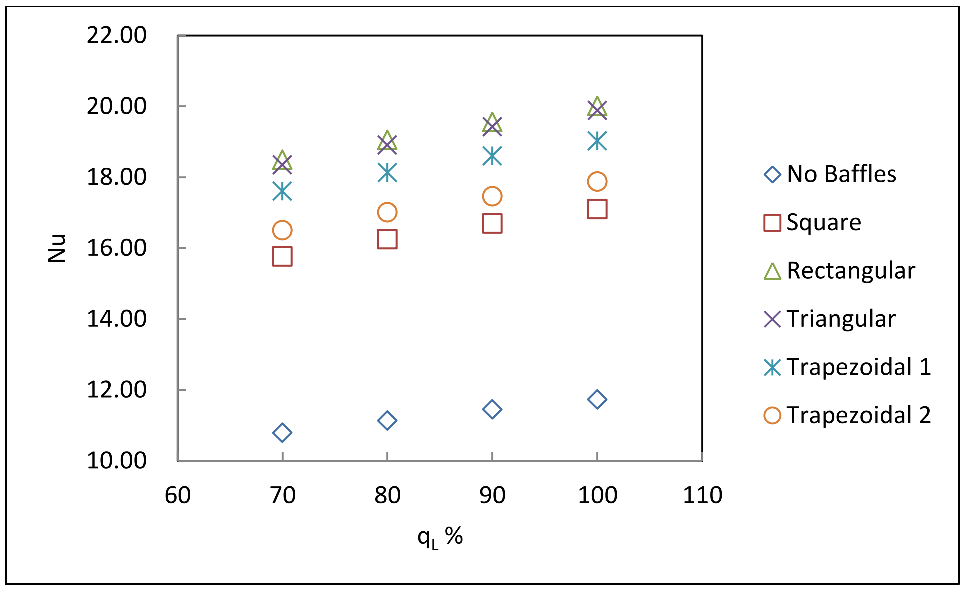

Figure 6.6: Variation of the Nu with heat flux load, where $Q_{in} = 3x10^{-7}$ m^3/s and T_{in}=303 K.

The results in this section show that the most effected parameter is heat flux load. The heat transfer shows small improvements when varying the flow rate Q_{in} at the range of $3x10^{-7}$ and $6.06x10^{-7}$ m^3/s and the inlet temperature T_{in} is varied from 303 and 318 K.

6.3.2 Investigation of best heat transfer parameter

The study in this section is based on the best heat transfer model with different baffles cross section. The greatest heat transfer situation is when the heat flux load is at 100%, the flow rate is $3x10^{-7}$ m^3/s and the inlet temperature is 303 K.

Figure 6.7, the average flow rate between the baffles has been taken along the server to show the variation of flow rate for different baffles cross section. The flow rate between all baffle cross sections is nearly zero from the bottom of the server to the edge of the heat sink. Then it steeply

increases and after passing the heat sink it decreases then it increases again. This is due to the buoyancy force, which creates the natural convection fluid flow circulation. All flow rates between baffles have shown nearly the same trend.

On further insight of the variation of flow rate in Figure 6.7, it is observed that the rectangular cross section achieved higher flow rate in the server than other baffles cross section. However, the biggest surface area is triangular baffle cross section and the second surface area is rectangular as presented in Table 6.2. In fact, it is more than the surface area that indicates the best heat transfer enhancement, since the flow rate also has a major effect on the heat transfer. Therefore, the best heat transfer performance is rectangular and the second is the triangular baffle cross section with marginal difference as shown in Figure 6.6.

Table 6.2: Baffles cross section surface area that contact with fluid

	Baffles surface area (mm^2)
Rectangular	4600
Triangular	4902.8
Square	3288
Trap 1	4026.4
Trap 2	3626.4

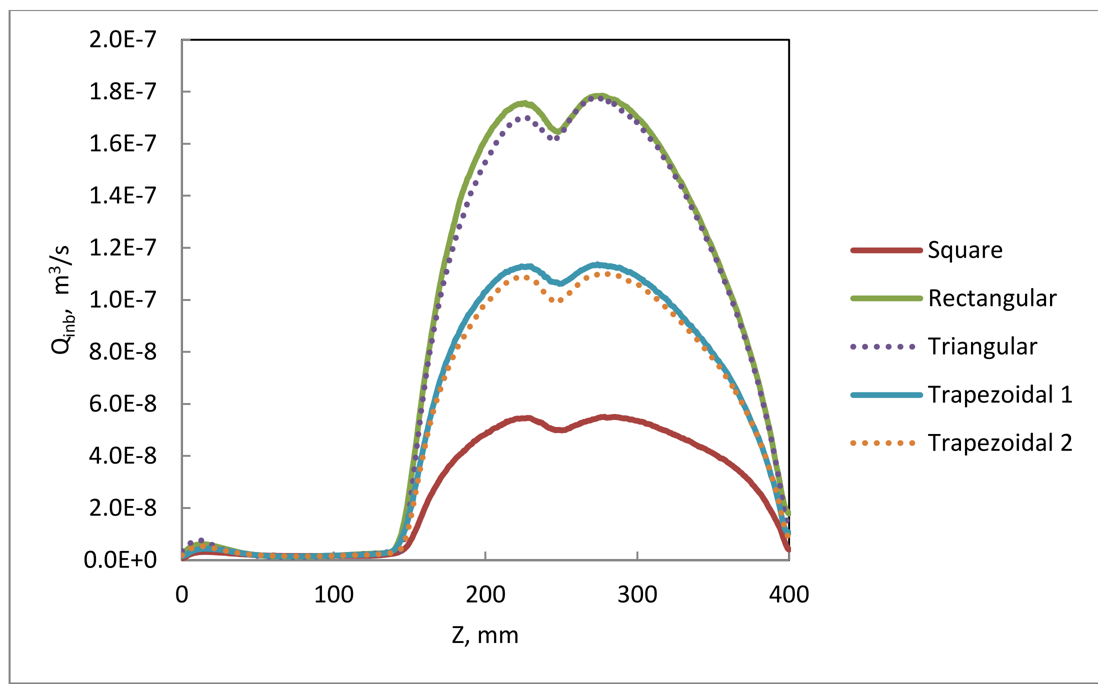

Figure 6.7: Flow rate between the baffles for a different baffles cross section area along the server.

The temperature contour in the 3D cut plane for different baffles cross section with constant parameters is presented in Figure 6.8. It can be noted that the highest temperature in all models occurs at the centre of the CPU and it decreases steeply form the CPU to the fluid. The lowest temperature of the T_{case} is for the rectangular baffles cross section (332 K) while the highest temperature obtained is for the server with no baffles (352 K), show a 20 K difference.

So far, the best heat transfer performance is the rectangular baffle cross section compare to other baffle cross section. Thus, it is lowest temperature and fastest dielectric liquid flow in the server.

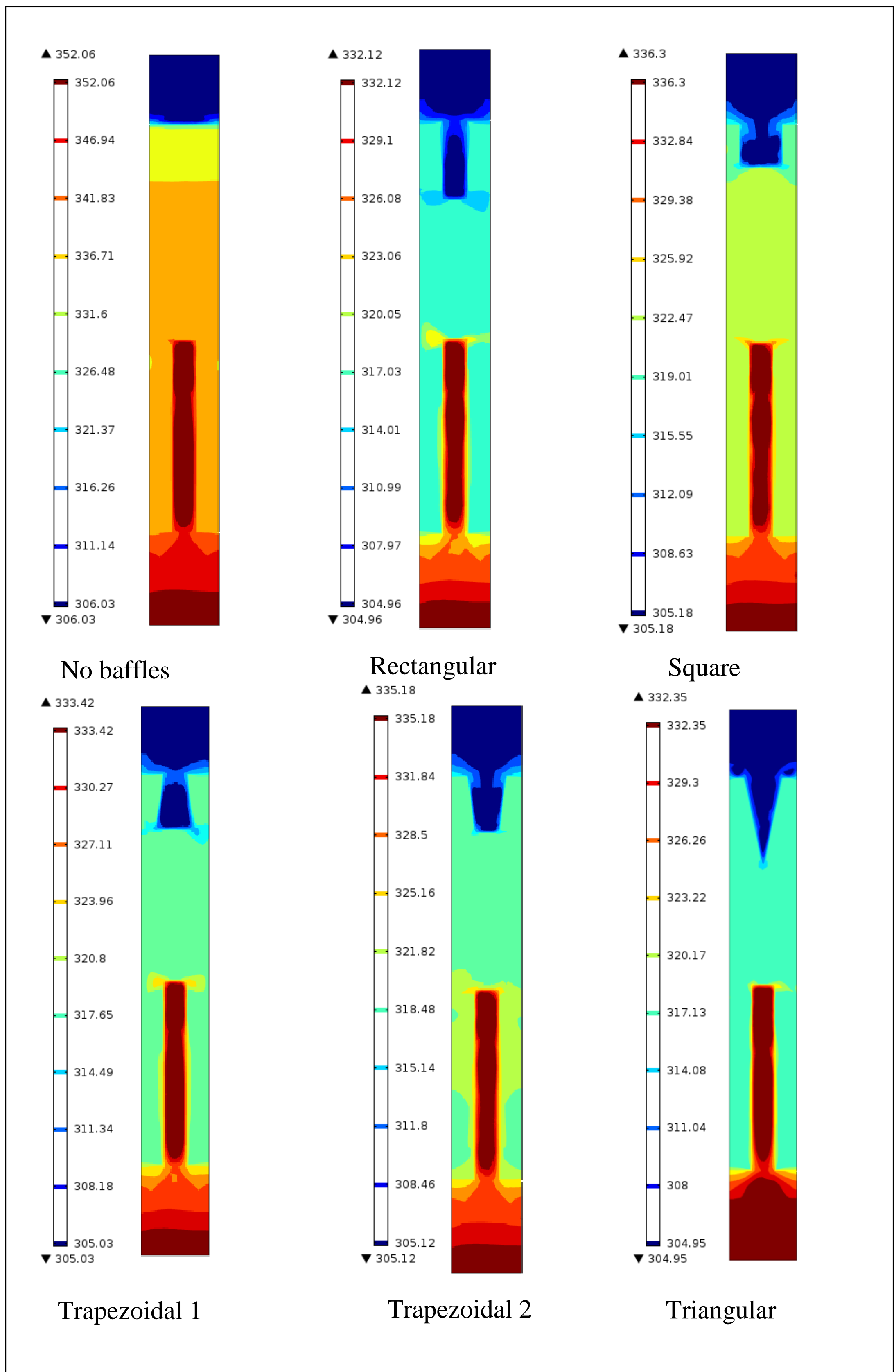

Figure 6.8: Temperature contour of Cut-plane in centre of the server for different baffles cross sections

6.3.3 Study of effect the heat flux on best baffle cross section

The previous sections have demonstrated that the most effective parameter for the immersed server model is the heat flux load, which provides the best heat transfer for rectangular baffles with the greatest convection speeds. The results in this section are based on the effect of the heat flux load on the rectangular baffle cross section. Figure 6.9 shows the variation of flow rate between rectangular baffles for a different heat load varying from 70% to 100%. It observed that the flow rate trend between the rectangular baffles of the HFE 7300 dielectric liquid in the server seems to be the same for all heat flux load. However, the flow rate of the HFE 7300 dielectric liquid increases with the increasing heat flux load. This is easily understood to be because of the increase in the buoyancy force with increase heat flux load.

Figure 6.10 presents the temperature behaviour between the baffle for different heat flux loads. The curves show the temperature along the centre line between consecutive baffles it is noted that the temperature for all heat flux load steeply increases from the bottom of the server to the edge of the heat sink with similar trends and also the temperature along the baffle increases with heat flux load. The higher the heat flux loads, the higher the temperature increases from the heat sink to the top of the server. This leads to interesting results that for immersed servers as described here, are only affected by the heat and buoyancy force from the bottom edge of the heat sink and above. Thus, further investigation is required to determine what enhancement of heat transfer is possible in an immersed server by changing the heat sink and CPU location.

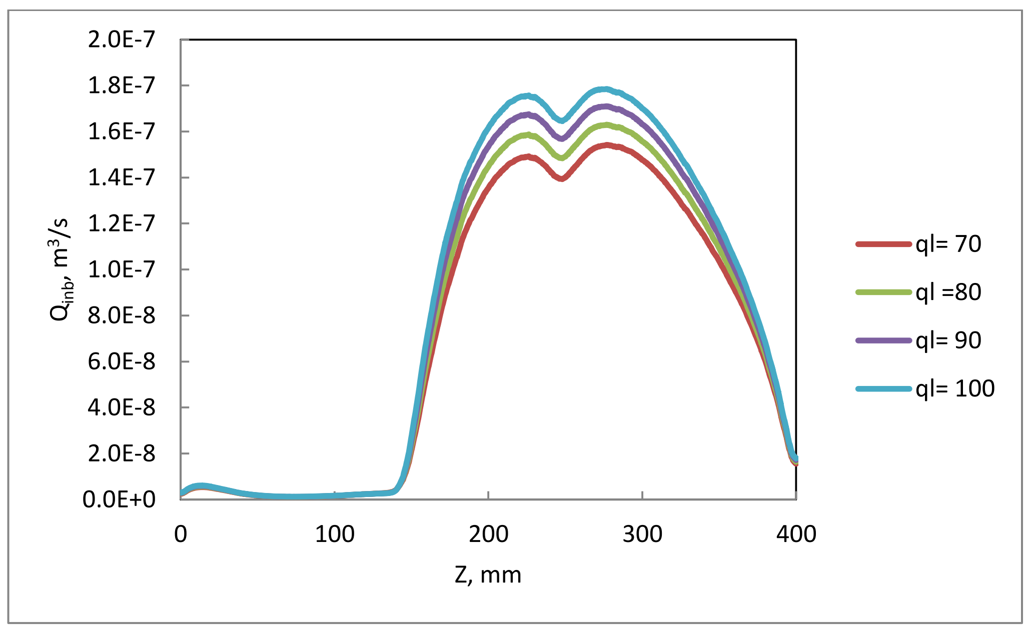

Figure 6.9: Flow rate long the server between the rectangular baffle for a different heat flux load.

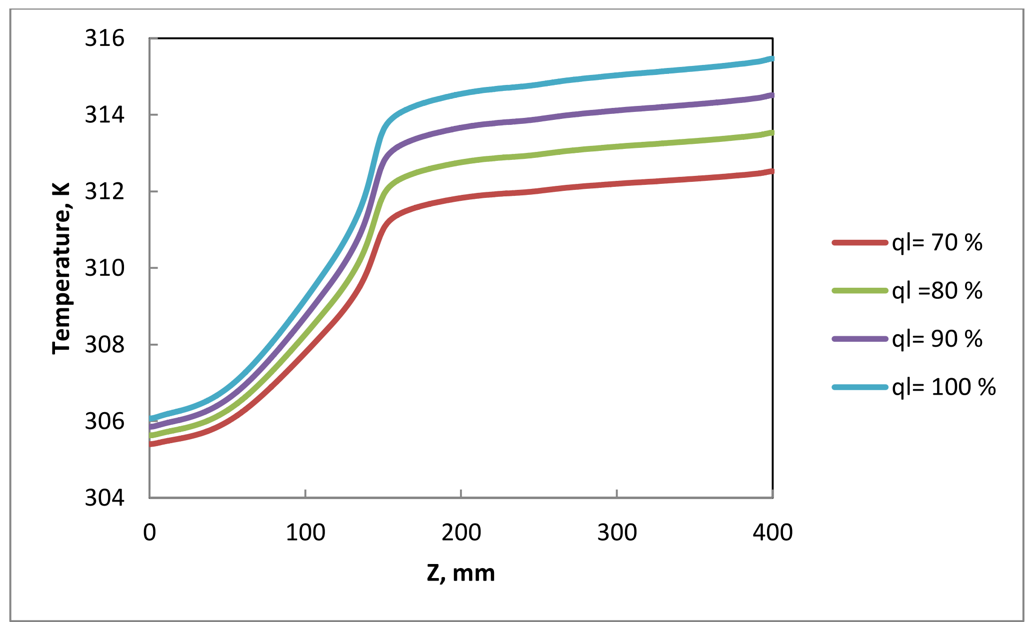

Figure 6.10: Temperature in centre line between rectangular baffles along the server for different heat flux load

6.3.4 Effect of CPU location on heat transfer

The following investigation is to determine the effect of the CPU and heat sink location on the heat transfer within the immersed server model with rectangular baffles. The CPU and heat sink locations are varied as shown in Figure 6.11. The variation is from the top to the bottom of the server and the CPU location defined as (S) where the values are shown in Table 6.3.

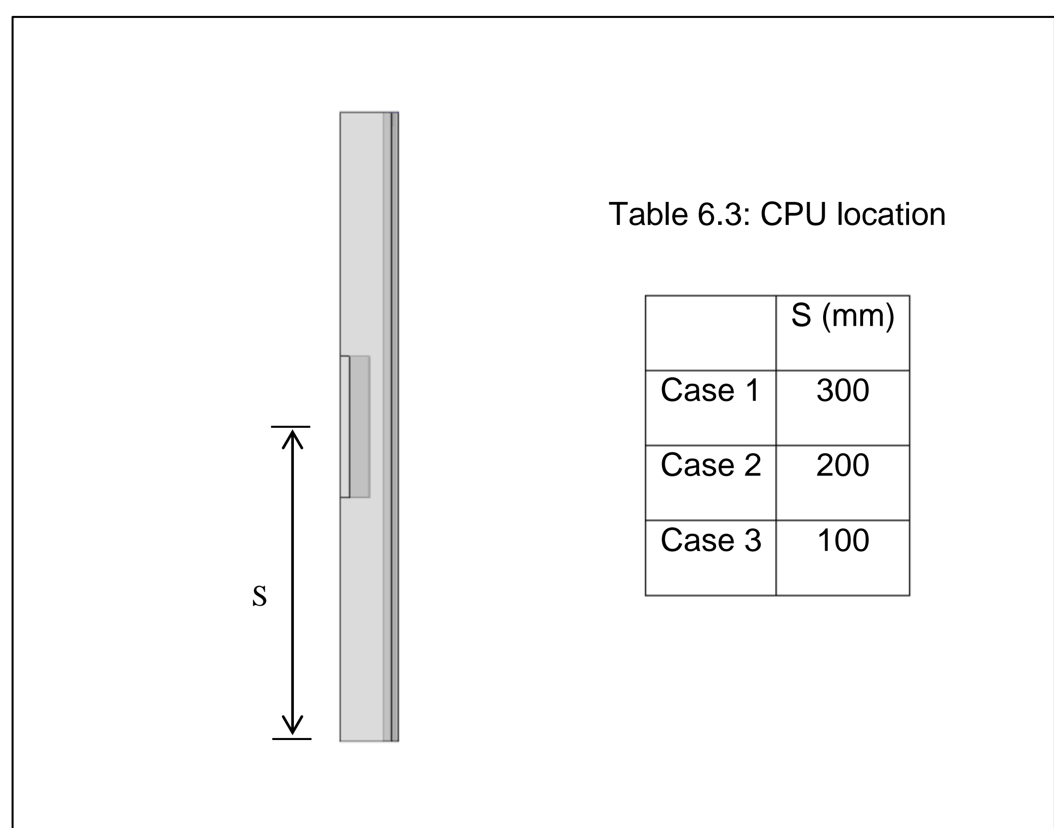

Table 6.3: CPU location

	S (mm)
Case 1	300
Case 2	200
Case 3	100

Figure 6.11: CPU locations, where S is varying as shown in Table 6.3

The effect of the CPU and heat sink location on Nu is presented in Figure 6.13. The heat flux load is also varying from 70 to 100% while the flow rate and inlet temperature were kept constant at 3×10^{-7} m^3/s and 303 K respectively. The highest Nu implies the best heat transfer performance and it occurs when the CPU is located in the bottom at S= 100 mm which is for

case 3. Figure 6.13 shows that the Nu is increased by 89% from the S= 300 to 100 mm. This indicted that the CPU and heat sink location has great effect on the heat transfer performance. This result shows that practicalities of placing a server motherboard and CPUs into an immersed situation are equivalent to air-cooled systems, since the hottest components are at the front of the board as shown in Figure 6.12. Therefore, for immersed servers placed vertically the hottest components will be at the bottom.

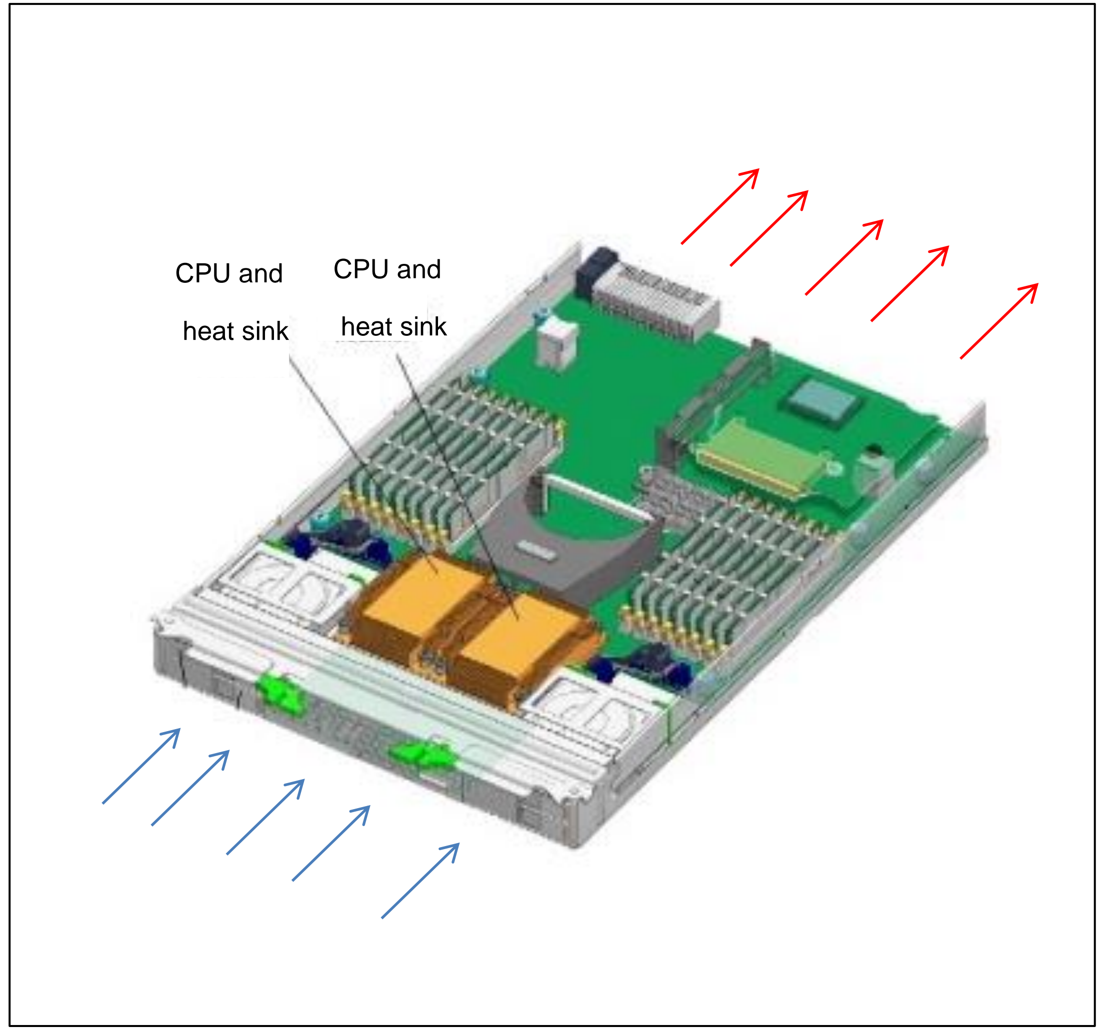

Figure 6.12: the location of CPU for server using air for cooling [109].

As the HFE 7300 dielectric liquid is heated the density decreasing which aids the fluid to traverse to the top of the server, the density then increases

again once it becomes adjacent to the cold plates and the liquid then travels down. This buoyancy force creates the circulation of the fluid and hence transfers the heat from the heat sink to the cold plate. In the case of the CPU located at the bottom of the server the buoyancy force is greater than when the CPU is located at the top. So the circulation of the fluid is stronger and the velocity of fluid flow is larger and this leads to an enhanced heat transfer natural convection performance. The effect of the CPU location in the velocity and circulation inside the server can be shown clearly in Figure 6.14. These velocity profiles are selected for the best heat transfer performance when the heat flux load is 100%, flow rate is $3x10^{-7}$ m^3/s and water inlet temperature is 303 k. The velocity of the HFE 7300 dielectric liquid on the bottom of the CPU and heat sink in the vertical orientation is very small that has no effect on the heat transfer performance.

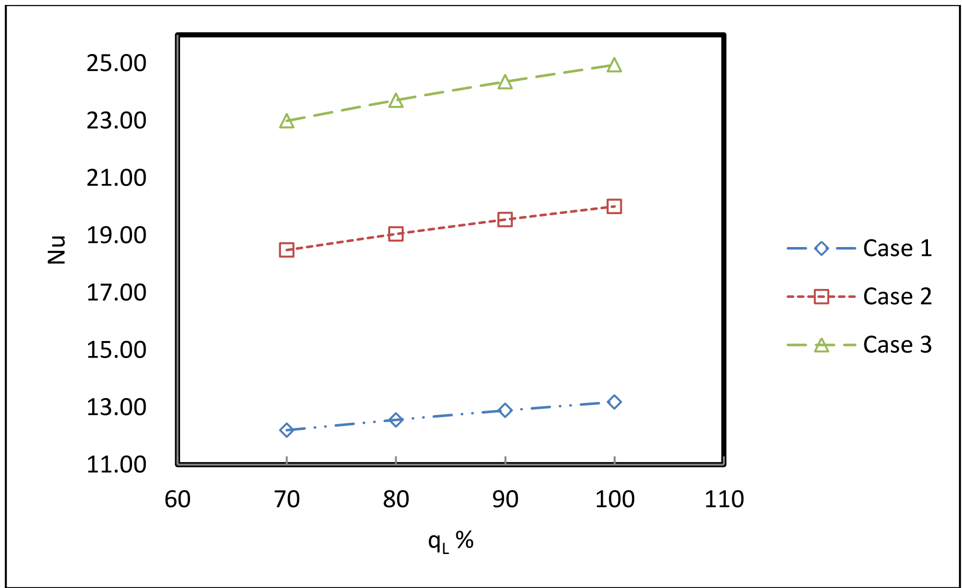

Figure 6.13: variation of heat flux load for different CPU location.

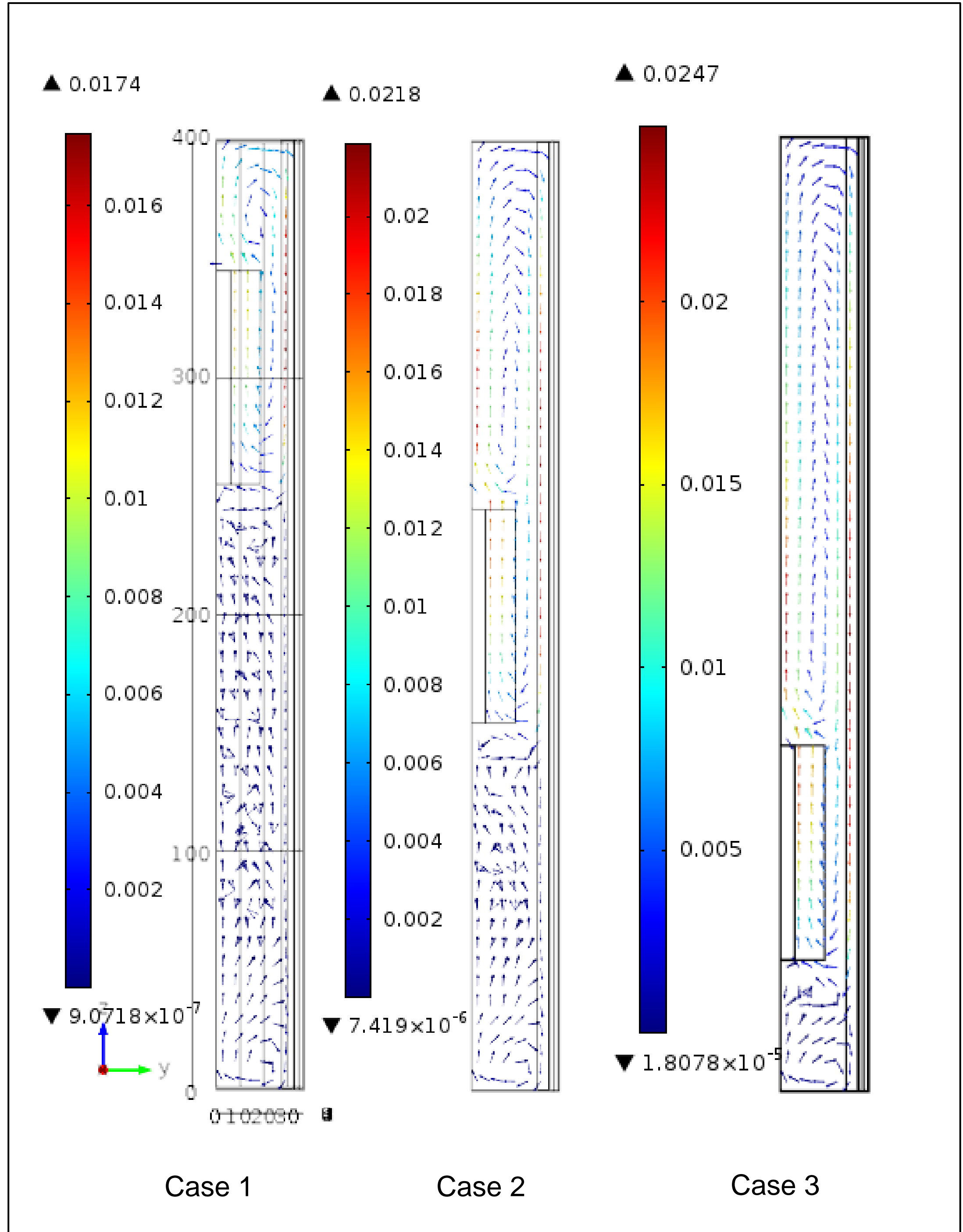

Figure 6.14: Effect of the CPU location on the velocity for different cases at q_L= 100%, Q_{in}= $3x10^{-7}$ m^3/s and T_{in}= 303 k

6.4 Summary

A computational study was carried out to investigate the different baffles cross sectional shapes for heat transfer in immersed servers with cold plates. The conjugate heats are coupled using COMSOL 4.3 for two different fluid physical flow conditions; one turbulent fluid (for the dielectric liquid) and the other laminar (for the water). The CPU generates heat which is conducted to the heat sink and then heat is convected naturally by the HFE 7300 dielectric liquid in which the server is immersed to the cooled water loop channel inside the cold plate. The heat flux load, water flow rate and inlet water temperature were varied for each baffle cross section, namely square, rectangular, triangular and two trapezoidal. The results show that all baffles can offer better heat transfer performance when compared to no baffles. It is further noted that a baffle with a rectangular cross section has the best heat transfer performance. The Nu for the rectangular baffles was improved by 71% and T_{case} dropped by 20K. In the case of different CPU locations, which have been investigated in this study it is found that the CPU should be located at the bottom of the server enclosure, since it offers the best heat transfer performance. This study yielded an overall boost of 89% in Nu value for the different CPU locations.

CHAPTER 7:

COOLING SYSTEM ANALYSIS FOR A DATA CENTRE USING LIQUID IMMERSED SERVERS

7.1 Introduction

The main interest in this chapter involves the integration of liquid immersed servers in the whole data centre cooling system. The cooling system in this study consists of a dry air cooler and buffer heat exchanger, together they can reject the heat from racks via liquid loops. The cooling system is explained in detail in the next sections. The ambient temperature for the calculations in this work are taken for the city of Leeds [110]. A MATLAB program is used to calculate the inlet water temperature to the rack based on the ambient temperature and pump flow rates. With the evaluated rack inlet flow rate and temperature, a computational model based on COMSOL is used to determine pressure drop for the immersed servers. The power of the pumps can be determined for the pressure drop and flow rate. The power usage effectiveness (PUE) of the data centre is calculated from

the IT power consumption and power consumed by the pumps and fans in the cooling loops. The variation of PUE is determined with varying rack load and is also presented.

7.2 Cooling data centre system

A schematic diagram of the data centre cooling system that is used in this section is shown in Figure 7.1. On the right of the figure is a dry air cooler and fan, which moves the air at the ambient outside temperature (T_5) through the heat exchanger. A pump circulates the water from the dry air cooler heat exchanger to a buffer (liquid-to-liquid) heat exchanger at a flow rate, Q_{inr}, to reject the heat from the data centre. On the left side of the figure the immersed servers are housed in the rack and are connected to the buffer heat exchanger via a liquid loop inside the data centre. A second pump circulates water between the buffer heat exchanger and the racks at a flow rate, Q_{ins}. The cold (supply) temperature to the buffer heat exchanger is T_3 and the inlet (supply) water temperature to the servers is, T_1.

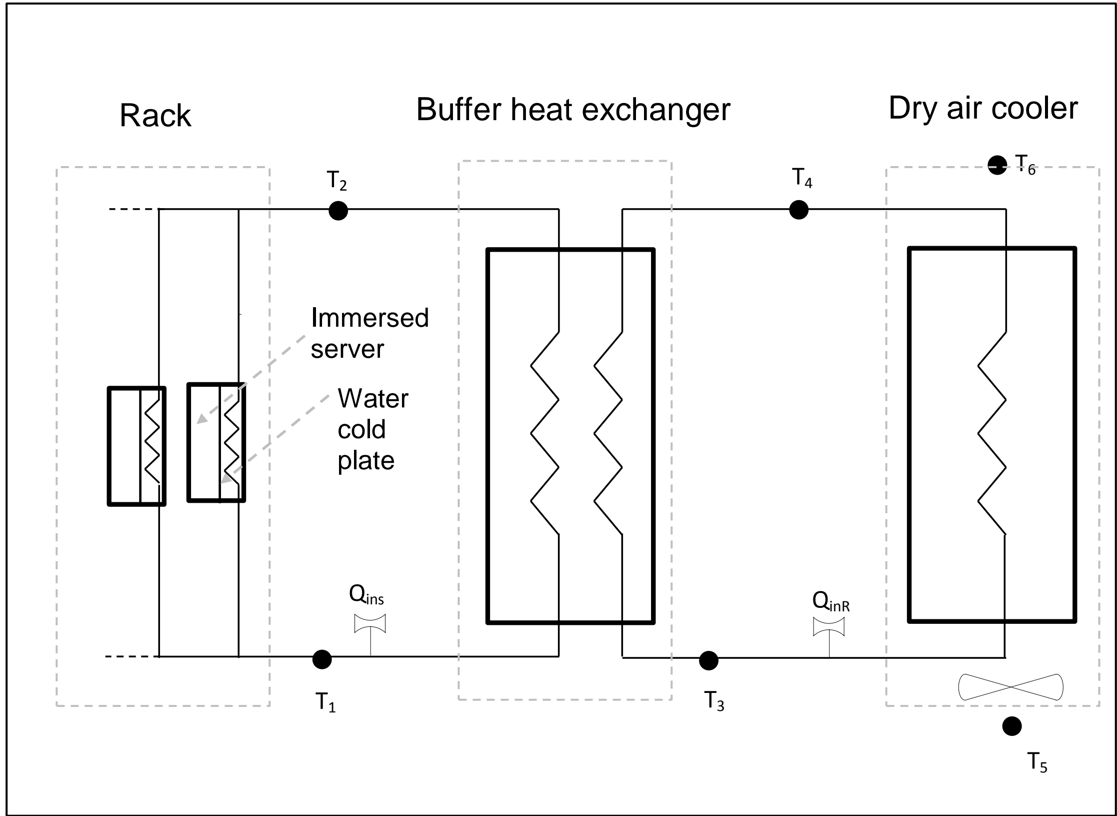

Figure 7.1: Schematic diagram of the data centre cooling system

The model using COMSOL is applied to simulate the heat transfer at the server level only. However, the data for the dry cooler and buffer heat exchanger are taken from an experimental study [111]. They studied a data centre cooling system experimentally, which had a cooling system arrangement that included a dry cooler, buffer heat exchanger and servers that were cooled by a combination of pumped water cold plates on the CPU and air, via fans, for the rest of the server.

In this study, the server is fully immersed without any air cooling used and therefore, the relative humidity is not considered in the system. This gives an advantage of limiting the number of variables to be only the temperature. The ambient temperature, T_5, is chosen for the city of Leeds, England [110]. The annual average temperature of Leeds is shown in Figure 7.2.

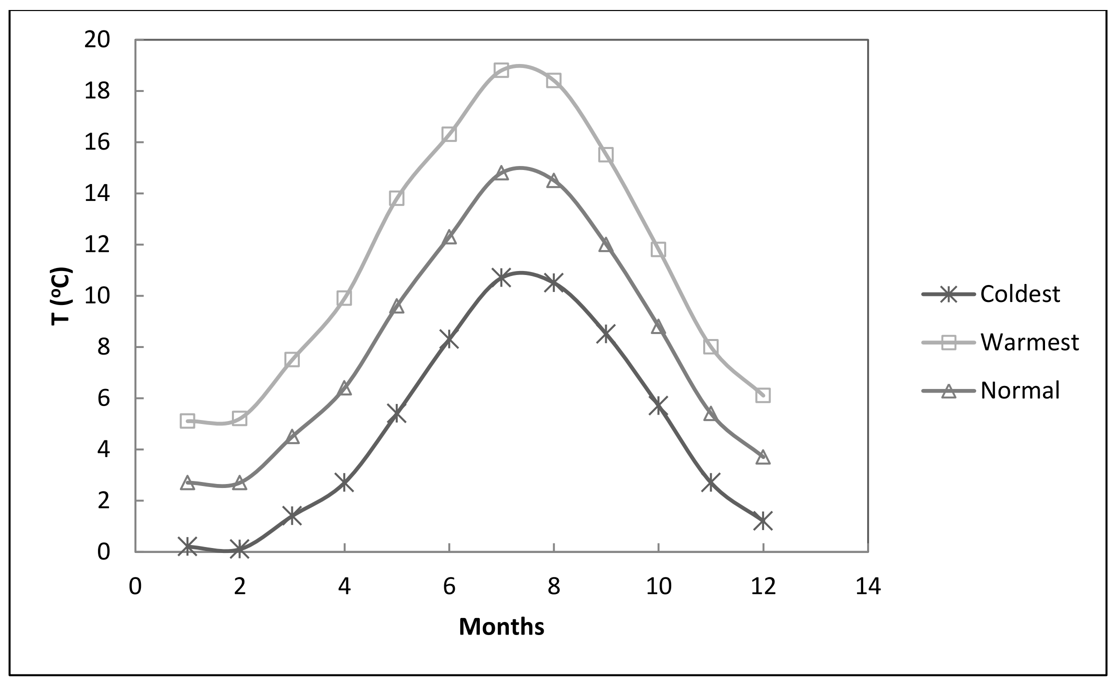

Figure 7.2: Average temperature of Leeds, England [110].

7.3 Methodology of flow rate and temperature calculations

In the previous section, the data centre cooling system and method of obtaining the ambient temperature, T_5, was explained. This section develops an approach to determine the other system parameters, which are the flow rate from the dry cooler to the buffer heat exchange, Q_{inr}, the flow rate from the buffer heat exchanger to the rack, Q_{ins}, the cold (supply) water temperature entering the buffer heat exchanger, T_3, and the water inlet temperature of servers, T_1.

The flow rates, Q_{ins} and Q_{inr}, each take one of the values, 5, 7.5, 10 GPM, which are aligned to the experimental work [111] as explained in section 7.2. In [111], a graph is plotted between ΔT_{apr} and the flow rate, Q_{inr}, for dry cooler fan speeds of 169 rpm. The ΔT_{apr} is the temperature difference between the ambient temperature, T_5, and the inlet water temperature of

buffer heat exchanger, T_3. The flow rate, Q_{ins}, and dry air cooler fan speed used are taken directly from [111], however the cooling load is different. In [111] the ΔT_{apr} is plotted against Q_{inr} at a cooling load of 15,000 W, whereas the rack cooling load in this work is 5000 W (each server load is 100 W and the number of servers in one rack is 50 servers). As the flow rate and fan speed are the same as used in [111] and the heat load is different, the ΔT_{apr} is scaled down by interpolating between two rack heat load, 5000W and 15000W. Figure 7.3 shows the variation of ΔT_{apr} at different flow rates, Q_{inr}, where the fan of dry cooler is spinning at 196 rpm and a cooling load of 5000 W.

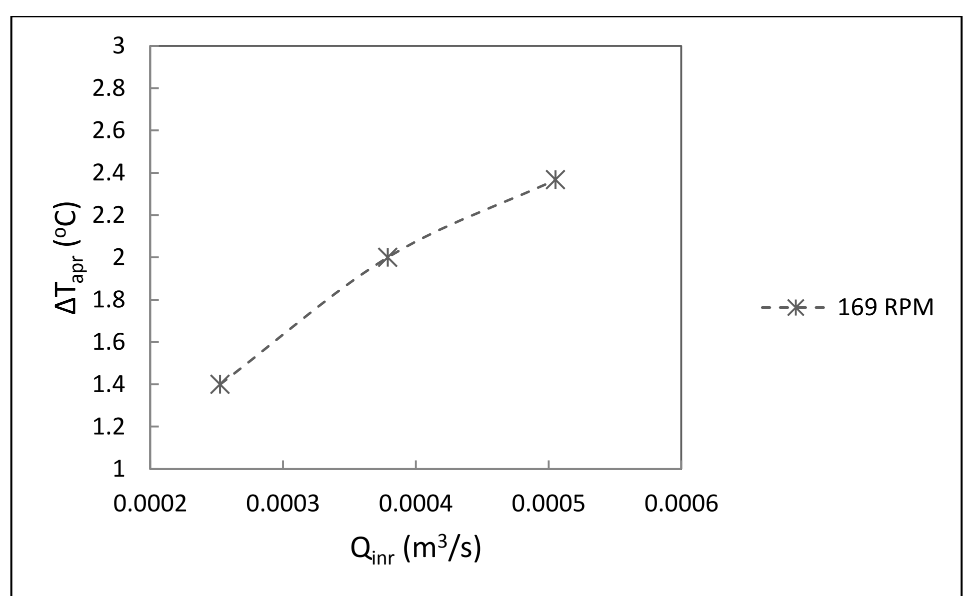

Figure 7.3: The variation of ΔT_{apr} with flow rate Q_{inr}, dry cooler fan spins at 169 rpm

The flow rate, Q_{inr}, is a function of ΔT_{apr} and this function is obtained from curve fitting the graph in Figure 7.3, it is expressed as:

$$\Delta T_{apr} = -7x10^6 Q_{inr}^2 + 9366.8 Q_{inr} - 0.5 \quad (7.1)$$

The flow rate between the dry cooler and the buffer heat exchanger, Q_{inr}, is known, so the ΔT_{apr} can be calculated from the equation above and the inlet water temperature to the buffer heat exchanger, T_3, can then be evaluated using

$$T_3 = T_5 + \Delta T_{apr} \tag{7.2}$$

Having obtained the value of T_3, the next step is to determine the inlet water temperature to the servers, T_1. The value of T_1 is based on ΔT_{aps}, which is the temperature difference between the water temperature entering the buffer heat exchanger, T_3, and the inlet water temperature to the rack, T_1, based on the following relationship

$$T_1 = T_3 + \Delta T_{aps} \tag{7.3}$$

The value of ΔT_{aps} is obtained from relationships with Q_{ins} and Q_{inr}. The values of Q_{ins} and Q_{inr} take values from 5, 7.5 and 10 GPM. In [111] the graph lines for ΔT_{aps} varying with Q_{ins} and Q_{inr} which is done at cooling load 15,000 W . In this section the rack cooling load is for 5000 W and the flow rate is kept the same as in the experimental work, [111], however the cooling load is different so ΔT_{aps} is scaled down as explained before. Figure 7.4 shows the variation of ΔT_{aps} for a 5000 W cooling load for different flow rates from the dry air cooler heat exchanger to the buffer heat exchanger and from the rack to the buffer heat exchanger.

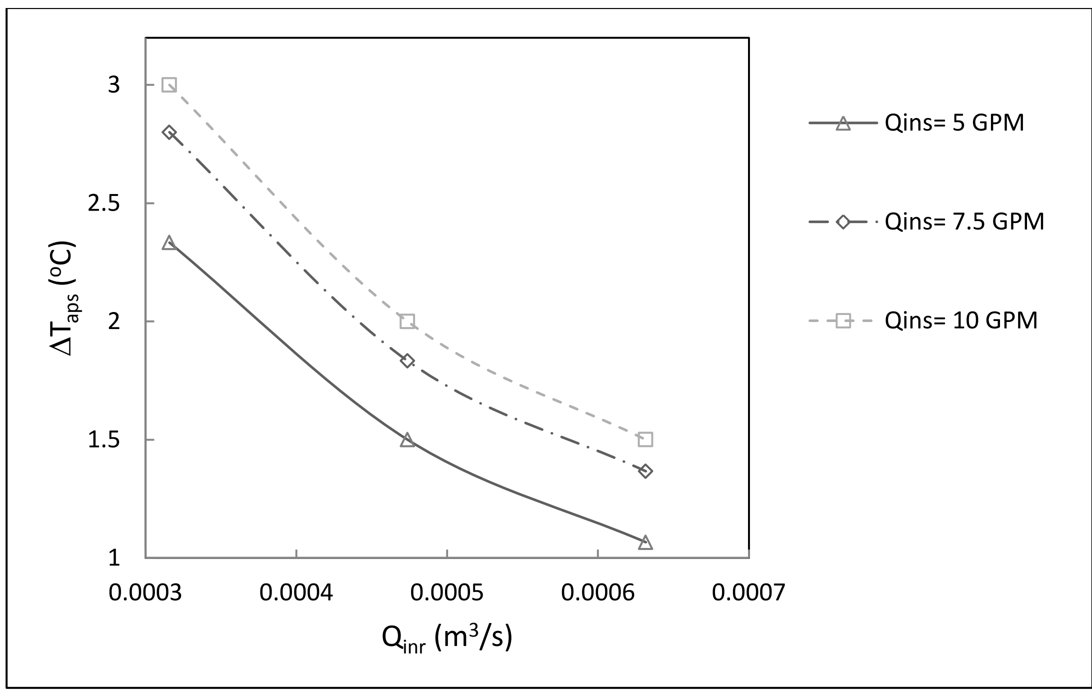

Figure 7.4: The variation of ΔT_{aps} with Q_{ins} and Q_{inr}

The ΔT_{aps} is affected by the values of Q_{ins} and Q_{inr} and the relationship is obtained by fitting curves from the results in Figure 7.4. The equations of ΔT_{aps} can be expressed as:

At Q_{ins} = 5 GPM

$$\Delta T_{aps} = 8x10^6 Q_{inr}^2 - 11609 Q_{inr} + 5.2 \quad (7.4)$$

At Q_{ins} = 7.5 GPM

$$\Delta T_{aps} = 1x10^7 Q_{inr}^2 - 14037 Q_{inr} + 6.23 \quad (7.5)$$

At Q_{ins} = 10 GPM

$$\Delta T_{aps} = 1x10^7 Q_{inr}^2 - 14248 Q_{inr} + 6.5 \quad (7.6)$$

A M script in MATLAB v7.11 is developed and applied to solve all of the above equations to find the inlet water temperature of the rack, T_1. The flow chart of the programing steps is shown in Figure 7.5.

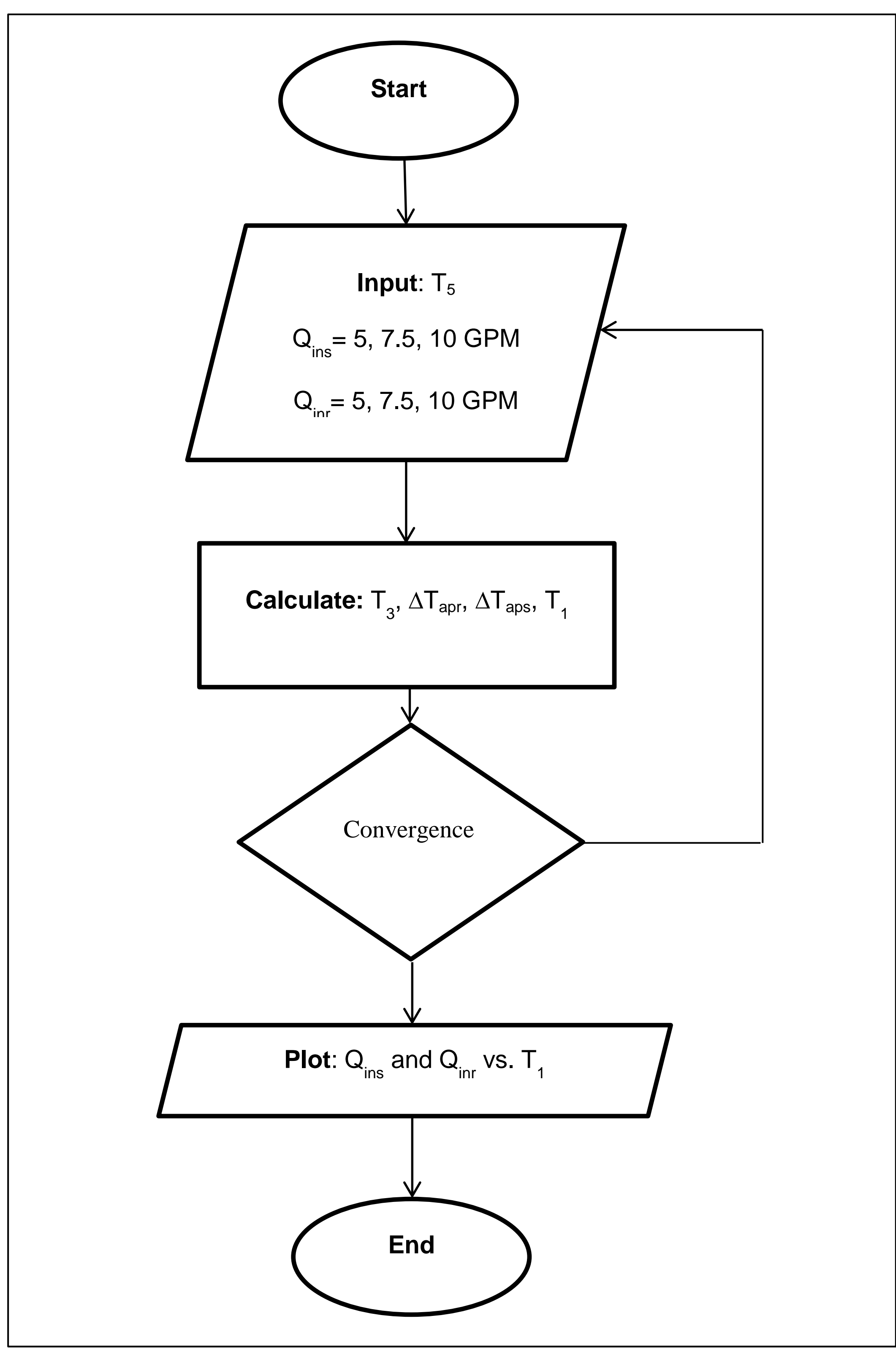

Figure 7.5: Flow chart of calculations to find T_1 using MATLAB v7.11.

7.4 Results of rack inlet temperature and the simulation model

This section presents the results of the rack water inlet temperature, T_1, which is obtained from the MATLAB program. The ambient temperature that is selected from Figure 7.2 is T_5 = 19 ^oC which is the highest temperature of the year in Leeds [110]. There are two flow rates through the buffer heat exchanger the first one is the flow rate from the dry air cooler heat exchanger to the buffer heat exchanger, Q_{inr}, and the second flow rate is from the buffer heat exchanger to the rack, Q_{ins}. The flow rates, Q_{ins} and Q_{inr}, are set independently to a value from 5, 7.5 and 10 GPM.

The effects of varying the flow rates on the rack water inlet temperature, T_1, are presented in Figure 7.6. Both flow rates, Q_{ins} and Q_{inr}, are varied independently between the three values 5, 7.5 and 10 GPM. The results show that T_1 decreases with increasing Q_{inr} and decreasing Q_{ins}. The lowest T_1 value is found to occur, at the highest Q_{inr} and lowest Q_{ins} as expected from the experimental result [111].

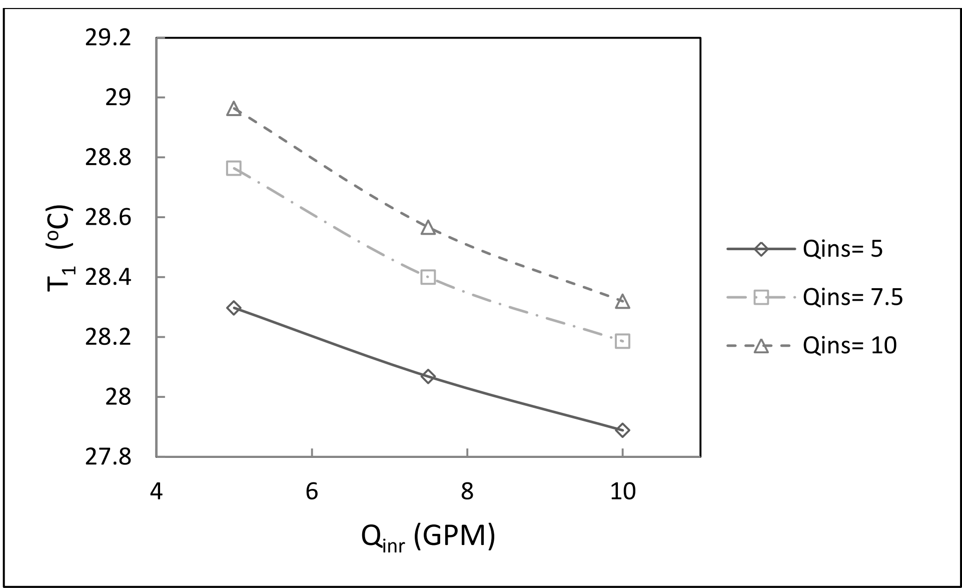

Figure 7.6 : Water inlet temperature of rack (T_1) varying Q_{inr} for different Q_{ins}

From the above results the lowest water inlet temperature to the rack is found to be T_1= 27.9 ^oC at Q_{ins}= 5 GPM. The geometry and boundary condition of the liquid immersed server model is shown in Figure 7.7. Heat is generated from the CPU underneath the heat sink and cooled by the water that passes through the cooler solid block representing the water jacket at T_1= 27.9 ^oC and Q_{ins}= 5 GPM.

The simulation model based on COMSOL 4.3 is now used to determine pressure drop in order to calculate the required pump power (see chapter 5 and 6).

The water inlet temperature of the server channel is T_{in}= T_1= 27.9 ^oC. The flow rate of the rack is Q_{ins} = 5 GPM and the flow rate used in the server cold plate water channel is:

Flow rate for one water channel

$$Q_{inc} = \frac{\mathrm{F.R.R(GPM)}}{\mathrm{N.O.Sx\ N.O.C.S}}$$

$$= \frac{5}{50\mathrm{x}\ 55\mathrm{x}\ 15852} = 1.15\ x10^{-7}\ \frac{m^3}{s}$$

Where F.R.R is flow rate to the rack, N.O.S is number of servers per rack and N.O.C.S is the number of water channels in one server.

The pressure drop across the water channel (ΔP_{ch}) is found to be 11.6 Pa from the simulation model with a temperature inlet to the server water channel equal to 27.9 ^{o}C and the water flow rate inlet server channel is 1.15x10^{-7} m^3/s.

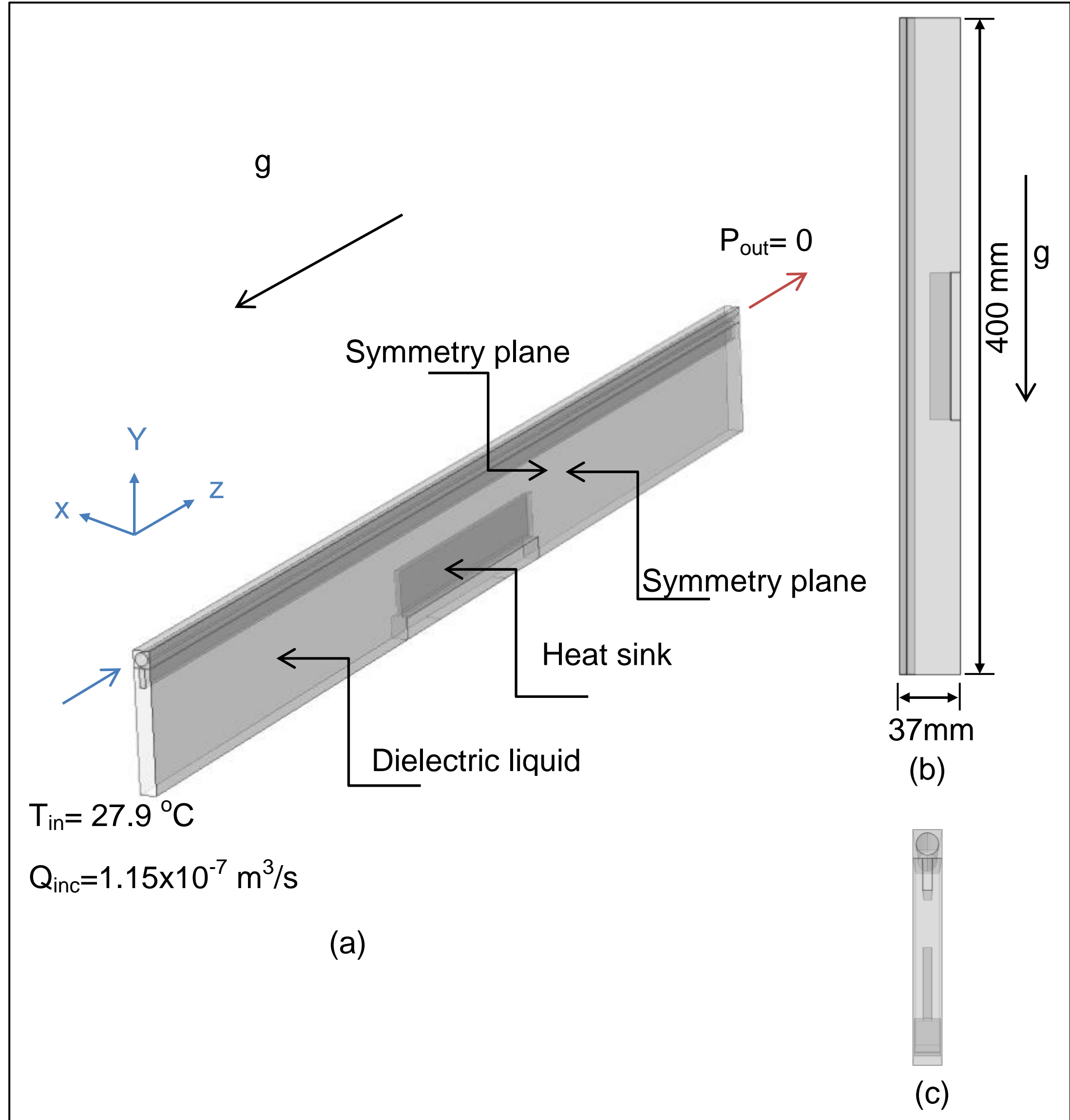

Figure 7.7: the geometry of the symmetry simulation model used in COMSOL a) Isometric view b) Side view c) Front View

7.5 PUE of the cooling system

The power usage effectiveness (PUE) is used to indicate the effectiveness of the data centre cooling systems and is calculated on the basis of the total power consumed by the data centre relative to power that is supplied to the IT. A PUE of 1 means that the data centre has achieved the best data centre efficiency [37]. The equation that is used to calculate the PUE is [38, 39]

$$PUE = \frac{Total\ Power}{IT\ Power} = \frac{P_{IT} + P_c}{P_{IT}} \quad (7.7)$$

The power of data centre utilities and power of IT is required to calculate the PUE. The power consumed by the IT in this work is obtained from the rack power which is

P_{IT} = 50 x100W= 5.0 kW

In this study there are two pumps to circulate water between the heat exchangers and fans to reject heat outside of the data centre from the dry air cooler. The power of the pump, P_{ps}, that circulates the water between the rack and buffer heat exchanger is determined by [112]

$$P_{ps} = \frac{\Delta P_s\, Q_{ins}}{\epsilon} \quad (7.8)$$

Where, Q_{ins} is flow rate between the rack and buffer heat exchanger, ϵ is the pump efficiency. The pressure drop from the simulation model for one channel is ΔP_{ch} =11.6 Pa

The pressure drop for the rack is given by,

ΔP_s= N.O.S x N.O.C.S x ΔP_{ch} =50x55x11.6 = 31.9 kPa

Where N.O.S is number of servers per rack and N.O.C.S is the number of water channels in one server.

Pump efficiencies are between 0.5 and 0.6 [113], in this study the pump efficiency is chosen to be 0.5 for the worst case scenario. The power required pumping the water between the rack and buffer heat exchanger is

$$P_{ps} = \frac{\Delta P_s \, Q_{ins}}{\epsilon} = \frac{31900x \; 0.000316}{0.5} = 20.15 \; W$$

The power required by the dry air cooler heat exchanger fans is based on the flow rate and pressure drop. The power of the fans calculated from,

$$P_f = \frac{\Delta P_f \, Q_f}{\epsilon} \quad (7.9)$$

Where the P_f is fans power, ΔP_f is pressure drop across the dry air cooler heat exchanger and Q_f is air flow rate. The ΔP_f is calculated from [114] which is written as:

$$\Delta P_f = \frac{2 f N_r \mathrm{G}^2}{\rho_a} \quad (7.10)$$

Where f is fanning friction factor, N_r number of tube rows, ρ_a is the air density and air flow rate, G, is calculated from

$$G = \rho_a V_f \quad (7.11)$$

The fanning factor friction f can be determined by the flowing expression

$$f = 18.93 R_e^{-0.316} (\frac{P_T}{D_r})^{-0.927} \quad (7.12)$$

Where Re is Reynolds number, D_r is root diameter and P_T tube pitch. This correlation from experimental work for six rows of bank tube with parameters range:

$$2000 < Re < 50000 \quad (7.13)$$

$$0.0186m < D_r < 0.041m \quad (7.14)$$

$$0.0428m < P_T < 0.114m \quad (7.15)$$

The Re needs to be calculated to check if this case can be applied to the experimental correlation in determining the fanning factor friction. The fans of the dry air cooler spins at rotational speeds (N) of 169 RPM and the diameter of the fans is D_f= 0.4 m. Hence, the velocity is

$$V_f = \frac{\pi\, D_f N}{60} = 3.54\, m/s \quad (7.16)$$

At the ambient temperature of T_5 =19 ^oC, the thermal properties are [115]; ρ_a= 1.2 kg/m^3 and μ_a= 1.8x10^{-4} Pa. s

The Reynolds number can be calculated from:

$$Re = \frac{\rho_a V_f D_r}{\mu_a} = 5925.5 \quad (7.17)$$

This value is within the range of the experimental correlation (see the range in equation (7.13)). The D_r and P_T parameters are selected a D_r= 0.0254 m and P_T=0.0762 m within the range of the correlation limits, thus the fanning factor fraction can be defined as:

$$f = 18.93 R_e^{-0.316} \left(\frac{P_T}{D_r}\right)^{-0.927} = 0.438$$

And G = ρ_a V_f = 4.26 kg/m^2.s

The pressure drop across the dry air cooler heat exchanger from equation (7.10) is

$$\Delta P_f = \frac{2 \text{ x } 0.438\text{x } 6\text{x } 4.26^2}{1.2} = 79.4\ Pa$$

The flow rate is

$$\mathrm{Q}_f = \frac{\pi}{4} D_f^2 V_f = 0.444\ \frac{m^3}{s}$$

The power required for one fan in the dry air cooler is,

$$P_f = \frac{\Delta P_f\ Q_f}{\epsilon} = 70.5\ W$$

The dry air cooler has 5 fans and the power required for all fans yielding P_{tf} = 352 W.

To calculate P_c, which is the total power required for cooling P_c= p_{ps}+ p_{pr}+ p_{tf}. To calculate the power of the pump that circulates the water between the dry air cooler heat exchanger and the buffer heat exchanger, p_{pr}, requires an estimate of the pressure drop. However, the pressure drop in the rack is greater than the pressure drop in the dry air cooler heat exchanger and since Q_{inr} is double Q_{ins}, assuming P_{pr} to be double to P_{ps} is a worst case scenario. The pumps, fans and IT power are all determined and hence the PUE can be calculated as:

$$PUE = \frac{Total\ Power}{IT\ Power} = \frac{P_{IT} + P_{ps} + P_{pr} + P_{tf}}{P_{IT}} = \frac{5000 + 20.15 + 40.3 + 352}{5000}$$

$$= 1.08$$

Chi [116] has carried out a comparison between The PUE of the fully immersed ICETOPE cooling and an equivalent air water data center cooling. The study found that the PUE for full system is 1.14 and 1.48 for immersed and air water cooling system respectively. The study included the PUE for cooling only and the PUE is found to be 1.081.

7.6 PUE for different number of servers

In the previous section the PUE is determined for a full rack with 50 servers. This section investigates the effect of decreasing the number of servers in a rack on the PUE. The pressure drop per server is 638 Pa. However, the flow rate passing through the rack is varying based on the number of servers. This affects the power that is required by the pumps as shown in equation.

$$P_{ps} = \frac{\Delta P_s \, Q_{ins}}{\epsilon}$$

Where, P_{ps} is the pumping power ΔP_s is the pressure drop across the rack, Q_{ins} is the flow rate between the rack and buffer heat exchanger, ϵ is the pump efficiency. In this section, the number of servers per rack is changing from 10 to 50 servers and based on that the rack cooling load start from 1,000 to 5,000 W. The required pumping power to circulate the water between the rack and buffer heat exchanger is varying from 0.8 to 20 W. The power of circulating the water between the buffer heat exchanger and the dry air cooler heat exchanger, P_{pr}, is again assumed to be double, P_{ps}. The fan power of the dry air cooler is unchanged.

Figure 7.8 shows the effect of the number of server per rack on the PUE. The results show that the PUE decrease by 26% for the full rack load of 50 compared to a 20% partial rack load. Increasing the number of servers per rack decreases the PUE since the power required for the pumps, is not significantly changing with number of servers added.

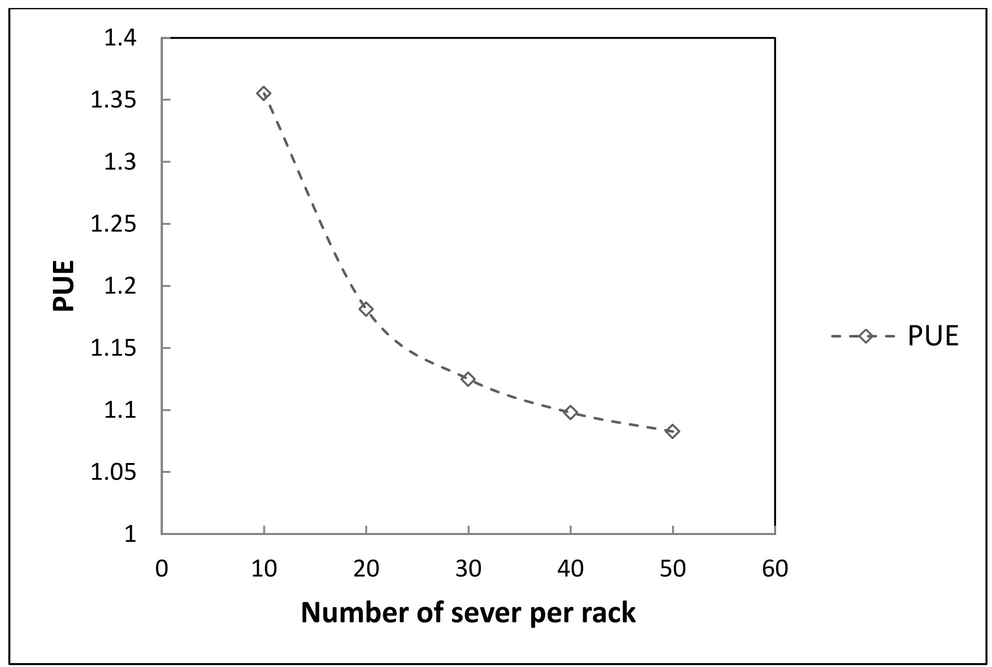

Figure 7.8: variation of PUE by changing the number of the servers per rack

7.7 Summary

The data centre cooling system in this study consists of a dry air cooler and a buffer heat exchanger to dissipate the heat from a liquid cooled rack. Temperatures in the full heat rejection system are determined by combining empirical data with full CFD simulations and are based on a real geographical ambient temperature used for the dry air cooler, T_5, of 19 ^oC. The data centre cooling system parameters are calculated using MATLAB to

obtain the inlet temperature, T_1, and flow rate, Q_{ins}, which are used as boundary conditions for the liquid immersed server model using COMSOL to determine the pressure.

The power of the pumps is determined from the flow rates and pressure drops, which enables the PUE of the data centre to be calculated, yielding a PUE of 1.08. The effect of the PUE for different rack loads is investigated and it is found that the PUE increases by 26% as rack-server occupancy drops to 20% of maximum capacity. This is due to the pump power dropping with decreasing pressure drop.

CHAPTER 8:

CONCLUSION

8.1 General discussion

The data centre power consumption is increasing due to the high demand in digital services together with the increased penetration of broadband globally. The cooling of the data centres that house all of the digital services has a major share of the power consumption, in fact over 30% of the total power consumption [4, 5]. There are two approaches of cooling data centres, one based on air and the other on liquid. The liquid cooling method can be classified into three categories which are back door cooler heat exchanger, immersed server and on chip heat exchanger (Cold plate). In this thesis the study has been focused on immersion of the server, where CFD is applied to simulate heat transfer from the processor into the dielectric liquid and transferred by buoyancy to cold plates. Buoyancy drives the flow inside the server due to temperature differences. The validation of the buoyancy driven flow is achieved by contrasting results for the benchmark cavity problem (section 4.2). Further validation has been carried out with a rectangular cavity that contains three heat sources attached

(chips). In addition, validation for fluid flow regimes was assessed for finned rectangular enclosures where the flow is consider being turbulent. All of the validations demonstrated very good agreement and they demonstrate that the COMSOL multiphysics modelling software is a capable tool to simulate an immersed server model. COMSOL uses the finite element method which is a robust and recommended approach to solving the combined heat transfer and fluid flow problems such as cooling electronic components [76].

The second phase in this thesis was to develop an immersed server model (Chapter 5). The computational domain for this complex geometry was based on symmetry conditions, where the heat flux is generated by a CPU and the heat is conducted to a heat sink made of copper and the heat removed by dielectric liquid between the heat sink and cold plate under the action and buoyancy, then the liquid is cooled by the cold plate. The study in this phase uses the optimisation approach to find the optimum value between the two different heights, namely the heat sink fin height and the distance from the CPU to the cold plate.

After finding the suitable fin and cold plate heights based on the top centre CPU temperature T_{case}, the third phase is mainly developing heat transfer improvements of the immersed server cooling by adopting the use of baffles attached on the dielectric facing side of the cold plate (Chapter 6). The study investigated different cross sectional areas of baffles using rectangular, square, triangular and two trapezoidal shapes. The baffles have the same cross sectional area and the same material density consequently they have same weight and cost. The cross section shape of the baffles was the only variable, which in turn was found to affect the temperature and velocity of

fluid flow. The results show that the rectangular shape cross sectional area baffles improves the heat transfer performance by 71% compared to no baffles and Tcase dropped by 20 K.

The last phase of this thesis has developed a data centre model for the PUE, which is based on the immersed server model when a number of servers are installed in racks (Chapter 7). The cooling system of the data centre for this phase is taken from experimental work [111], and incorporates an air dry cooler and a water heat exchanger. The primary water cooling is recirculated between the rack (servers) and the heat exchanger and the other (secondary) water recirculation is from the heat exchanger to the air dry cooler. The flow rate applied to simulate a data centre rack of immersed servers is based on the flow rate from the heat exchanger and the rack. Pressure drops in water circuits are used to determine the pump power required and therefore to calculate the PUE.

The conclusions of this thesis can be written based on the results of the above phases as follows:

1. In chapter 4, section 4.4 the comparison was done between three different CFD packages which are COMSOL and Fluent. Fluent is using finite volume whereas COMSOL use finite element and the reason of using COMSOL because it solves multiphysics problems like the conjugate heat transfer problem in this thesis. The comparison between the CFD packages is done for square cavity where there is a buoyancy driven flow. The fluids that are used in the cavity are water and a dielectric, which is a hydrofluoroether HFE

7300. The Ra is smaller than 10^6 to make sure that the fluid inside the cavity is laminar. The results of the comparison show that the there is no significant difference between of prediction the various packages for buoyancy driven flow problems.

2. Multiple heat sink fin simulations have been investigated to ascertain if the symmetry condition for the immersed server model affects the solution. Two and three fin solutions are used in this study. The results in chapter 5 section 5.2.5 proves that the changing the number of fins has very little effect on T_{case}. However, using one simplifies the model, reduces the computational time and decreases the mesh size by 48%.
3. The study of two design variables which are fin height and cold plate height for immersed server is done in chapter 5. The optimum value for the fin height and the cold plate height in the parameter range were found to be H_{fin} = 23.9 mm and H_{plate} = 30 mm. The optimum solution was found to drop the T_{case} by 16.4 K. The optimisation approach made use of the Optimal Latin Hypercube design of experiments and the Genetic Algorithm optimisation method, both of which were an effective approach to find the optimum heat transfer scenario for the immersed server. The response surface is simple in this case, the results of which laid on the boundary of the domain, and however the approach could be used for more complicated geometries.
4. Using a typical flow rate in a cold plate water channel on the top of immersed server has been presented with the water flow being

laminar, see chapter 6. The water inlet flow rate must be defined as a developed flow in order to compare it with the heat balance equation ($\dot{Q}$ =m c_p (T_{in}-T_{out})). The conclusion of this validation is that in case of not defining the water inlet as developed flow will produce an error between the T_{out} from the simulation model and the T_{out} from the heat balance equation. The error for T_{out} between the simulation model and heat balance equation without a defined developed flow is 4.7% however with a defined flow rate that has developed flow, the error was 0.11%.

5. The study of using different cross section area of baffles in chapter 6 shows that the heat transfer performance can be improved by using baffles. The study concluded that the best shape among the baffles is the rectangular baffle with the same cross sectional area. The Nu number of rectangular baffles showed a 71% increase when compared to no baffles.
6. The study in chapter 6, section 6.3.4 also considered the effect of the heat sink and CPU location on the heat transfer in the immersed server model. Three different locations were investigated, namely 100, 200 and 300 mm from the bottom of the server. The best location is at 100 mm from the bottom of the server where the CPU and heat sink are close to the bottom of the server. Placing the CPU and heat sink in the bottom of the server can increase the Nu by 89%. This is due to the CPU and heat sink creating large fluid recirculation which promotes the fluid to flow faster, which gives rise to a better heat transfer coefficient.

7. In chapter 7 the immersed server model was placed in a data centre with a cooling system that comprised of a liquid-to-liquid heat exchanger and a dry air cooler. The study is theoretical, but is based on experimental work, which investigated a data centre cooling system for servers using a similar mixed cooling (water cold plate for the CPU and air used to cool the rest of server IT equipment) system and cooling plant comprising a dry air cooler and water heat exchanger. Based on the outside temperature and flow rate between the dry air cooler, water heat exchanger and servers in the rack, the inlet water temperature and flow rate through the water jacket of the immersed sever was determined. From the flow rate and the inlet temperature to the rack it is also possible to determine the pressure drop across the immersed server's water jacket. Based on the pressure drops and flow rates, the power required for the rack pump can be calculated. It then follows that a PUE can be obtained based on the fans and pump power. The PUE of a fully populated rack was found to be 1.08. However, the study concluded that the PUE is increases when reducing the number of servers and therefore the full rack load yields a better PUE.

8.2 Future Work

The study in this thesis is carried out for immersed server by using CFD. The validation has been done for different cases that showed the CFD is capable of simulating buoyancy driven flow for heat transfer in an immersed sever. The different shapes of baffle is investigated and the PUE of a data centre is calculated for cooling systems that use the air dry cooler and water heat exchanger combination. The following are suggestions for future studies:

1. The experiment of immersed server is desired in order to carry out a detailed parametric study and to validate the immersed server model using CFD.
2. Using different cooling dielectric liquids for immersed server and compare their cooling performance.
3. The comparison between different baffles cross section area is done in this thesis at same area, and the best baffle cross section area of the baffles is found to be rectangular as shown in chapter 6. It is good to find the optimum of the rectangular width and height.
4. The baffles are parallel with fluid flow in a vertical orientation. The baffles could be oriented horizontally across the fluid flow which may be investigated in a further study.
5. In general, perforated fin or baffle could improve the heat transfer and it could be investigated for fin or baffle in immersed server as well as the adoption of venturis and mechanisms for enhancing the flow inside the immersed server.

6. The immersed servers are likely to be configured for much more powerful situations, so looking at much higher fluxes would also be of interest.
7. The cooling system of a data centre in this study is performed in Leeds. In further work, the cooling system could be applied in a different city as well as further investigations into cooling plan configurations.

REFERENCES

1. Almaneea, A., et al., *Optimal Heat Sink Fin and Cold Lid Heights for Liquid Immersed Servers*, in *COMSOL* 2013: Rotterdam.
2. Almaneea, A., et al., *Cooling System Analysis for a Data Center using Liquid Immersed Servers.* International Journal of Thermal Technologies, 2014. **4**(3): p. 200-207.
3. Almaneea, A., et al., *The Effect of CPU Location in Total Immersion of Microelectronics.* Engineering and Technology International Journal of Electrical, Computer, Electronics and Communication Engineering 2015. **9**(4): p. 370-273.
4. Shah, A., et al. *Impact of rack-level compaction on the data center cooling ensemble*. in *Thermal and Thermomechanical Phenomena in Electronic Systems, 2008. ITHERM 2008. 11th Intersociety Conference on*. 2008: IEEE.
5. Greenberg, S., et al., *Best practices for data centers: Lessons learned from benchmarking 22 data centers.* Proceedings of the ACEEE Summer Study on Energy Efficiency in Buildings in Asilomar, CA. ACEEE, August, 2006. **3**: p. 76-87.
6. 42U. *Hot-Aisle/Cold Aisle Layout for Data Center Racks*. 2014; Available from: http://www.42u.com/cooling/hot-aisle-cold-aisle.htm.
7. PacificGasandElectrical. *HIGH PERFORMANCE DATA CENTERS*. 2011 [cited 2012 01/06]; Available from:

http://hightech.lbl.gov/documents/data_centers/06_datacenters-pge.pdf.

8. AL-Moli, A.M., *AIR FLOW MANAGEMENT INSIDE DATA CENTRES*, in *Mechanical Engineering*. 2013, University of Leeds: Leeds. p. 211.

9. Yang, C.-Y., et al. *An in-situ performance test of liquid cooling for a server computer system*. in *Microsystems Packaging Assembly and Circuits Technology Conference (IMPACT), 2010 5th International*. 2010: IEEE.

10. Tuma, P.E. *The merits of open bath immersion cooling of datacom equipment*. in *Semiconductor Thermal Measurement and Management Symposium, 2010. SEMI-THERM 2010. 26th Annual IEEE*. 2010: IEEE.

11. Naidu, S. and V. Kamaraju, *High Voltage Engineering*. 2009: Tata McGraw Hill Education Private Limited.

12. Lee, T.S., G.H. Son, and J.S. Lee, *Numerical study on natural convection in three-dimensional rectangular enclosures.* KSME Journal, 1989. **3**(1): p. 50-55.

13. He, Y., W. Yang, and W. Tao, *Three-dimensional numerical study of natural convective heat transfer of liquid in a cubic enclosure.* Numerical Heat Transfer, Part A: Applications, 2005. **47**(9): p. 917-934.

14. Frederick, R.L. and F. Quiroz, *On the transition from conduction to convection regime in a cubical enclosure with a partially heated wall.* International journal of heat and mass transfer, 2001. **44**(9): p. 1699-1709.

15. Holman, J., *Heat transfer, 9th*. 2002, McGraw-Hill. p. 335-337.

16. Phan-Thien, Y.L., Nhan, *An optimum spacing problem for three chips mounted on a vertical substrate in an enclosure.* Numerical Heat Transfer: Part A: Applications, 2000. **37**(6): p. 613-630.

17. Chuang, S.-H., J.-S. Chiang, and Y.-M. Kuo, *Numerical simulation of heat transfer in a three-dimensional enclosure with three chips in various position arrangements.* Heat transfer engineering, 2003. **24**(2): p. 42-59.

18. Frederick, R.L. and S.G. Moraga, *Three-dimensional natural convection in finned cubical enclosures.* International journal of heat and fluid flow, 2007. **28**(2): p. 289-298.

19. Nada, S., *Natural convection heat transfer in horizontal and vertical closed narrow enclosures with heated rectangular finned base plate.* International Journal of Heat and Mass Transfer, 2007. **50**(3): p. 667-679.

20. Yucel, N. and H. Turkoglu, *Numerical analysis of laminar natural convection in enclosures with fins attached to an active wall.* Heat and mass transfer, 1998. **33**(4): p. 307-314.

21. Shehabi, A., *Energy Implications of Economizer Use in California Data Centers.* 2008.

22. McNevin, A. *UK DATA CENTERS WOULD COVER 900 FOOTBALL PITCHES*. 2011 [cited 2013 10 April]; Available from: http://www.datacenterdynamics.com/focus/archive/2011/12/uk-data-centers-would-cover-900-football-pitches.

23. Rolander, N., *An approach for the robust design of air cooled data center server cabinets*. 2005, Georgia Institute of Technology.

24. Calban, J.M. *University of Southern California Data Center*. 2012 [cited 2013 12/4]; Available from: http://www.mattconstruction.com/project-detail/mission-critical-data-centers/usc-data-center.

25. Miller, R. *Estimate: Facebook Running 180,000 Servers*. 2012 [cited 2013; Available from: http://www.datacenterknowledge.com/archives/2012/08/15/estimate-facebook-running-180000-servers/.

26. Bailey, J. *Five Reasons Not to Cut Disaster Recovery from Your Budget*. 2013 [cited 2014; Available from: http://www.datacenterjournal.com/it/reasons-cut-disaster-recovery-budget/.

27. *WORLD INTERNET USAGE AND POPULATION STATISTICS June 2012*. 2012 [cited 2013; Available from: http://www.internetworldstats.com/stats.htm.

28. PacificGasandElectrical. *HIGH PERFORMANCE DATA CENTERS*. 2011 January; Available from: http://hightech.lbl.gov/documents/data_centers/06_datacenters-pge.pdf.

29. Romadhon, R., et al. *Optimization of cooling systems in data centre by computational fluid dynamics model and simulation*. 2009: IEEE.

30. SMITH, V., *The Green Grid Energy Policy Research For Data Centers.* White Paper 25, 2009.

31. Domestic-energy-price-statistics. *Statistical data set Annual domestic energy bills*. 2014 [cited 2014; Available from: https://www.gov.uk/government/statistical-data-sets/annual-domestic-energy-price-statistics.

32. Data_Center_Dynamic. *DCD Industry Census 2011*. 2011 [cited 2011; Available from: www.dcd-intelligence.com/content/.../CENSUS_marketgrowth.pdf.

33. Christian, T., et al. *Automated synthesis of sustainable data centers*. in *2009 IEEE International Symposium on Sustainable Systems and Technology (ISSST), 18-20 May 2009*. 2009. Piscataway, NJ, USA: IEEE.

34. Barroso, L.A. and U. Hölzle, *The datacenter as a computer: An introduction to the design of warehouse-scale machines.* Synthesis Lectures on Computer Architecture, 2009. **4**(1): p. 1-108.

35. Koomey, J.G., *Worldwide electricity used in data centers.* Environmental Research Letters, 2008. **3**: p. 034008.

36. Rasmussen, N., *Avoidable Mistakes that Compromise Cooling Performance in Data Centers and Network Rooms.* White Paper, 2003. **49**: p. 2003-0.

37. Rouse, M. *power usage effectiveness (PUE)*. April 2009 [cited 2014 23 March]; Available from: http://searchdatacenter.techtarget.com/definition/power-usage-effectiveness-PUE.

38. Haywood, A., et al., *Thermodynamic feasibility of harvesting data center waste heat to drive an absorption chiller.* Energy Conversion and Management, 2012. **58**: p. 26-34.

39. BELADY, C. *The green grid data centre power efficiency metrics: PUE and DCiE. White paper # 6.* 2007; Available from: http://www.thegreengrid.org/~/media/WhitePapers/White_Paper_6_-_PUE_and_DCiE_Eff_Metrics_30_December_2008.pdf?lang=en.

40. Sheehab, S., *PUE calculations: the model and myths* CCG Whitepaper, 2013.

41. Avelar, V., *Guidance for Calculation of Efficiency (PUE) in Data Centers.* Schneider Electric, Rueil Malmaison, France, White Paper, 2010. **158**.

42. Nelson, G.M., *Development of an Experimentally-Validated Compact Model of a Server Rack.* 2007.

43. Hannemann, R. and H. Chu, *Analysis of Alternative Data Center Cooling Approaches.* InterPACK paper. **1176**.

44. Bhopte, S., et al. *Optimization of data center room layout to minimize rack inlet air temperature*. 2005: ASME.

45. Sharma, R.K., C.E. Bash, and C.D. Patel. *Dimensionless parameters for evaluation of thermal design and performance of large-scale data centers*. 2002: Citeseer.

46. Wang, D. *Cooling challenges and best practices for high density data and telecommunication centers*: IEEE.

47. Niemann, J., *Hot aisle Vs. Cold aisle containment.* APC white paper.

48. Hartley, J., *e Cool: Cold Aise Containment*, in *International Conference on Sustainable Data Center Design and Operation*. 2011, University of Leeds: Leeds.

49. *HOT AISLE CONTAINMENT COOLING SOLUTIONS*. 2011.

50. Rasmussen, N., *Improving Rack Cooling Performance Using Airflow Management™ Blanking Panels.* White Paper 44

51. Hannaford, P., *Ten cooling solutions to support high-density server deployment.* APC white paper, 2006. **42**.

52. *2010 Best Practices for the EU Code of Conduct on Data Centres.* 2010.

53. Cho, J., T. Lim, and B.S. Kim, *Measurements and predictions of the air distribution systems in high compute density (Internet) data centers.* Energy and Buildings, 2009. **41**(10): p. 1107-1115.

54. ASHRAE-TC9.9. *Thermal guidelines for data centre processing environments*. 2011; Available from: http://ecoinfo.cnrs.fr/IMG/pdf/ashrae_2011_thermal_guidelines_data_center.pdf.

55. Evans, T., *Humidification strategies for data centers and network rooms.* White Paper, 2004. **58**: p. 2004-0.

56. Baker, E., *Liquid immersion cooling of small electronic devices.* Microelectronics Reliability, 1973. **12**(2): p. 163-173.

57. Chu, R.C., et al., *Review of cooling technologies for computer products.* Device and Materials Reliability, IEEE Transactions on, 2004. **4**(4): p. 568-585.

58. 451-RESEARCH, *Liquid-Cooled IT: A Flood of Disruption for the Datacenter?* 2014.

59. Almoli, A., et al., *Computational fluid dynamic investigation of liquid rack cooling in data centres.* Applied Energy, 2011.

60. Ellsworth, M., et al. *The evolution of water cooling for IBM large server systems: Back to the future*. 2008: IEEE.

61. Udakeri, R., V. Mulay, and D. Agonafer. *Comparison of Overhead Supply and Underfloor Supply with Rear Heat Exchanger in High Density Data Center Clusters*: IEEE.

62. Anubhav, K. and J. Yogendra. *Use of airside economizer for data center thermal management*. 2008: IEEE.

63. frigel. *Free Cooling*. 2011 [cited 2014; Available from: http://www.frigel.com/why_frigel/performance/free-cooling/.

64. Yang, C.Y. and W.C. Liu, *Development of a Mini Liquid Cooling System for High-Heat-Flux Electronic Devices.* Heat Transfer Engineering, 2011. **32**(7-8): p. 690-696.

65. Anandan, S.S. and V. Ramalingam, *Thermal management of electronics: A review of literature.* Thermal Science, 2008. **12**(2): p. 5-26.

66. Kandlikar, S.G. and C.N. Hayner, *Liquid Cooled Cold Plates for Industrial High-Power Electronic Devices—Thermal Design and Manufacturing Considerations.* Heat Transfer Engineering, 2009. **30**(12): p. 918-930.

67. Chien-Yuh, Y., et al. *An in-situ performance test of liquid cooling for a server computer system*. in *2010 5th International Microsystems,*

Packaging, Assembly and Circuits Technology Conference (IMPACT 2010), 20-22 Oct. 2010. 2010. Piscataway, NJ, USA: IEEE.

68. Miller, R. *The Iceotope Liquid Cooling System in Action*. 2013 [cited 2013; Available from: http://www.datacenterknowledge.com/archives/2013/03/04/iceotope-liquid-cooling-in-action/.

69. Tuma, P.E. *Fluoroketone C2F5C(O)CF(CF3)2 as a heat transfer fluid for passive and pumped 2-phase applications*. in *SEMI-THERM '08. 2008 24th Annual IEEE Semiconductor Thermal Measurement and Management Symposium, 16-20 March 2008*. 2008. Piscataway, NJ, USA: IEEE.

70. Tuma, P.E. *The Merits of Open Bath Immersion Cooling of Datacom Equipment*. in *2010 IEEE/CPMT 26th Semiconductor Thermal Measurement, Modeling & Management Symposium (SEMI-THERM), 21-25 Feb. 2010*. 2010. Piscataway, NJ, USA: IEEE.

71. CHESTER, D., et al., *COOLED ELECTRONIC SYSTEM*. 2010, WO Patent 2,010,130,993.

72. Chester, D., *Icoetope Immersed data centre*. 2011, University of Leeds: Leeds.

73. Henk Kaarle Versteeg, W.M., *An introduction to computational fluid dynamics: the finite volume method*. 2007: Pearson Education Ltd. 1-4.

74. Jiyuan Tu, G.H.Y., Chaoqun Liu, *Computational fluid dynamics: a practical approach*. 2008: Elsevier Inc.

75. Patankar, S., *Numerical heat transfer and fluid flow*. 1980: CRC Press.

76. Lewis, R.W., P. Nithiarasu, and K.N. Seetharamu, *Front Matter*. 2004: Wiley Online Library.

77. Rambo, J. and Y. Joshi, *Modeling of data center airflow and heat transfer: state of the art and future trends.* Distributed and Parallel Databases, 2007. **21**(Copyright 2007, The Institution of Engineering and Technology): p. 193-225.

78. Versteeg, H.K. and W. Malalasekera, *An introduction to computational fluid dynamics: the finite volume method*. 2007: Pearson Education.

79. Çengel, Y.A., R. H. Turner, et al, *Fundamentals of thermal-fluid sciences* 2008. p. 797.

80. Mechanical-and-Mechatronic-Engg. *Fully Developed Laminar Flow*. [cited 2014; Available from: http://www-mdp.eng.cam.ac.uk/web/library/enginfo/aerothermal_dvd_only/aero/fprops/pipeflow/node10.html.

81. Wilcox, D.C., *Turbulence modeling for CFD*. Vol. 2. 1998: DCW industries La Canada, CA.

82. COMSOL, *Wall Functions*. 2013, COMSOL.

83. Kuzmin, D., O. Mierka, and S. Turek, *On the implementation of the κ-ε turbulence model in incompressible flow solvers based on a finite element discretisation.* International Journal of Computing Science and Mathematics, 2007. **1**(2): p. 193-206.

84. COMSOL, *CFD II: Turbulent and High Mach Number Flow*, in *COMSOL Conference Rotterdam*. 2013, COMSOL: Rotterdam. p. 43.

85. Potter, M., D. Wiggert, and B. Ramadan, *Mechanics of Fluids SI Version*. 2011: Cengage Learning.

86. Çengel, Y.A., R.H. Turner, and J.M. Cimbala, *Fundamentals of thermal-fluid sciences* 2008. p. 534.

87. TRITTON, D.J., *Physical Fluid Dynamics*. 1988, Oxford: University of Oxford.

88. Almoli, A.M., *Air flow management in data centres*. 2013, Univesity of Leeds.

89. Hirsch, C., *Numerical computation of internal and external flows: the fundamentals of computational fluid dynamics*. Vol. 1. 2007: Butterworth-Heinemann.

90. Launder, B.E. and D. Spalding, *The numerical computation of turbulent flows.* Computer methods in applied mechanics and engineering, 1974. **3**(2): p. 269-289.

91. Rundle, C. and M. Lightstone. *Validation of turbulent natural convection in a square cavity for application of CFD modelling to heat transfer and fluid flow in atria geometries*. in *2nd Canadian Solar Buildings Conference, Calgary*. 2007.

92. Zitzmann, T., et al. *Simulation of steady-state natural convection using CFD*. in *Proc. of the 9th International IBPSA Conference Building Simulation 2005*. 2005: Montréal: IBPSA.

93. Aounallah, M., et al., *Numerical investigation of turbulent natural convection in an inclined square cavity with a hot wavy wall.*

International Journal of Heat and Mass Transfer, 2007. **50**(9): p. 1683-1693.

94. Abe, K., T. Kondoh, and Y. Nagano, *A new turbulence model for predicting fluid flow and heat transfer in separating and reattaching flows—I. Flow field calculations.* International Journal of Heat and Mass Transfer, 1994. **37**(1): p. 139-151.

95. de Vahl Davis, G., *Natural convection of air in a square cavity: a bench mark numerical solution.* International Journal for Numerical Methods in Fluids, 1983. **3**(3): p. 249-264.

96. de Vahl Davis, G. and I. Jones, *Natural convection in a square cavity: a comparison exercise.* International Journal for numerical methods in fluids, 1983. **3**(3): p. 227-248.

97. Ammour, D.I., H and Craft, T.J, *MODEL VALIDATION FOR BOUYANCY-DRIVEN FLOWS INSIDE DIFFERENTIALLY HEATED CAVITIES*. 2011: The University of Manchester.

98. Kamel, J. *Buoyancy Flow in Free Fluids*. 2011 [cited 2011 10/10]; Available from: http://www.comsol.nl/showroom/gallery/665/.

99. Khan, A., *Model of Natural convection in square cavity using fluent*. 2012, University of Leeds.

100. Barakos, G., E. Mitsoulis, and D. Assimacopoulos, *Natural convection flow in a square cavity revisited: laminar and turbulent models with wall functions.* International Journal for numerical methods in fluids, 1994. **18**(7): p. 695-719.

101. AAVID-THERMALL. *HI-CONTACTTM LIQUID COLD PLATES FOR POWER APPLICATIONS*. 2013 [cited 2013; Available from:

http://www.aavid.com/sites/default/files/products/liquid/pdf/liquid-cold-plate-datasheet-hicontact.pdf.

102. Vijiapurapu, S. and J. Cui, *Performance of turbulence models for flows through rough pipes.* Applied Mathematical Modelling, 2010. **34**(6): p. 1458-1466.

103. Joshi, Y. and P. Kumar, *Energy efficient thermal management of data centers*. 2012: Springer.

104. COMSOL. *Water Purification Reactor*. 2013 [cited 2014; Available from: http://www.uk.comsol.com/model/download/176391/models.cfd.water_purification_reactor.pdf.

105. Narayanan, A., et al., *Simultaneous model building and validation with uniform designs of experiments.* Engineering Optimization, 2007. **39**(5): p. 497-512.

106. 3M. *HEF 7300 Data sheet*. 2009 [cited 2013 20/9]; Available from: http://www.scribd.com/doc/49617639/data-sheet-HFE-7300.

107. COMSOL, *Convection Cooling of Circuit Boards 2D Natural Convection*, COMSOL, Editor. 2014.

108. Cengel, Y.A., *Heat Transfer A Practical Approach* 1998, New York: McGraw-Hill. 29.

109. Sun-Microsystems. *Introduction to the Sun Blade X6250 Server Module*. 2009 [cited 2014; Available from: http://docs.oracle.com/cd/E19045-01/blade.x6250/820-1185-17/intro.html.

110. Jensen, I.S. *Weather statistics for Leeds, England (United Kingdom)*. 2013 [cited 2014 19/03]; Available from: http://www.yr.no/place/United_Kingdom/England/Leeds/statistics.html.

111. Iyengar, M., et al. *Server liquid cooling with chiller-less data center design to enable significant energy savings*. in *Semiconductor Thermal Measurement and Management Symposium (SEMI-THERM), 2012 28th Annual IEEE*. 2012: IEEE.

112. Incropera, F.P., A.S. Lavine, and D.P. DeWitt, *Fundamentals of heat and mass transfer*. 2011: John Wiley & Sons.

113. Stone, T.L. *ENERGY EFFICIENCY IN PUMPING TECHNOLOGY*. 2012 [cited 2014; Available from: http://www.dovercorporation.com/globalnavigation/our-markets/fluids/energy-efficiency-in-pumping-technology.

114. Serth, R.W., *Process heat transfer: principles and applications*. 2007: Elsevier Academic Press New York.

115. Çengel, Y.A., R.H. Turner, and J.M. Cimbala, *Fundamentals of thermal-fluid sciences*. 2008: McGraw-Hill New York. 1020.

116. Chi, Y.Q., et al. *Case study of a data centre using enclosed, immersed, direct liquid-cooled servers*. in *Semiconductor Thermal Measurement and Management Symposium (SEMI-THERM), 2014 30th Annual*. 2014: IEEE.